THYROID HORMONE MODULATION OF DNA METHYLATION IN THE DEVELOPING BRAIN

by

Yasuhiro Kyono

A dissertation submitted in partial fulfillment
of the requirements for the degree of
Doctor of Philosophy
(Neuroscience)
in the University of Michigan
2015

Doctoral Committee:

Professor Robert J. Denver, Chair
Assistant Professor Laura Buttitta
Professor Kenneth M. Cadigan
Professor Cunming Duan
Professor Daniel Goldman
Assistant Professor Andrzej Wierzbicki

To my family

ACKNOWLEDGEMENTS

First and foremost, I would like to thank my thesis advisor Dr. Robert Denver for working with me diligently for the past eight years. He has been an excellent mentor, and without his guidance, support and encouragement, I cannot imagine myself standing where I am today. As I move on to the next phase of my career, I hope that experience and knowledge I have acquired in the Denver lab will take me far to make a strong contribution to science.

I also would like to thank my committee members, Dr. Laura Buttitta, Dr. Kenneth Cadigan, Dr. Cunming Duan, Dr. Daniel Goldman and Dr. Andrzej Wierzbicki, for providing me with their insight and valuable feedback over the years. Without their expertise and willingness to help, my research would not have come this far.

I would like to thank collaborators and people who have helped my research, particularly Drs. Laurent Sachs, Nicolas Buisine and Alexis Grimaldi at Muséum National d'Histoire Naturelle in Paris, France. Their help and expertise on *Xenopus* genomics were indispensable for the completion of my thesis research. I would also like to thank Dr. Sachs' family, Claire, Luc and Rémi for their warm welcome during my stay in France. I would like to thank Robert Weymouth at Xenopus One, Inc. for generously providing us with tadpoles.

I would like to thank staff members in both Neuroscience Graduate Program (Valerie Smith, Rachel Harbach) and in the Department of MCDB (Marry Carr, Diane Durfy and Kristi Rork) for their administrative support and accommodations.

I would like to thank my funding sources: Ruth L. Kirschstein National Research Service Award (NRSA) for Individual Predoctoral Fellowship, Rackham Merit Fellowship and Rackham Graduate Student Research Grant. I am humble to be recognized and receive such an honor. I hope that I strive in the future to reciprocate their investment.

I would like to thank many past and current members of the Denver lab. I was very fortunate to be surrounded by labmates who made it enjoyable to come to work every day. My special thanks goes to Pia Bagamasbad who taught me essentially all molecular biology techniques I conducted in my thesis research.

I would like to thank everyone with whom I had a chance to meet while I was in Ann Arbor. I particularly would like to thank Takeshi Akama, Toshiya Hoshikawa, Yukiko Koizumi, Yuki Matsuba, Yoshinari Miyata, Mikiko Nagashima and Yuta Suzuki for making my life in Ann Arbor enjoyable all these years. My special thanks goes to Toshiya with whom I shared great memories throughout my graduate career. I hope to have a great continuing friendship with him in the coming years. Another special thanks goes to Yukiko and Yuki who provided me with emotional support and encouragement towards the end of my graduate career.

TABLE OF CONTENTS

LIST OF TABLES

LIST OF FIGURES

LIST OF APPENDICES

APPENDIX

ABSTRACT

Postembryonic brain development is dependent on thyroid hormone (T_3). The actions of T_3 are mediated by T_3 receptors (TRs) that bind T_3 response elements (T_3REs) in the genome and regulate gene transcription through recruitment of histone-modifying enzymes. Methylation of DNA is another critical epigenetic modification that controls gene transcription. Using mouse and frog (T_3 controls tadpole metamorphosis), I investigated T_3-dependent modulation of DNA methylation, regulation of genes that control this epigenetic modification, and roles of DNA methylation in regulation of gene expression programs in the brain.

I discovered that TRs directly activate the transcription of the *de novo* DNA methyltransferase 3a (*Dnmt3a*) gene that encodes a key enzyme that establishes genome-wide patterns of DNA methylation in the developing brains of mouse and frog. I identified two functional T_3REs that support T_3-dependent transactivation of the *Dnmt3a* genes. I found strong sequence conservation of the mouse T_3REs among eutherian mammals.

I found that the tadpole brain genome became demethylated during metamorphosis, which correlated with activation of genes that are involved in active DNA demethylation (*tet2, tet3, apobec2, gadd45β, gadd45γ* and *tdg*). Treating premetamorphic tadpoles with exogenous T_3 induced *tet3, gadd45γ* and *tdg* mRNAs. I found that T_3REs for known T_3-regulated genes (*klf9* and *dnmt3a*) became demethylated during metamorphosis and in response to T_3. *In vitro* methylation of DNA fragments containing these T_3REs subcloned into reporter plasmids abrogated T_3-dependent transactivity, suggesting that DNA demethylation of T_3REs activates T_3-regulated genes.

To identify gene expression programs that are regulated by DNA methylation, I conducted methylated DNA capture sequencing and RNA-sequencing in tadpole brain. I identified ~142,000 genomic regions enriched for methylated DNA and 855 regions that showed changes during metamorphosis. More than 5,000 genes showed changes in expression, and I identified thirteen patterns of expression dynamics and enriched biological pathways among these genes. I found an inverse correlation between changes in expression of genes found within 50 kb neighborhood of regions that became differentially methylated..

My findings support that T_3 modulates DNA methylation in the developing brain, and that these changes may be important for the coordination of gene expression programs during postembryonic neurological development.

Chapter 1

INTRODUCTION TO THESIS

Thyroid hormone (TH) plays crucial roles in normal neurological development. Acting through its cognate nuclear hormone receptor, TH exerts pleiotropic actions on neural cell development by controlling gene transcription through modulation of posttranslational modification of histones. While this molecular action of TH is well established, a potential role for TH in modulating DNA methylation, another key epigenetic modification that controls gene transcription, has not been investigated. In my dissertation research I investigated if TH modulates DNA methylation to regulate developmental gene expression programs during neurological development.

Roles of thyroid hormone in postembryonic neurological development

The synthesis of TH is controlled by the hypothalamus-pituitary-thyroid (HPT) axis (1). In mammals thyrotropin-releasing factor (TRH) from the hypothalamus stimulates the anterior pituitary to release thyroid-stimulating hormone (TSH), which in turn stimulates the thyroid gland to release TH into the circulation primarily as thyroxine (T_4). At target tissues T_4 is actively transported into cells and locally converted into more biologically active form of TH (3,5,3' triiodothyronine - T_3) by active removal of iodine from T_4 catalyzed by actions of type 1 and type 2 deiodinases.

The developing brain is one of the most important target tissues of TH. In humans TH starts to influence fetal brain development around 8-10 weeks of gestation, as fetuses express detectable levels of TH receptors (2). Thyroid hormone influences various aspects of neural cell development, including cell proliferation, migration, differentiation, apoptosis, morphology and function (3). Severe deficiency of TH during this period of development leads to an irreversible neurological condition known as cretinism characterized by mental retardation and growth defects.

The molecular actions of TH are mediated by TH receptors (TR) that are encoded by two genes in vertebrate genomes (*Thra* and *Thrb)*; the *Thra* gene encodes TRα, while the *Thrb* gene encodes TRβ (4). The TRs preferentially heterodimerize with another nuclear hormone receptor Retinoid X receptor (RXR) and regulate the transcription of target genes by binding to *cis*-regulatory elements in the genome (T_3 response elements; T_3REs). The TR-RXR heterodimers preferentially recognize T_3REs that are direct repeats of hexanuleotide half sites (5' AGGTCA 3') separated by a four-nucleotide spacer (DR+4), although the half sites could be arranged in an inverted, everted or palindromic manner, with a variable length (1-5 bp) of the spacer in between (4). The TRs have dual roles in gene transcription as activators and repressors, and binding of TH to the receptors modulates their transcriptional activity. In the absence of TH, TRs interact with a corepressor complex (NCoR1 – nuclear corepressor; SMRT – silencing mediator of retinoid and thyroid hormone receptors) that further recruits histone deacetylases to create a chromatin environment that is not permissible for transcription. When TH binds to the receptors, this induces a conformational change of TRs to dissociate the corepressor complex, and in exchange recruits a coactivator complex that contains histone acetyltransferases (p300, CBP) to

promote gene transcription (reviewed in Shi 2009) (5). However, the molecular mechanism by which TH controls various aspects of neural cell development is still poorly understood.

Amphibian metamorphosis is a postembryonic process controlled by TH. Therefore, amphibian species such as *Xenopus laevis* and *X. tropicalis* have been valuable research models to study TH action on tissue morphogenesis including the brain (6). There are several advantages of using amphibian tadpoles over mammalian species to study molecular action of TH on tissue morphogenesis. First, because tadpoles develop and grow as free-swimming larvae, this removes the confounding influence of maternal TH. Second, the hormonal status of tadpoles can be easily manipulated by adding TH or TH signaling inhibitors (e.g. the goitrogen, methimazole) to their rearing water.

The HPT axis controls the synthesis and release of TH in amphibians, except that corticotropin-releasing factor, instead of TRH, stimulates the release of TSH from the pituitary (reviewed in Denver 2013 (7)). At the onset of metamorphosis (NF stage 50) TH level is low. Plasma [T_3] and [T_4] start to elevate during early prometamorphosis (NF stage 54), dramatically increase and peak at metamorphic climax (NF stage 62), and then decline at the completion of metamorphosis (NF stage 66) (Fig 1.1) (8). The surge of TH drives a dramatic morphological transformation of tadpoles that involves tissue generation (e.g. limbs), remodeling of existing organs (e.g. brain, intestine) and removal of body parts that are no longer necessary as a frog (e.g. tail) (8). Thyroid hormone single-handedly orchestrates these morphological changes in a coordinated fashion by activating tissue-specific gene expression programs (9,10).

DNA methylation and enzymes that establish genome-wide patterns of DNA methylation (DNA methyltransferases)

DNA methylation refers to the transfer of a methyl group ($-CH_3$) from a donor substrate, *S*-adenosylmethionine (SAM), onto the fifth carbon position of cytosines in the genome (5-methylcytosine; 5-mC). DNA methylation in vertebrate genomes predominantly occurs on cytosines of cytosine-guanine (CpG) dinucleotides, and 60-80% of CpG dinucleotides in the genome are methylated by actions of enzymes that catalyze DNA methylation, DNA methyltrasferases (DNMTs) (11). Three genes encode DNMTs in vertebrate genomes: *Dnmt1, Dnmt3a* and *Dnmt3b* (in *Xenopus* genome only *dnmt1* and *dnmt3a* genes have been identified). Genome-wide patterns of DNA methylation are first established by DNMT3a and DNMT3b (*de novo* DNMTs), and then maintained through cell divisions by DNMT1 (maintenance DNMT). All of these enzymes are essential for normal development; mice carrying mutations for these genes are embryonic lethal or die prematurely shortly after birth (12,13). Neural cell-specific deletion of DNMT genes in mice causes abnormal neurological development accompanied by defective cell differentiation, neurodegeneration and deficits in learning and memory (14-17).

Recent research has also shown that DNA methylation also occurs on cytosines in the context of non-CpG (or CpH, where H = C, T, or A) dinucleotides. CpH methylation was first discovered in human embryonic stem (ES) cells (18) and later in somatic cells (19-22); interestingly, CpH methylation is most enriched in neural cells (21). The enzyme that catalyzes CpH methylation is currently unknown; however, a number of studies support DNMT3a as a likely candidate. For example, a recent genome-wide analysis of 5-mC in early postnatal mouse and human brain found that a dramatic increase in CpH methylation occurs in parallel with upregulation of the *Dnmt3a* gene (20). Furthermore, other studies have shown that knocking down DNMT3a reduces the abundance of CpH methylation in mouse germinal vesicle oocytes (23), mouse and human ES cells (24,25), and in mouse brain (19,26).

Enzymes that catalyze active DNA demethylation ("DNA demethylases")

DNA demethylation refers to the process of removing the methyl group from methylated cytosines. In mammals global DNA demethylation occurs during embryogenesis in pre-implantation embryos and in primordial germ cells (reviewed in Hackett and Surani, 2013) (27); *Xenopus* embryos undergo similar DNA demethylation (28). Genomes can be demethylated through passive and active mechanisms. Passive DNA demethylation occurs when the newly synthesized DNA does not inherit the pattern of DNA methylation during cell divisions, which may occur through exclusion of the maintenance DNMT (DNMT1) from the nucleus (29). It has been long speculated that global DNA demethylation during mammalian embryogenesis also involved active mechanisms because the decline of 5-mC occurs with faster kinetics than predicted by passive mechanisms alone (29). However, the identity of the enzymes that catalyze active DNA demethylation remained unknown until 2009 when it was discovered that a family of Ten-eleven translocation (TET) enzymes catalyze the conversion of 5-mC to 5-hydroxymethylcytosine (5-hmC), an oxidized form of 5-mC that is enriched in neural cells (30,31). Since this initial discovery, later studies found that 5-hmC serves as a substrate for other pathways to complete the process of DNA demethylation (Fig. 1.2). The first pathway involves de-amination of 5-hmC to 5-hmU (5-hydroxymethyluracil) by combined actions of activity-induced cytidine deaminase (AID) and apolipoprotein B mRNA editing enzyme, catalytic polypeptide (APOBEC), followed by removal of 5-hmU through the base-excision repair (BER) pathway catalyzed by thymine DNA glycosylase (TDG) (29). Another pathway involves further oxidation of 5-hmC by TET proteins to 5-formylcytosine (5-fC), then to 5-carboxylcytosine (5-caC) (32,33). 5-fC and 5-caC can be then removed by the TDG-mediated BER pathway (32,34),

or by the nucleotide excision repair pathway mediated by growth arrest and DNA damage (GADD45) proteins (35).

DNA methylation and gene regulation

Prior studies have established a role for DNA methylation in transcriptional regulation. Once cytosines become methylated by actions of DNMTs, methylated DNA can either directly block binding of transcription factors when their recognition motifs contains CpG dinucleotides, or recruit additional proteins that have affinity for methylated cytosines, such as a family of methyl-CpG binding proteins (MBD: MeCP2, MBD1-4) (36). These MBD proteins interact with a protein complex that contains histone deacetylases such as Sin3A (37) to establish chromatin architecture that is not permissive for transcription. Therefore, in general, DNA methylation is associated with gene repression, while DNA demethylation promotes gene activation.

DNA methylation at gene regulatory regions follow this general rule, as there is an inverse correlation between expression of nearby genes and DNA methylation at promoters, around transcription start site, within intragenic region (gene body), and cell-type specific active enhancers (20,38,39). There is also a strong positive correlation between the level of 5-hmC within the gene body and the transcript abundance of the associated genes (40-42), which is consistent with 5-hmC being an intermediate of active DNA methylation. In vertebrate genomes CpG dinucleotides are often present in clusters (termed 'CpG islands'), and many CpG islands overlap with promoters of constitutively active (i.e. house-keeping) genes; these regions are generally free of DNA methylation to keep the promoters active (43).

On the other hand, there are examples where DNA methylation does not correlate with gene repression. For example, Wu et al. (2010) showed that DNA methylation of non-promoter

regions led to gene activation by preventing the recruitment of Polycomb repressor complex (PRC) 2 that catalyzes the deposition of tri-methylation on lysine residue 27 of histone 3 (H3K27me3), which is a repressive histone mark. It has also been shown that MeCP2, which is normally a repressor, could activate genes by associating with a transcriptional coactivator CREB1 (44). Therefore, the repressive role of CpG methylation appears to be dependent on the location within the genome and the nature of proteins recruited by MBDs. The regulatory role of CpH methylation is still not well understood because of its recent discovery in vertebrate genomes. However, available data suggests that it is also a repressive mark like CpG methylation. For example, Lister et al. (2013) showed that intragenic CpH methylation inversely correlated with the amount of transcript for the associated genes (20).

DNA methylation plays a number of important roles during development, such as X-chromosome inactivation and imprinting. X-chromosome inactivation refers to the dosage-compensation mechanism in mammals to silence one of X-chromosomes in XX females (reviewed in Deng et al., 2014 (45)). Silencing of X-chromosome is regulated by *Xist* long non-coding RNA, which is actively transcribed from the inactive X-chromosome, whereas it is silenced on the active X-chromosome. The 5' region of the *Xist* gene is differentially methylated between active and inactive X-chromosomes; it is hypermethylated on the active X-chromosome to silence the *Xist* gene and hypomethylated on the inactive X-chromosome to keep *Xist* gene transcription active (46). It has been shown that disrupting this differential pattern of DNA methylation leads to abnormal reactivation of the inactive X-chromosome (47,48). Imprinting refers to the pattern of differential gene expression between the two alleles, where one parental copy is preferentially expressed over the other depending on the sex of the parent transmitting the allele. For example, the *Igf2 (*insulin-like growth factor 2) gene in mammals is expressed

only from the paternal allele (reviewed in Nordin et al., 2014 (49)). Almost all imprinted genes are associated with differentially methylated regions (DMRs) (50), and previous studies have established a direct linkage between the *Igf2* gene transcription and the methylation state of DMRs associated with the gene (49).

Role of DNA methylation in neurological development

In humans Rett syndrome best exemplifies the critical role that DNA methylation plays in postembryonic neurological development. Rett syndrome is caused by mutations in the X-linked gene that codes for MeCP2, which binds to methylated cytosines through its methyl-CpG binding domain (51). The affected individuals develop normally up to ~6 months of age, then start to display symptoms such as mental retardation, loss of speech and abnormal gait (51). Mice carrying mutations in the homologous *MeCP2* gene recapitulate the neurological and behavioral symptoms seen in humans (52,53). These disease-associated phenotypes can be partially rescued by re-expressing MeCP2 in post-mitotic neurons (54), suggesting their roles in mature neuronal cells. Indeed, the MeCP2 protein is expressed as abundantly as histone proteins in post-mitotic neurons (55).

Although MeCP2 was originally identified as a protein that binds to methylated CpG dinucleotides (hence the name 'methyl-CpG binding'), it also binds to methylated CpA dinucleotides with a similar affinity to methylated CpGs (26). Recent studies have shown that MeCP2 preferentially binds to brain-specific genes in a manner that is dependent on the density of CpA methylation and the transcript length (26,56), suggesting a role for CpA methylation in Rett syndrome. A recent, comprehensive genome-wide mapping of 5-mC revealed a dramatic increase in CpA methylation in the developing mammalian brains, coincident with the period of

synaptogenesis and synaptic pruning (20), further suggesting roles for DNA methylation in normal neurological development.

Thesis Summary

In this thesis I describe studies that investigated T_3-dependent modulation of DNA methylation during postembryonic brain development. In Chapter 2, I describe work that investigated T_3-dependent transcriptional regulation of the DNA methylatransferase 3a (*Dnmt3a*) gene that codes for a key enzyme that catalyzes *de novo* DNA methylation. I discovered that the *Dnmt3a* gene is directly activated by TRs in the developing brains of mouse and frog. I also identified and characterized two DR+4 T_3REs associated with the gene. Although sequence alignment analysis did not support orthology between mouse and frog *Dnmt3a* T_3REs, I found a strong conservation for both of the mouse *Dnmt3a* T_3REs among eutherian mammals, suggesting that transcriptional regulation of the *Dnmt3a* gene by T_3 is an evolutionary conserved and ancient mechanism to modulate DNA methylation in the developing brain.

Published work and my findings in Chapter 2 suggested that the neural cell genome undergoes changes in DNA methylation during postembryonic development, and I further investigated this in Chapter 3 using *Xenopus* tadpoles. Contrary to what I expected from findings in Chapter 2, I discovered that the genome of tadpole neural cells became demethylated during metamorphosis, which correlated with increases in mRNAs for genes that code for enzymes that catalyze active DNA demethylation (*tet2, tet3, apobec2, gadd45β, gadd45γ* and *tdg*); *tet3, gadd45γ* and *tdg* mRNAs also showed T_3-dependent increases in premetamorphic tadpole brain. I also discovered that regions that contain T_3RE for known T_3-regulated genes (krüppel-like factor 9 – *klf9* and *dnmt3a*) became demethylated in tadpole brain during metamorphosis, and

this correlated with increases in *klf9* and *dnmt3a* mRNAs. I further showed that *in vitro* methylation of DNA fragments that encompassed *klf9* and *dnmt3a* T_3REs impaired T_3-dependent transactivity, suggesting that modulation of DNA methylation at T_3REs may regulate transcriptional activation of T_3-regulated genes in the developing brain.

Findings in Chapter 3 suggest that modulation of DNA methylation support T_3-dependent gene expression changes in tadpole brain during metamorphosis. To identify gene expression programs that are regulated by changes in DNA methylation, I conducted methylated DNA capture sequencing (MethylCap-seq) and RNA-sequencing (RNA-seq) in *Xenopus* tadpole brain at different stages of metamorphosis, which is described in Chapter 4. I identified ~142,000 genomic regions that are enriched for methylated DNA; however, only a small number of regions (855) exhibited changes in DNA methylation (differentially methylated regions – DMRs). On the other hand, I identified more than 5,000 differentially expressed genes in tadpole brain during metamorphosis. By combining MethylCap-seq and RNA-seq data I investigated the potential correlation between changes in DNA methylation and expression of genes that are found in 50 kb vicinity of DMRs. While the majority of genes did not show correlated changes in expression, my analysis supported an inverse correlation between changes in DNA methylation and gene expression changes.

In summary, my findings support that T_3 modulates DNA methylation in the developing brain via activation of genes that are involved in DNA methylation and active DNA demethylation. My discoveries have important implications for understanding the mechanisms by which T_3 regulates gene expression programs that underlie tissue morphogenesis during postembryonic development.

References

1. Nunez J, Celi FS, Ng L, Forrest D. Multigenic control of thyroid hormone functions in the nervous system. Molecular and cellular endocrinology 2008; 287:1-12

2. Bernal J. Thyroid hormone receptors in brain development and function. Nature clinical practice Endocrinology & metabolism 2007; 3:249-259

3. Anderson GW, Schoonover CM, Jones SA. Control of thyroid hormone action in the developing rat brain. Thyroid : official journal of the American Thyroid Association 2003; 13:1039-1056

4. Cheng SY, Leonard JL, Davis PJ. Molecular aspects of thyroid hormone actions. Endocrine reviews 2010; 31:139-170

5. Shi YB. Dual functions of thyroid hormone receptors in vertebrate development: the roles of histone-modifying cofactor complexes. Thyroid : official journal of the American Thyroid Association 2009; 19:987-999

6. Tata JR. Amphibian metamorphosis as a model for the developmental actions of thyroid hormone. Molecular and cellular endocrinology 2006; 246:10-20

7. Denver RJ. Neuroendocrinology of amphibian metamorphosis. Current topics in developmental biology 2013; 103:195-227

8. Shi Y-B. Amphibian Metamorphosis: From Morphology to Molecular Biology. New York: John Wiley and Sons, Inc.

9. Buchholz DR, Heimeier RA, Das B, Washington T, Shi YB. Pairing morphology with gene expression in thyroid hormone-induced intestinal remodeling and identification of a core set of TH-induced genes across tadpole tissues. Developmental biology 2007; 303:576-590

10. Das B, Cai L, Carter MG, Piao YL, Sharov AA, Ko MS, Brown DD. Gene expression changes at metamorphosis induced by thyroid hormone in Xenopus laevis tadpoles. Developmental biology 2006; 291:342-355

11. Suzuki MM, Bird A. DNA methylation landscapes: provocative insights from epigenomics. Nature reviews Genetics 2008; 9:465-476

12. Li E, Bestor TH, Jaenisch R. Targeted mutation of the DNA methyltransferase gene results in embryonic lethality. Cell 1992; 69:915-926

13. Okano M, Bell DW, Haber DA, Li E. DNA methyltransferases Dnmt3a and Dnmt3b are essential for de novo methylation and mammalian development. Cell 1999; 99:247-257

14. Fan G, Martinowich K, Chin MH, He F, Fouse SD, Hutnick L, Hattori D, Ge W, Shen Y, Wu H, ten Hoeve J, Shuai K, Sun YE. DNA methylation controls the timing of astrogliogenesis through regulation of JAK-STAT signaling. Development 2005; 132:3345-3356

15. Feng J, Zhou Y, Campbell SL, Le T, Li E, Sweatt JD, Silva AJ, Fan G. Dnmt1 and Dnmt3a maintain DNA methylation and regulate synaptic function in adult forebrain neurons. Nature neuroscience 2010; 13:423-430

16. Hutnick LK, Golshani P, Namihira M, Xue Z, Matynia A, Yang XW, Silva AJ, Schweizer FE, Fan G. DNA hypomethylation restricted to the murine forebrain induces cortical degeneration and impairs postnatal neuronal maturation. Human molecular genetics 2009; 18:2875-2888

17. Nguyen S, Meletis K, Fu D, Jhaveri S, Jaenisch R. Ablation of de novo DNA methyltransferase Dnmt3a in the nervous system leads to neuromuscular defects and

shortened lifespan. Developmental dynamics : an official publication of the American Association of Anatomists 2007; 236:1663-1676
18. Lister R, Pelizzola M, Dowen RH, Hawkins RD, Hon G, Tonti-Filippini J, Nery JR, Lee L, Ye Z, Ngo QM, Edsall L, Antosiewicz-Bourget J, Stewart R, Ruotti V, Millar AH, Thomson JA, Ren B, Ecker JR. Human DNA methylomes at base resolution show widespread epigenomic differences. Nature 2009; 462:315-322
19. Guo JU, Su Y, Shin JH, Shin J, Li H, Xie B, Zhong C, Hu S, Le T, Fan G, Zhu H, Chang Q, Gao Y, Ming GL, Song H. Distribution, recognition and regulation of non-CpG methylation in the adult mammalian brain. Nature neuroscience 2014; 17:215-222
20. Lister R, Mukamel EA, Nery JR, Urich M, Puddifoot CA, Johnson ND, Lucero J, Huang Y, Dwork AJ, Schultz MD, Yu M, Tonti-Filippini J, Heyn H, Hu S, Wu JC, Rao A, Esteller M, He C, Haghighi FG, Sejnowski TJ, Behrens MM, Ecker JR. Global epigenomic reconfiguration during mammalian brain development. Science 2013; 341:1237905
21. Varley KE, Gertz J, Bowling KM, Parker SL, Reddy TE, Pauli-Behn F, Cross MK, Williams BA, Stamatoyannopoulos JA, Crawford GE, Absher DM, Wold BJ, Myers RM. Dynamic DNA methylation across diverse human cell lines and tissues. Genome research 2013; 23:555-567
22. Xie W, Barr CL, Kim A, Yue F, Lee AY, Eubanks J, Dempster EL, Ren B. Base-resolution analyses of sequence and parent-of-origin dependent DNA methylation in the mouse genome. Cell 2012; 148:816-831
23. Shirane K, Toh H, Kobayashi H, Miura F, Chiba H, Ito T, Kono T, Sasaki H. Mouse oocyte methylomes at base resolution reveal genome-wide accumulation of non-CpG methylation and role of DNA methyltransferases. PLoS genetics 2013; 9:e1003439
24. Arand J, Spieler D, Karius T, Branco MR, Meilinger D, Meissner A, Jenuwein T, Xu G, Leonhardt H, Wolf V, Walter J. In vivo control of CpG and non-CpG DNA methylation by DNA methyltransferases. PLoS genetics 2012; 8:e1002750
25. Ziller MJ, Muller F, Liao J, Zhang Y, Gu H, Bock C, Boyle P, Epstein CB, Bernstein BE, Lengauer T, Gnirke A, Meissner A. Genomic distribution and inter-sample variation of non-CpG methylation across human cell types. PLoS genetics 2011; 7:e1002389
26. Gabel HW, Kinde B, Stroud H, Gilbert CS, Harmin DA, Kastan NR, Hemberg M, Ebert DH, Greenberg ME. Disruption of DNA-methylation-dependent long gene repression in Rett syndrome. Nature 2015;
27. Hackett JA, Surani MA. DNA methylation dynamics during the mammalian life cycle. Philosophical transactions of the Royal Society of London Series B, Biological sciences 2013; 368:20110328
28. Stancheva I, Meehan RR. Transient depletion of xDnmt1 leads to premature gene activation in Xenopus embryos. Genes & development 2000; 14:313-327
29. Wu H, Zhang Y. Reversing DNA methylation: mechanisms, genomics, and biological functions. Cell 2014; 156:45-68
30. Tahiliani M, Koh KP, Shen Y, Pastor WA, Bandukwala H, Brudno Y, Agarwal S, Iyer LM, Liu DR, Aravind L, Rao A. Conversion of 5-methylcytosine to 5-hydroxymethylcytosine in mammalian DNA by MLL partner TET1. Science 2009; 324:930-935
31. Kriaucionis S, Heintz N. The nuclear DNA base 5-hydroxymethylcytosine is present in Purkinje neurons and the brain. Science 2009; 324:929-930

32. He YF, Li BZ, Li Z, Liu P, Wang Y, Tang Q, Ding J, Jia Y, Chen Z, Li L, Sun Y, Li X, Dai Q, Song CX, Zhang K, He C, Xu GL. Tet-mediated formation of 5-carboxylcytosine and its excision by TDG in mammalian DNA. Science 2011; 333:1303-1307
33. Ito S, Shen L, Dai Q, Wu SC, Collins LB, Swenberg JA, He C, Zhang Y. Tet proteins can convert 5-methylcytosine to 5-formylcytosine and 5-carboxylcytosine. Science 2011; 333:1300-1303
34. Maiti A, Drohat AC. Thymine DNA glycosylase can rapidly excise 5-formylcytosine and 5-carboxylcytosine: potential implications for active demethylation of CpG sites. The Journal of biological chemistry 2011; 286:35334-35338
35. Schafer A. Gadd45 proteins: key players of repair-mediated DNA demethylation. Advances in experimental medicine and biology 2013; 793:35-50
36. Hendrich B, Bird A. Identification and characterization of a family of mammalian methyl-CpG binding proteins. Molecular and cellular biology 1998; 18:6538-6547
37. Nan X, Ng HH, Johnson CA, Laherty CD, Turner BM, Eisenman RN, Bird A. Transcriptional repression by the methyl-CpG-binding protein MeCP2 involves a histone deacetylase complex. Nature 1998; 393:386-389
38. Guo JU, Ma DK, Mo H, Ball MP, Jang MH, Bonaguidi MA, Balazer JA, Eaves HL, Xie B, Ford E, Zhang K, Ming GL, Gao Y, Song H. Neuronal activity modifies the DNA methylation landscape in the adult brain. Nature neuroscience 2011; 14:1345-1351
39. Hon GC, Rajagopal N, Shen Y, McCleary DF, Yue F, Dang MD, Ren B. Epigenetic memory at embryonic enhancers identified in DNA methylation maps from adult mouse tissues. Nature genetics 2013; 45:1198-1206
40. Colquitt BM, Allen WE, Barnea G, Lomvardas S. Alteration of genic 5-hydroxymethylcytosine patterning in olfactory neurons correlates with changes in gene expression and cell identity. Proceedings of the National Academy of Sciences of the United States of America 2013; 110:14682-14687
41. Song CX, Szulwach KE, Fu Y, Dai Q, Yi C, Li X, Li Y, Chen CH, Zhang W, Jian X, Wang J, Zhang L, Looney TJ, Zhang B, Godley LA, Hicks LM, Lahn BT, Jin P, He C. Selective chemical labeling reveals the genome-wide distribution of 5-hydroxymethylcytosine. Nature biotechnology 2011; 29:68-72
42. Szulwach KE, Li X, Li Y, Song CX, Wu H, Dai Q, Irier H, Upadhyay AK, Gearing M, Levey AI, Vasanthakumar A, Godley LA, Chang Q, Cheng X, He C, Jin P. 5-hmC-mediated epigenetic dynamics during postnatal neurodevelopment and aging. Nature neuroscience 2011; 14:1607-1616
43. Deaton AM, Bird A. CpG islands and the regulation of transcription. Genes & development 2011; 25:1010-1022
44. Chahrour M, Jung SY, Shaw C, Zhou X, Wong ST, Qin J, Zoghbi HY. MeCP2, a key contributor to neurological disease, activates and represses transcription. Science 2008; 320:1224-1229
45. Deng X, Berletch JB, Nguyen DK, Disteche CM. X chromosome regulation: diverse patterns in development, tissues and disease. Nature reviews Genetics 2014; 15:367-378
46. Norris DP, Patel D, Kay GF, Penny GD, Brockdorff N, Sheardown SA, Rastan S. Evidence that random and imprinted Xist expression is controlled by preemptive methylation. Cell 1994; 77:41-51
47. Beard C, Li E, Jaenisch R. Loss of methylation activates Xist in somatic but not in embryonic cells. Genes & development 1995; 9:2325-2334

48. Panning B, Jaenisch R. DNA hypomethylation can activate Xist expression and silence X-linked genes. Genes & development 1996; 10:1991-2002
49. Nordin M, Bergman D, Halje M, Engstrom W, Ward A. Epigenetic regulation of the Igf2/H19 gene cluster. Cell proliferation 2014; 47:189-199
50. Reik W, Walter J. Genomic imprinting: parental influence on the genome. Nature reviews Genetics 2001; 2:21-32
51. Amir RE, Van den Veyver IB, Wan M, Tran CQ, Francke U, Zoghbi HY. Rett syndrome is caused by mutations in X-linked MECP2, encoding methyl-CpG-binding protein 2. Nature genetics 1999; 23:185-188
52. Chen RZ, Akbarian S, Tudor M, Jaenisch R. Deficiency of methyl-CpG binding protein-2 in CNS neurons results in a Rett-like phenotype in mice. Nature genetics 2001; 27:327-331
53. Guy J, Hendrich B, Holmes M, Martin JE, Bird A. A mouse Mecp2-null mutation causes neurological symptoms that mimic Rett syndrome. Nature genetics 2001; 27:322-326
54. Luikenhuis S, Giacometti E, Beard CF, Jaenisch R. Expression of MeCP2 in postmitotic neurons rescues Rett syndrome in mice. Proceedings of the National Academy of Sciences of the United States of America 2004; 101:6033-6038
55. Skene PJ, Illingworth RS, Webb S, Kerr AR, James KD, Turner DJ, Andrews R, Bird AP. Neuronal MeCP2 is expressed at near histone-octamer levels and globally alters the chromatin state. Molecular cell 2010; 37:457-468
56. Sugino K, Hempel CM, Okaty BW, Arnson HA, Kato S, Dani VS, Nelson SB. Cell-type-specific repression by methyl-CpG-binding protein 2 is biased toward long genes. The Journal of neuroscience : the official journal of the Society for Neuroscience 2014; 34:12877-12883

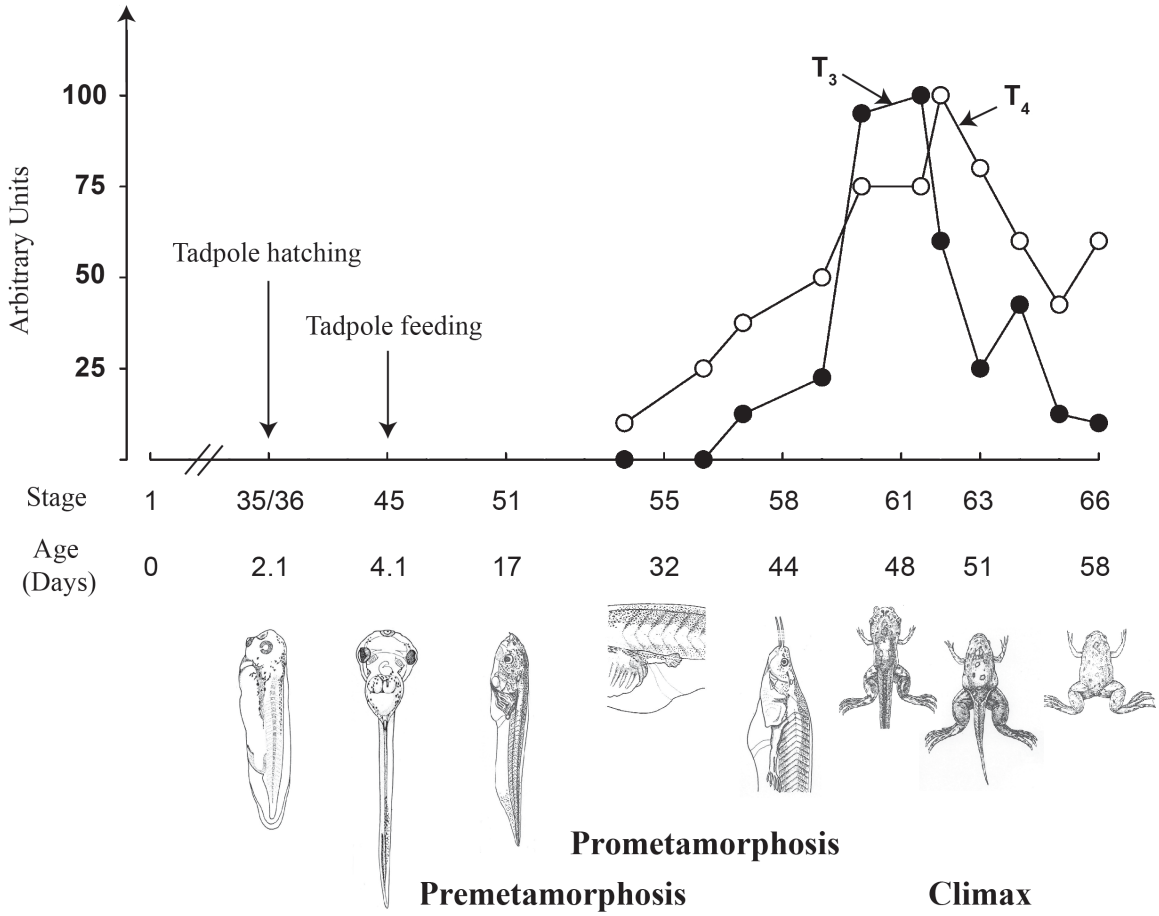

Fig. 1.1. Correlation of plasma thyroid hormone (T_3 and T_4) concentration with *Xenopus laevis* metamorphosis. Developmental stage is assigned according to the normal table of *X. laevis* (Nieuwkoop and Faber, 1956). The figure was recreated with permission based on a figure in Shi (2000).

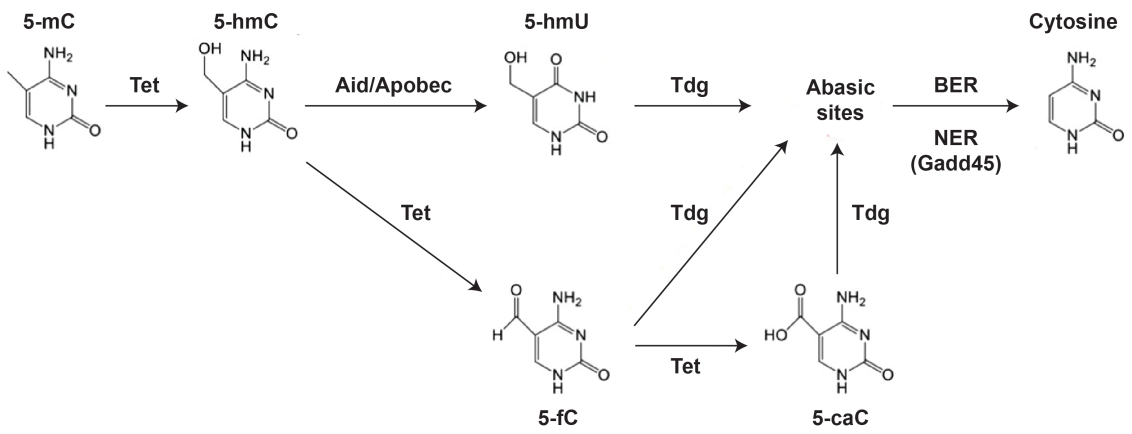

Fig. 1.2. Active DNA demethylation pathways. Ten-eleven translocation (TET) enzymes initiate the process of active DNA demethylation by catalyzing the conversion of 5-methylcytosine (5-mC) to 5-hydroxymethylcytosine (5-hmC). The first pathway involves de-amination of 5-hmC to 5-hmU (5-hydroxymethyluracil) by combined actions of activity-induced cytidine deaminase (AID) and apolipoprotein B mRNA editing enzyme, catalytic polypeptide (APOBEC). This is followed by removal of 5-hmU through the base-excision repair (BER) pathway catalyzed by thymine DNA glycosylase (TDG). The second pathway involves TET-mediated oxidation of 5-hmC to 5-formylcytosine (5-fC), then to 5-carboxylcytosine (5-caC). 5-fC and 5-caC are then removed by the TDG-mediated BER pathway, or by the nucleotide excision repair pathway mediated by growth arrest and DNA damage (GADD45) proteins (adapted and modified from Wu and Zhang (2010) with permission)

Chapter 2

THYROID HORMONE RECEPTORS DIRECTLY REGULATE TRANSCRIPTION OF THE *DE NOVO* DNA METHYLTRANSFERASE *DNMT3A* GENE IN THE DEVELOPING BRAIN

Abstract

Thyroid hormone (T_3) is essential for vertebrate neurological development. Thyroid hormone receptors control gene transcription by modulating chromatin structure through posttranslational modifications of histones. Methylation of DNA is another key epigenetic modification influencing gene transcription. Patterns of DNA methylation are established by the *de novo* DNA methyltransferases (DNMT) 3a and 3b, and maintained by DNMT1. Using *Xenopus* tadpole metamorphosis, a T_3-dependent process, I discovered that *dnmt3a* mRNA increased in tadpole brain during spontaneous metamorphosis and could be induced in premetamorphic tadpoles by exogenous T_3. I identified two T_3 response elements (T_3REs) within *dnmt3a* at -7.4 kb and +4.7 kb relative to the predicted translation start site to explain T_3 regulation of the gene. In mouse brain the postnatal rise in plasma T_3 and expression of *Dnmt3a* are positively correlated. I therefore investigated whether *Dnmt3a* was similarly regulated by T_3 in mouse as in frog. Injection of T_3 into postnatal day 6 mice increased *Dnmt3a* mRNA in the brain. Treatment of the mouse neuroblastoma cell line Neuro2a[TRβ1] with T_3 caused a rapid increase in *Dnmt3a* mRNA. I identified two functional T_3REs within the mouse *Dnmt3a* locus at

+30.1 kb and +49.0 kb from the transcription start site; they are highly conserved among mammalian species, but do not appear to be orthologous with the frog *dnmt3a* T_3REs. Thyroid regulation of *Dnmt3a* may be an ancient feature in vertebrates, but the ancestral genomic sites responsible for hormone regulation may have diverged, or arisen by convergent evolution. I hypothesize that T_3 regulation of *Dnmt3a* is an important mechanism for modulating global changes in DNA methylation during postnatal neurological development.

Introduction

DNA methylation of the carbon-5 position of cytosines (5-methylcytosines; 5-mC) is an epigenetic modification that is critical for controlling gene expression. In most vertebrate cells cytosine methylation in DNA occurs predominantly in the context of cytosine-guanine (CpG) dinucleotides, but recent findings showed that it is also present as a form of CpH methylation (where H = A, T or G) (1). Genome-wide DNA methylation pattern is established during embryogenesis by the *de novo* by DNA methyltransferases DNMT3a and 3b, and maintained through rounds of cell division by DNMT1. DNA methylation at gene regulatory loci can lead to gene silencing through direct inhibition of transcription factor binding or recruitment of methyl-CpG binding domain (MBD) proteins, such as MeCP2, that recruit chromatin modifying enzymes such as histone deacetylases to establish a repressive chromatin state (2).

In addition to established roles in X-chromosome inactivation, genomic imprinting and silencing of transposable elements during embryogenesis (3), DNA methylation plays crucial roles in postembryonic maturation of the developing brain. For example, a recent comprehensive genome-wide analysis of 5-mC in the developing frontal cortices in human and mouse found a dramatic increase in the abundance of 5-mC, mostly in the CpA context, that coincides with a period of synaptogenesis during early postnatal weeks (4). Mutations in the X-linked *MECP2* gene in humans causes Rett syndrome, where affected individuals gradually lose acquired speech and motor skills and develop mental retardation by 6-18 months of age (5). *Dnmt3a* knock-out mice die prematurely at four weeks of age (6) with signs of defective neurogenesis in the subventricular zone (SVZ) of the brain (7).

Thyroid hormone plays critical roles in vertebrate development, which was first shown in the amphibian tadpole where TH is necessary and sufficient to induce metamorphosis. The

hormone has pleiotropic actions in neurological development, influencing neural cell proliferation, migration, differentiation, apoptosis, morphology and function, but the molecular basis for these actions are poorly understood (8). Thyroid hormone acts to control gene transcription via ligand-modulated transcription factors (TRs) that bind T_3 response elements (T_3RE) in the genome typically in heterodimerization with retinoid X receptor (RXR). For genes that are activated by T_3, unliganded TRs repress transcription through interaction with a corepressor complex that recruits histone-modifying enzymes such as histone deacetylases to create a closed chromatin structure. By contrast, liganded TRs activate transcription through recruitment of a coactivator complex that includes histone acetyltransferases that acetylate lysine residues on histone tails to generate an open chromatin structure (9).

While the roles of TRs in controlling histone modifications have been extensively studied, it is not known whether TH acting through TRs can influence DNA methylation. In the present study I investigated T_3 regulation of the *Dnmt3a* gene in *Xenopus* and mouse brain, and in mouse neurobastoma cells (Neuro2a[TRβ1]). I found that *Dnmt3a* is regulated in a developmental stage and T_3-dependent manner in both species. Furthermore, I identified and characterized functional T_3REs in *Xenopus* and mouse *Dnmt3a* genes. My findings support the hypothesis that TH influences DNA methylation in the developing brain through direct regulation of *Dnmt3a*.

Materials and Methods

Animal care and thyroid hormone (T_3) treatment of animals

Xenopus laevis tadpoles were obtained by in-house breeding, reared in dechlorinated tap water (21 – 23 °C), maintained at 12L:12D photoperiod and fed *ad libitum* with pulverized frog brittle powder (NASCO, Fort Atkinson, WI). The normal table of Nieuwkoop and Faber (NF)

(1994) was used to assign developmental stages.

For gene expression analyses I placed premetamorphic *X. laevis* tadpoles (NF stage 50) in aquaria containing two liters of water 24 hr prior to hormone treatment. Thyroid hormone (3,5,3′-L-triiodothyronine; T_3 sodium salt; Sigma-Aldrich, St. Louis, MO) was first dissolved in dimethylsulfoxide (DMSO) and directly added to the aquarium water. I treated animals with vehicle (0.0003% DMSO) or T_3 (5 nM) for different times before harvest. Twenty-four hours after hormone treatment was initiated, the water was exchanged and T_3 was replenished. Tadpoles were killed by rapid decapitation, brains were dissected, and either snap frozen in liquid nitrogen and stored at –80 °C until RNA extraction, or fixed for *in situ* hybridization histochemistry (ISHH; described below).

I purchased wild-type C57BL/6J mice from the Jackson Laboratory (Bar Harbor, ME) and maintained them at 12L:12D photoperiod with food and water provided *ad libitum*. Neonatal mice were obtained by in-house breeding. For gene expression analysis I administered intraperitoneal (i.p.) injections at postnatal day 6 (PND6) of vehicle (corn oil + EtOH) or T_3 (25 μg/kg body weight - BW). The T_3 was first dissolved in EtOH at high concentration and then added dropwise to corn oil with vigorous mixing (final concentration 0.05% EtOH). Mice were killed by rapid decapitation one hr after injection. The hippocampal region of the brain was dissected, snap frozen in liquid nitrogen and stored at –80 °C until RNA extraction.

For chromatin immunoprecipitation (ChIP) assays, I administered i.p. injections of T_3 (25 μg/kg BW) to PND14 mice of mixed sexes (n=5). Mice were killed by rapid decapitation four hrs after injection. Frontal cortex, the hippocampus and the cerebellum were dissected, and chromatin was extracted immediately after dissection, snap frozen in liquid nitrogen and stored at –80 °C until ChIP assays were conducted (see below). All procedures involving animals were

conducted in accordance with the guidelines of the University Committee on the Care and Use of Animals of the University of Michigan.

RNA extraction and reverse transcriptase real-time quantitative PCR (RT-qPCR)

I extracted total RNA from tissues or cells using TRIZOL reagent (Invitrogen Life Technologies, Carlsbad, CA). Prior to cDNA synthesis, I treated the total RNA with 20 units of deoxyribonuclease I (DNAse I) (Invitrogen) in the presence of RNAse inhibitor (Roche Applied Sicence, Indianapolis, IN). I reverse transcribed cDNA using the High Capacity cDNA Synthesis Kit (Applied Biosystems Inc. (ABI), Foster City, CA). I conducted real-time qPCR using ABsolute Blue qPCR SYBR Low ROX Mix (ABgene Thermo Scientific, Surrey, UK) and Fast 7500 Real-Time PCR System (ABI) or StepOne Real Time PCR Systems (Life Technologies). Primers were designed to span exon/exon boundaries for each target gene (Supplemental Table 2.1). A relative quantification method (10,11) was used to compare gene expression levels across developmental stages or among treatments by generating standard curves for each gene with a pool of cDNAs. *Xenopus laevis dnm3a* mRNA (Genbank Accession# BJ059684) was normalized to *alpha-actinin* mRNA (NM_001090829.1), and mouse *Dnmt3a* mRNA (NM_007872) was normalized to *GAPDH* mRNA (NM_008084). Both *alpha-actinin* and *GAPDH* mRNAs did not change across development or with hormone treatment.

***In situ* hybridization histochemistry (ISHH)**

I analyzed the spatial distribution of *dnmt3a* mRNA in *X. laevis* tadpole brain using ISHH as previously described (12). I isolated a partial cDNA for *X. laevis dnmt3a* (591 bp), subcloned it into the pGEM-T Easy cloning vector (Promega, Fitchburg, WI) and verified the

orientation and sequence by direct DNA sequencing. I synthesized sense and antisense riboprobes from the linearized plasmid using the DIG RNA Labeling Kit (Sp6/T7) (Roche). I hybridized 200 ng of sense or antisense riboprobes to cryosections (12 μm) at 65°C overnight. The RNA hybrids were detected using monoclonal sheep anti-digoxigenin antibody cojugated to alkaline phosphatase (1:500; Roche). Primary immune complexes were detected by colorimetric reaction with NBT/BCIP (nitro-blue tetrazolium chloride and 5-bromo-4-chloro-3'-indolyphosphate p-toluidine) (Roche). The specificity of the riboprobe was determined by: 1) the absence of signal with sense probe on the adjacent sections (Supplemental Fig. 2.1); and/or 2) the absence of signal with antisense probe in cryosections of vehicle-treated animals. All sections were carefully matched for anatomical level, and digital micrographic images were captured using an Olympus IX81 inverted microscope (Olympus, Tokyo, Japan). Brightness, contrast, and evenness of illumination were adjusted uniformly for images shown in the figures using Adobe Photoshop CS5 (Adobe Systems, Inc., San Jose, CA).

Plasmid constructs

Xenopus tropicalis dnmt3a T_3REs: A chromatin interaction analysis by paired-end tag sequencing (ChIA-PET) with TR as the target protein was conducted on chromatin isolated from *X. tropicalis* tadpole tail fin to identify TR binding sites and their long range interactions in chromatin (L. Sachs and N. Buisine, unpublished data). This analysis identified three putative TR binding sites in the frog *dnmt3a* gene. The coordinates of these three genomic loci (regions A, B and C) are provided in Supplemental Table 2.2. I subcloned genomic fragments corresponding to regions A (281 bp) and B (322 bp) into the pGL4.23 luciferase vector (Promega) at the KpnI

and SacI sites. Region C was not subcloned because I did not find TR association in the tadpole brain by chromatin immunoprecipitation (ChIP) analysis (see Results).

Mouse Dnmt3a T_3REs: I used data from TR ChIP sequencing (ChIP-seq) analyses conducted on chromatin isolated from mouse liver (13) or the C17.2 mouse cerebellar cell line (14) to identify putative TR binding sites at the mouse *Dnmt3a* locus. This analysis, described in the Results, identified two candidate genomic regions, one at +30.1 kb and another at +49.0 kb relative to the TSS (these fell within the second and third introns, respectively, of the mouse *Dnmt3a* gene). I subcloned 500 bp genomic fragments corresponding to these regions into the pCpGL luciferase vector (gift of Michael Rheli) at the BglII and HindIII sites (+30.1 kb fragment), or into pGL4.23 at the KpnI and SacI sites (+49.0 kb fragment).

I generated point mutations in predicted T_3REs within the subcloned genomic fragments by site-directed mutagenesis (primer sequences in Supplemental Table 2.3) using the QuikChange II Site-Directed Mutagenesis Kit (Agilent Technologies, Santa Clara, CA).

Chromatin immunoprecipitation (ChIP) assays

I conducted ChIP assays as previously described (15) with minor modifications. For *X. laevis, I* prepared chromatin from the whole brain of premetamorphic tadpoles (NF stage 50; 18 pooled per sample, n=4) treated with vehicle (0.0003% DMSO) or T_3 (5 nM) for 48 hr, and from untreated tadpoles at metamorphic climax (NF stage 62; 5 pooled per sample, n=4). For mouse, I prepared chromatin from Neuro2a[TRβ1] cells treated with vehicle (0.1% DMSO) or T_3 (30 nM) for 24 hr (n=4/treatment), and chromatin from the frontal cortex of the brain of PND14 mouse that received i.p. injection of T_3 (25 μg/kg BW) four hr before sacrifice (n=5). I sonicated all chromatin samples to ~500 bp using a sonic dismembrator 100 (Fisher, Fair Lawn, NJ) for a total of 200 seconds per sample (20 cycles of 10-second sonication with 1 minute rest between each

cycle) at an output rating of 5-6 watts. All chromatin samples were snap frozen in liquid nitrogen and stored at -80 °C until analysis.

I used the following primary antibodies for ChIP assays: a rabbit polyclonal antiserum raised against the full-length *X. laevis* TRβ (PB antiserum, which recognizes both TRα and TRβ in frog and mouse; 5 μl; gift of Yun-Bo Shi) (15), anti-histone 3 (H3) (5 μl; Millipore, Billerica, MA; #07-670), or anti-acetylated H3 (AcH3) (5 μl; Millipore #06-599). Negative controls for the assay included the replacement of the primary antibody with straight normal rabbit serum (NRS, for the PB antiserum) or IgG purified from NRS (16). I measured ChIP DNA by real-time qPCR using SYBR Green assays.

Electrophoretic mobility shift assays (EMSA)

I conducted EMSA as previously described (17). *Xenopus* TRβ and retinoid X receptor alpha (RXRα) proteins were *in vitro* synthesized using pSp64a-TRβ and pSp64a-RXRα plasmids (gift of Yun-Bo Shi) and the TnT SP6 Quick-Coupled Translation System (Promega). I used radioinert duplex oligonucleotides (1 μM) as competitors in competitive EMSA (Supplemental Table 2.3).

Cell culture and transient transfection assays

Neuro2a is a neuroblastoma cell line that was derived from a spontaneous brain tumor of a strain A albino mouse (American Type Culture Collection). I used Neuro2a engineered to express the TRβ1 isoform (Neuro2a[TRβ1]) (18). I cultured cells as previously described (15) in DMEM/F12 containing 10% fetal bovine serum that had been stripped of thyroid hormone (19) and was supplemented with hygromycin B (500 μg/ml). I plated cells at a density of 0.5 X 10^6

per well in 6-well plates for RNA analysis, 1.25 X 10^6 per well in 6-well plates for ChIP, and 0.15 X 10^6 per well in 24-well plates for transient transfection-reporter assays.

For RNA analysis and ChIP assay, I incubated cells overnight before treatment with vehicle (0.1% DMSO) or T_3 (30 nM) for different times before harvest.

I transfected cells with luciferase reporter constructs (described above; 200 ng per well plus 10 ng pRenilla-tk) using FuGene 6 transfection reagent (Promega, Madison, WI) when cells had reached 60-70% confluency. Twenty-four hr after transfection I treated cells with vehicle (0.1% DMSO) or T_3 (30 nM) for 5 or 24 additional hr before harvest for analysis by dual luciferase assay (Promega). I consistently observed a ~2 fold reduction of the relative light units (RLU) in the T3-treated group transfected with the pGL4.23 empty vector. For this reason I corrected the RLU for the T_3-treated groups by multiplying it by a correction factor. The correction factor was calculated by dividing the RLU from the vehicle treated groups transfected with pGL4.23 empty plasmid by the RLU in the T_3-treated groups transfected with pGL4.23 empty plasmid, which was approximately 2.

To determine whether T_3-induction of *dnmt3a* mRNA required ongoing protein synthesis, I treated cells with 10 μg/ml cycloheximide (CHX) (Sigma-Aldrich) for a total of 7 hr before harvest, 1 hr before and 6 hr during T_3 treatment (the CHX suppressed ongoing protein synthesis by >95% - Bagamasbad et al. 2015).

Data analysis and statistics

I analyzed data using SPSS statistical software (version 19; SPSS Inc., Chicago, IL). I conducted one-way ANOVA followed by Fisher's least significant difference (Fisher's LSD) *post hoc* test and Student's independent sample *t*-test (α=0.05). Data were Log10-transformed

before statistical analysis for the derived values or when the variances were found to be heterogeneous.

I searched for putative direct repeat with four base spacer (DR+4) T_3REs using the sequence analysis program Vector NTI (version 10; Invitrogen) with "TGWCCYnnnnTGWCCY" as a search term with 3 base-pair mismatches allowed. I used AlignX module of Vector NTI for sequence alignment analyses shown in Supplemental Figures. 2.2, 2.6 and 2.8.

Results

Dnmt3a mRNA exhibits developmental and T_3–dependent changes in *Xenopus* tadpole brain

Using real-time RT-qPCR I found that treatment of premetamorphic (NF stage 50) *X. laevis* tadpoles with T_3 added to the aquarium water (5 nM) caused a time-dependent increase in *dnmt3a* mRNA in tadpole brain (Fig. 2.1A). I confirmed and extended these findings using ISHH, which showed expression in different brain regions including the anterior preoptic area, thalamic nuclei, the suprachiasmatic nucleus, the ventral hypothalamus and the optic tectum (Fig. 2.1B and 1C; shown are two transverse planes, the region of the ventral hypothalamus and thalamic nuclei [1] and the optic tectum and tegmentum [2]).

The *dnmt3a* mRNA level analyzed by RTqPCR (Fig. 2.1D) and by ISHH (Fig. 2.1E) exhibited dynamic changes in tadpole brain during spontaneous metamorphosis. It was low during premetamorphosis to early prometamorphosis (NF stages 50-54), increased during late prometamorphosis (from NF stage 54 to 58), peaked at metamorphic climax (NF stage 62) and declined at the end of metamorphosis (NF stage 66; hybridization with sense probe gave no signal – Supplemental Fig. 2.1). Treatment of late prometamorphic (NF stage 58) *X. laevis*

tadpoles with the goitrogen methimazole did not alter *dnmt3a* mRNA in tadpole brain, although this treatment reduced mRNA for a known direct TR target gene (*krüpple-like factor 9 - klf9)* (data not shown)

I detected ISHH signal in the same brain regions as for the premetamorphic tadpole (treated with T_3 for 48 hrs). However, unlike when the expression was induced by exogenous T_3 in the premetamorphic tadpole brain, during spontaneous metamorphosis *dnmt3a* mRNA was excluded from cells located in the ventricular and subventricular zones (VZ and SVZ; neurogenic regions) where neural stem cells proliferate and give rise to neurons and glia (Fig. 2.1E; Supplemental Fig. 2.1).

Identification of T_3 response elements at the frog *dnmt3a* locus

By analyzing data from a ChIA-PET experiment conducted on tadpole tail fin chromatin with TR as the target protein (L. Sachs and N. Buisine, unpublished data) I identified three putative TR binding sites within the *X. tropicalis dnmt3a* locus: one located at 7.4 kb upstream of the predicted translation start site ("region A"), a second at 4.7 kb downstream of the predicted translation start site within the intron between coding exons 1 and 2 ("region B"), and a third at 8.2 kb downstream of the predicted translation start site within the intron between coding exons 2 and 3 ("region C") (Fig. 2.2; see Supplemental Table 2.2 for genomic coordinates of these regions). The annotation for this locus in the *X. tropicalis* genome has not been resolved. While I are confident that these are the first three coding exons based on comparison of the predicted gene structure with that of the mouse *Dnmt3a* gene, I do not know the exact numbering of the exons or introns. For this reason I express distances relative to the predicted translation start site. I also identified homologous genomic loci in the *X. laevis* genome for each of these regions

(Supplemental Fig. 2.2).

I conducted targeted ChIP analysis for TR association with regions A, B and C in brain chromatin isolated from premetamorphic *X. laevis* tadpoles (NF stage 50) treated with or without T_3 for 48 hr, and in chromatin from tadpoles at metamorphic climax when endogenous plasma [T_3] peaks (20). This showed enrichment of the TR ChIP signal at region A in all treatments (Fig. 2.2). The TR ChIP signal was also enriched at region B, but only in metamorphic climax (NF stage 62) animals. The TR ChIP signal was at background levels in all treatments at region C (Fig. 2.2).

Computer analysis identified three putative DR+4 T_3REs located within each of the genomic regions A and B of the *X. tropicalis dnmt3a* locus (xT_3RE-A1-3 and xT_3RE-B1-3; Supplemental Fig. 2.2). Using comparative genomic sequence analysis of the homologous regions of the two *X. laevis dnmt3a* genes (*X. laevis* is pseudotetraploid, while *X. tropicalis* is diploid) I found sequence conservation for one of the T_3REs within each of these regions (xT_3RE-A1 and xT_3RE-B2) (Supplemental Fig. 2.2). Electrophoretic mobility shift assay using oligonucleotide probes containing these conserved T_3REs showed that TRβ-RXRα heterodimers bound to both sequences *in vitro* (Fig. 2.3A). Competitive EMSA confirmed that radioinert duplex olingonucleotides or genomic fragments containing these sequences displaced TRβ-RXRα from the radiolabled probe (Supplemental Fig. 2.3).

To test for functionality of these putative T_3REs I conducted transient transfection-reporter assays in Neuro2a[TRβ1] cells using luciferase reporter constructs containing *X. tropicalis* genomic fragments corresponding to regions A (300 bp) and B (326 bp). Treatment with T_3 caused a significant increase in luciferase activity in cells transfected with these constructs (Fig. 2.3B), which was abolished by single base mutations introduced into each of the

two half sites of the T_3RE-A1 and T_3RE-B2 sequences (Fig. 2.3B).

Dnmt3a mRNA exhibits developmental and T_3–dependent changes in neonatal mouse brain, and is induced by T_3 with rapid kinetics in mouse neuroblastoma cells

Given the strong developmental and T_3-dependent regulation of *dnmt3a* in *Xenopus* brain, I investigated whether the orthologous mouse gene was similarly regulated by TH, and thus if this was an evolutionarily conserved mechanism in vertebrates to control DNA methylation during postembryonic neural development. Published work supports that there is a parallel increase in circulating plasma [T_3] and [T_4] with *Dnmt3a* mRNA and protein in mouse brain during postnatal days 4 (PND4) to PND14 (4,21-23) (Supplemental Fig. 2.4). In addition, a recent meta-analysis of published microarray studies listed *Dnmt3a* as one of 734 candidate TH-regulated genes in rodent brain (24). I found that intraperitoneal injection of T_3 at PND6 increased *Dnmt3a* mRNA in neonatal mouse brain (hippocampal region) at 1 hr after injection, supporting TH regulation of the gene (data not shown). To further investigate TH regulation of *Dnmt3a* in mouse neuronal cells I treated the neuroblastoma cell line Neuro2a[TRβ1] with T_3 (30 nM). This caused a rapid, time-dependent increase in *Dnmt3a* mRNA (Fig. 2.4A), and this increase did not require ongoing protein synthesis (cycloheximide experiment; Fig. 2.4B), thus supporting that mouse *Dnmt3a* is a direct T_3-response gene.

Identification of T_3 response elements at the mouse *dnmt3a* locus

By analyzing data from TR ChIP-seq experiments conducted in mouse liver (13) and in the C17.2 mouse cerebellar cell line (14), I identified thirteen putative TR binding sites associated with the mouse *Dnmt3a* locus (see Supplemental Table 2.2 for genomic coordinates of

these putative TR binding sites). Using this information I conducted targeted ChIP assays for TR association at these genomic regions using chromatin isolated from mouse frontal cortex as published work (4,21) showed that DNMT3a is expressed throughout the mouse brain and that its peak expression occurs in the frontal cortex at PND14 (Supplemental Fig. 2.4). Of the thirteen predicted sites, I confirmed that TR associated with two, one within the second intron at +30.1 kb from the transcription start site (TSS) and another within the third intron at +49.0 kb from the TSS (Fig. 2.5). There was no signal within the second intron at +39.0 kb from the TSS where no T_3RE was predicted (negative control region).

In Neuro2a[TRβ1] cells I found enrichment of TR ChIP signal at the +30.1 kb, but not at the +49.0 kb region (Fig. 2.5). Chromatin immunoprecipitation assays for histone 3 (H3) and acetylated H3 (AcH3) showed that T_3 treatment reduced H3 and increased AcH3 at the +30.1kb region (Supplemental Fig. 2.5). Treatment with T_3 did not alter H3 signal, but increased AcH3 at the +39.0kb and +49.0kb regions (Supplemental Fig. 2.5). These data support that the +30.1 kb site is a *bona fide* T_3RE in N2a[TRb1] cells, and that the increased AcH3 signals at +39.0 and +49.0 kb may indicate spreading of histone acetylation across the locus initiated by T_3-TR action at the +30.1 kb T_3RE.

Computer analysis identified seven putative DR+4 T_3REs within a 500 bp region centered at +30.1 kb from the TSS of the mouse *Dnmt3a* gene (see Supplemental Fig. 2.6 for location of these predicted T_3REs). Competitive EMSA showed that radioinert duplex oligonucleotides with sequences of predicted T_3REs #2, 3, 4 (within a single oligonucleotide because these T_3REs overlap) and #6 displaced TRβ-RXRα heterodimers from the radiolabeled probe; predicted T_3REs #1, 5 and 7 did not compete for binding (Fig. 2.6A). I next tested whether these four predicted T_3REs could support T_3-dependent transactivity by conducting

transient transfection-reporter assays in Neuro2a[TRβ1] cells, using a luciferase reporter construct into which I sub-cloned a 500 bp fragment centered at +30.1 kb from the TSS of the mouse *Dnmt3a* gene. Treatment with T_3 for 5 hr induced ~50 fold increase in luciferase activity in cells transfected with the construct containing the native DNA sequence (Fig. 2.6B). Single base mutations introduced into each of the two half sites of the predicted T_3REs 2, 3 and 4 reduced T_3-dependent transactivity by ~2 fold; whereas, mutation of the predicted T_3RE #6 almost completely abolished transactivity (1.4-fold increase relative to control) (Fig. 2.6B). Competitive EMSA showed that radioinert genomic fragments that encompass these predicted T_3REs displaced TRβ-RXRα heterodimers from the radiolabeled probe; however, mutation of predicted the T_3RE #6 within the fragment abolished its ability to displace the probe (Supplemental Fig. 7A). Taken together, the data support a predominant role for the T_3RE #6 at the +30.1 kb region of the mouse *dnmt3a* gene.

Computer analysis identified a single DR+4 T_3RE within a 500 bp region centered at +49.0 kb from the TSS of mouse *Dnmt3a*. This T_3RE sequence was able to bind TRβ-RXRα heterodimers *in vitro* (Fig. 2.6C) and also supported T_3-dependent transactivation in transient transfection reporter assays in Neuro2a[TRβ1] cells, which was reduced by single base mutations introduced into each of the two half sites of the predicted T_3RE (Fig. 2.6D). Competitive EMSA showed that radioinert duplex oligonucleotides with the native sequence of the +49.0 kb T_3RE completely displaced TRβ-RXRα heterodimers from the radiolabeled probe, while the mutant sequence caused partial displacement (Supplemental Fig. 7B).

The mouse *Dnmt3a* T_3REs are highly conserved among mammalian species

I investigated DNA sequence conservation of the two *Xenopus* T_3REs among different

vertebrate taxa including mouse but found no clear orthology. However, I found strong sequence conservation of both mouse T_3REs (+30.1 and +49.0) among eutherian mammals (Supplemental Fig. 8). The mouse +49.0 kb T_3RE is also present in a metatherian, the wallaby, and in a monotreme, the platypus (Supplemental Fig. 8B). However, I found no sequence conservation of these mammalian *Dnmt3a* T_3REs in a bird (chicken) or in reptiles (lizard, alligator and turtle).

Discussion

Thyroid hormone plays a crucial role in normal neurological development. While TR regulation of gene transcription via posttranslational modifications of histones is well known (9), a potential role for TH modulation of DNA methylation has received little attention. Here I show that transcription of a gene that codes for a key enzyme controlling DNA methylation, *Dnmt3a*, is directly regulated by liganded TR in neural cells in the developing brains of frog and mouse. Although the frog and mouse T_3REs do not appear to be orthologous, I found strong conservation of the *Dnmt3a* T_3REs among mammalian species. To my knowledge, this is the first report that TRs directly regulate transcription of a gene that influences DNA methylation in the central nervous system.

Hormonal regulation of Dnmt3a in the developing brain and identification of T_3 response elements associated with the gene

I found that *dnmt3a* mRNA could be induced in premetamorphic *Xenopus* tadpole brain by treating them with T_3 added to the aquarium water. Also, *dnmt3a* mRNA increased in tadpole brain (diencephalon) during spontaneous metamorphosis, with peak expression at metamorphic climax when plasma [T_3] reaches its highest level (20). my ISHH analysis showed that *dnmt3a*

mRNA was widely expressed throughout the tadpole brain, but it was notably excluded from the neurogenic regions (the VZ and SVZ) where neural stem cells (NSCs) proliferate. In tadpole brain the rate of cell proliferation in the VZ/SVZ peaks at mid-prometamorphosis, then declines through late prometamorphosis and metamorphic climax (12). Because this developmental decline of cell proliferation inversely correlates with increase in *dnmt3a* mRNA in tadpole brain, DNMT3a may play a role in regulation of cell proliferation in the neurogenic region of the developing brain through regulation of cell cycle. In support of this, a recent microarray analysis conducted on NSCs derived from the SVZ of *Dnmt3a* knockout mice showed impaired neurogenesis in response to a differentiation signal accompanied by dysregulation of cell cycle genes (7). Further work is required to determine whether T_3 induces methylation changes at promoters regions of cell cycle control gene.

I further investigated whether *Xenopus dnmt3a* was a direct TR target gene in the developing tadpole brain. Using ChIP, gel shift, mutagenesis and transfection-reporter assays, I identified and characterized two functional DR+4 T_3REs associated with the *Xenopus dnmt3a* locus: one located at +7.4 kb (T_3RE-A) and the other at +4.7 kb (T_3RE-B) from the predicted translation start site. The third putative TR binding site at the *dnmt3a* locus (region C) identified by TR ChIA-PET on tadpole tail fin (L. Sachs and N. Buisine, unpublished data) was not bound by TR in tadpole brain. This may reflect tissue-specific differences in TR binding sites at the *dnmt3a* locus. Because I only investigated TR association in tadpole brain targeting putative TR binding sites identified in tadpole tail fin, it is possible that there are more T_3REs associated with this locus. Future TR ChIP-seq analysis of tadpole brain will be necessary to investigate this possibility.

While my evidence supports that *Xenopus dnmt3a* is a direct TR target gene, treatment of late prometamorphic tadpoles with the goitrogen methimazole did not reduce *dnmt3a* mRNA in tadpole brain, although this treatment reduceded mRNA for another known direct TR target (*klf9*) gene. This may suggest that while *dnmt3a* mRNA is initially induced by TH during early stages of metamorphosis, the maintenance of its expression may be independent of T_3 during later developmental stages. It is also possible that the lack of goitrogen effect on the *dnmt3a* gene may be related to how strongly these two genes are regulated by TH. Developmental increase in *klf9* mRNA during metamorphosis is very robust (40-50 fold) and the kinetics of its induction in premetamorphic tadpole brain is rapid with exogenous T3 treatment (upregulated by 6 hr). By contrast, I observed a relatively small developmental increase in *dnmt3a* mRNA (2-3 fold) during metamorphosis, and the kinetics of induction in premetamorphic tadpole brain is slow with T3 treatment (upregulated by 24 hrs). Because my goitrogen treatment did not even cause a strong reduction for *klf9* mRNA (~2-fold), it is possible that my experiment was not sensitive enough to detect the effect of goitrogen on weakly regulated genes, such as *dnmt3a*.

Given the strong developmental and T_3-dependent regulation of *dnmt3a* in *Xenopus* brain, and previous work showing a parallel increase in circulating plasma [T_3] and [T_4] with *Dnmt3a* mRNA and protein in mouse brain (4,21-23) (Supplemental Fig. 2.4), I hypothesized that T3 regulation of this gene is conserved in other vertebrate animals and tested this hypothesis using mouse brain and in mouse-derived neuroblastoma Neuro2a[TRβ1] cell line. I found that T_3 injection of PND6 mice rapidly induced *Dnmt3a* mRNA in brain. Treating the Neuro2a[TRβ1] cells with T_3 similarly induced *Dnmt3a* mRNA with rapid kinetics, and this was resistant to protein synthesis inhibition, further supporting that *Dnmt3a* is a direct TR target gene in mouse.

I also investigated TR association with the *Dnmt3a* locus in mouse frontal cortex at PND14 based on previous finding that the peak expression of the *Dnmt3a* gene occurs at this developmental time point (4),. I found that TR associated at genomic regions +30.1 and +49.0 kb from the TSS of the mouse *Dnmt3a* gene; the DR+4 T_3REs found within each locus supported T_3-dependent transactivation. Despite that the *Dnmt3a* gene was similarly regulated in mouse brain and in Neuro2a[TRβ1] cells, I found TR association only at the +30.1 kb region in Neuro2a[TRβ1] cells unlike in PND14 mouse frontal cortex. This may indicate that TR association at the *Dnmt3a* locus is cell type-dependent. However, since the brain tissue is composed of a heterogeneous population of neural cells (i.e. neurons and glia) at distinct stages of differentiation, I cannot distinguish if the TR interacts with both T_3REs in all neural cell types, if TR differentially interacts with one of the two identified T_3REs dependent on neural cell types (and/or at distinct stages of differentiation), or cell line does not recapitulate what may be occurring *in vivo,* and the absence of TR association at the +49.0 kb locus in Neuro2a[TRβ1] cells may be nothing to do with normal physiology.

Sequence conservation of Dnmt3a T_3REs

The frog T_3RE-B and the mouse +30.1 kb T_3RE are found within the intron between coding exons 1 and 2 of the respective *Dnmt3a* genes. This could indicate that the two regulatory elements arose by descent from a common ancestral sequence. However, comparative genomic analysis did not support orthology between these two T_3REs. I also did not find orthology between the frog T_3RE-A and either of the mouse *dnmt3a* T_3REs, or conservation of the two frog *dnmt3a* T_3REs with any other taxa. However, I do not know if T_3 regulation of *Dnmt3a* gene is

conserved in any other mammalian and amphibian species. More work is required to understand the origin(s) of the amphibian and mammalian Dnmt3a T_3REs.

By contrast, I found strong sequence conservation for both of the mouse *Dnmt3a* T_3REs among eutherians. This conservation extended to a metatherian, the wallaby, and to a monotreme, the platypus for the +49.0 kb but not the 30.1 kb T3RE. Interestingly, I found that the +49.0 kb T_3RE is a direct repeat plus four base spacer (DR+4) in the genomes of mouse, rat and Chinese hamster, while it is DR+5 in other species (Supplemental Fig. 8B). I estimate that the transition from DR+5 to DR+4 occurred at least 44 million years ago, since the T_3RE sequence is DR+4 in Chinese hamster, while it is DR+5 in kangaroo rat and naked mole rat (Supplemental Fig. 8). Previous work has shown that DR+5 T_3REs can bind TRβ-RXRα heterodimers *in vitro*, but whether they can support T_3-dependent transactivation may be dependent on the DR+5 sequence context and/or cell types used to test activity, as one study found support for T_3-dependent transactivity while the other did not (25,26). Further investigation is required to determine whether the DR+5 T_3RE at the +49.0 kb region of the mouse *Dnmt3a* locus can support T_3-dependent transactivation.

Although there is strong conservation of the *Dnmt3a* T_3REs among mammals, my analysis did not find similar regulatory elements in birds or reptiles. However, I do not know if this is due to divergent, missing or incomplete sequences of genomic regions that could potentially contain T_3REs in these lineages. I also do not know if the orthologous *Dnmt3a* genes in these two lineages are similarly regulated by TH. Further study is necessary to determine when in the evolution of tetrapods the gene came under TH control, whether this evolved once or multiple times, and whether the regulation has been lost in some lineages.

In conclusion, I show that liganded TR directly activates transcription of *Dnmt3a* genes in the developing brains of frog and mouse. This suggests that in addition to modulating posttranslational modification of histone, TH can influence global patterns of DNA methylation in the developing brain. Therefore, disruption of TH signaling through TH deficiency or exposure to endocrine disrupting chemicals during critical periods of brain development could impact normal neurological development by interfering with proper establishment of DNA methylation by DNMT3a.

Acknowledgements

I thank Dr. Michael Rehli (University Hospital Regensburg, Germany) for kindly providing the pCpGL plasmids, Yun-Bo Shi (National Institute of Child Health and Development, National Institutes of Health, Bethesda, MD) for kindly providing the PB antiserum, pSp64a-TRt and pSp64a-RXRi plasmids, Richard Harland (University of California, Berkley) for generously sharing draft *X. laevis* genome data (Build 5.0) and Pia Bagamasbad for technical assistance.

References

1. Lister R, Pelizzola M, Dowen RH, Hawkins RD, Hon G, Tonti-Filippini J, Nery JR, Lee L, Ye Z, Ngo QM, Edsall L, Antosiewicz-Bourget J, Stewart R, Ruotti V, Millar AH, Thomson JA, Ren B, Ecker JR. Human DNA methylomes at base resolution show widespread epigenomic differences. Nature 2009; 462:315-322

2. MacDonald JL, Roskams AJ. Epigenetic regulation of nervous system development by DNA methylation and histone deacetylation. Progress in neurobiology 2009; 88:170-183

3. Goll MG, Bestor TH. Eukaryotic cytosine methyltransferases. Annual review of biochemistry 2005; 74:481-514

4. Lister R, Mukamel EA, Nery JR, Urich M, Puddifoot CA, Johnson ND, Lucero J, Huang Y, Dwork AJ, Schultz MD, Yu M, Tonti-Filippini J, Heyn H, Hu S, Wu JC, Rao A, Esteller M, He C, Haghighi FG, Sejnowski TJ, Behrens MM, Ecker JR. Global epigenomic reconfiguration during mammalian brain development. Science 2013; 341:1237905

5. Amir RE, Van den Veyver IB, Wan M, Tran CQ, Francke U, Zoghbi HY. Rett syndrome is caused by mutations in X-linked MECP2, encoding methyl-CpG-binding protein 2. Nature genetics 1999; 23:185-188

6. Okano M, Bell DW, Haber DA, Li E. DNA methyltransferases Dnmt3a and Dnmt3b are essential for de novo methylation and mammalian development. Cell 1999; 99:247-257

7. Wu H, Coskun V, Tao J, Xie W, Ge W, Yoshikawa K, Li E, Zhang Y, Sun YE. Dnmt3a-dependent nonpromoter DNA methylation facilitates transcription of neurogenic genes. Science 2010; 329:444-448

8. Anderson GW, Schoonover CM, Jones SA. Control of thyroid hormone action in the developing rat brain. Thyroid : official journal of the American Thyroid Association 2003; 13:1039-1056

9. Cheng SY, Leonard JL, Davis PJ. Molecular aspects of thyroid hormone actions. Endocrine reviews 2010; 31:139-170

10. Crespi EJ, Denver RJ. Leptin (ob gene) of the South African clawed frog Xenopus laevis. Proceedings of the National Academy of Sciences of the United States of America 2006; 103:10092-10097

11. Yao M, Stenzel-Poore M, Denver RJ. Structural and functional conservation of vertebrate corticotropin-releasing factor genes: evidence for a critical role for a conserved cyclic AMP response element. Endocrinology 2007; 148:2518-2531

12. Denver RJ, Hu F, Scanlan TS, Furlow JD. Thyroid hormone receptor subtype specificity for hormone-dependent neurogenesis in Xenopus laevis. Developmental biology 2009; 326:155-168

13. Ramadoss P, Abraham BJ, Tsai L, Zhou Y, Costa-e-Sousa RH, Ye F, Bilban M, Zhao K, Hollenberg AN. Novel mechanism of positive versus negative regulation by thyroid hormone receptor beta1 (TRbeta1) identified by genome-wide profiling of binding sites in mouse liver. The Journal of biological chemistry 2014; 289:1313-1328

14. Chatonnet F, Guyot R, Benoit G, Flamant F. Genome-wide analysis of thyroid hormone receptors shared and specific functions in neural cells. Proceedings of the National Academy of Sciences of the United States of America 2013; 110:E766-775

15. Denver RJ, Williamson KE. Identification of a thyroid hormone response element in the mouse Kruppel-like factor 9 gene to explain its postnatal expression in the brain. Endocrinology 2009; 150:3935-3943
16. Bagamasbad P, Ziera T, Borden SA, Bonett RM, Rozeboom AM, Seasholtz A, Denver RJ. Molecular basis for glucocorticoid induction of the Kruppel-like factor 9 gene in hippocampal neurons. Endocrinology 2012; 153:5334-5345
17. Hoopfer ED, Huang L, Denver RJ. Basic transcription element binding protein is a thyroid hormone-regulated transcription factor expressed during metamorphosis in Xenopus laevis. Development, growth & differentiation 2002; 44:365-381
18. Lebel JM, Dussault JH, Puymirat J. Overexpression of the beta 1 thyroid receptor induces differentiation in neuro-2a cells. Proceedings of the National Academy of Sciences of the United States of America 1994; 91:2644-2648
19. Samuels HH, Stanley F, Casanova J. Depletion of L-3,5,3'-triiodothyronine and L-thyroxine in euthyroid calf serum for use in cell culture studies of the action of thyroid hormone. Endocrinology 1979; 105:80-85
20. Krain LP, Denver RJ. Developmental expression and hormonal regulation of glucocorticoid and thyroid hormone receptors during metamorphosis in Xenopus laevis. The Journal of endocrinology 2004; 181:91-104
21. Chestnut BA, Chang Q, Price A, Lesuisse C, Wong M, Martin LJ. Epigenetic regulation of motor neuron cell death through DNA methylation. The Journal of neuroscience : the official journal of the Society for Neuroscience 2011; 31:16619-16636
22. Feng J, Chang H, Li E, Fan G. Dynamic expression of de novo DNA methyltransferases Dnmt3a and Dnmt3b in the central nervous system. Journal of neuroscience research 2005; 79:734-746
23. Westberry JM, Trout AL, Wilson ME. Epigenetic regulation of estrogen receptor alpha gene expression in the mouse cortex during early postnatal development. Endocrinology 2010; 151:731-740
24. Chatonnet F, Flamant F, Morte B. A temporary compendium of thyroid hormone target genes in brain. Biochimica et biophysica acta 2015; 1849:122-129
25. Emi Y, Ikushiro S, Kato Y. Thyroxine-metabolizing rat uridine diphosphate-glucuronosyltransferase 1A7 is regulated by thyroid hormone receptor. Endocrinology 2007; 148:6124-6133
26. Shulemovich K, Dimaculangan DD, Katz D, Lazar MA. DNA bending by thyroid hormone receptor: influence of half-site spacing and RXR. Nucleic acids research 1995; 23:811-818

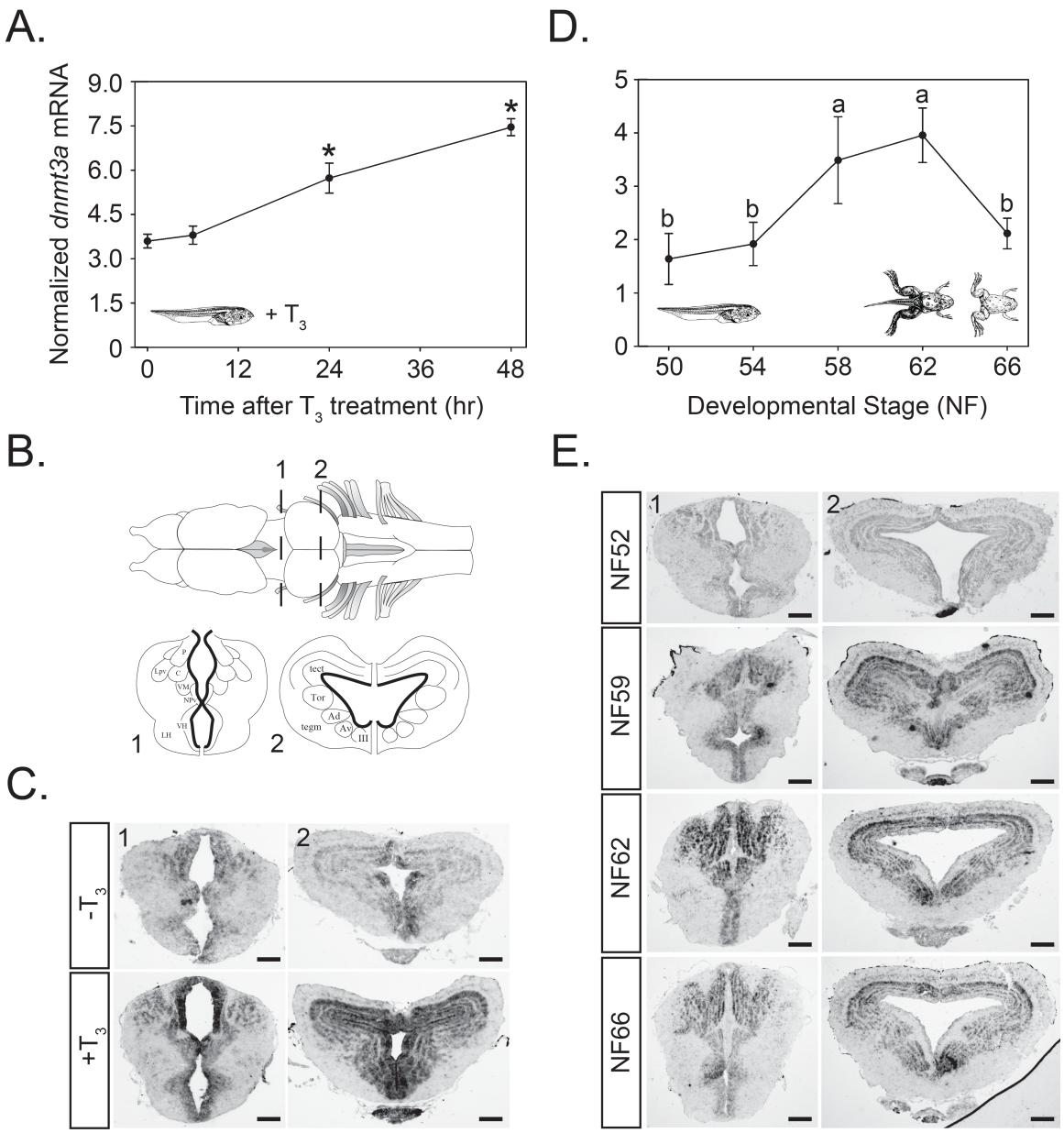
A.
Normalized dnmt3a mRNA
9.0
7.5
6.0
4.5
3.0
1.5
0
0
12
24
36
48
Time after T3 treatment (hr)
+ T3
*
*
D.
5
4
3
2
1
0
50
54
58
62
66
Developmental Stage (NF)
b
b
a
a
b
B.
1
2
C
Lpv
VM
NP
VII
LH
tect
Tor
Ad
Av
tegm
III
C.
-T3
+T3
1
2
E.
NF52
NF59
NF62
NF66
1
2

Fig. 2.1. *Dnmt3a* mRNA exhibits developmental and T_3-dependent increases in *Xenopus* tadpole brain. **(A.)** I treated premetamorphic (NF stage 50) *X. laevis* tadpoles with vehicle (0.0003% DMSO) or T_3 (5 nM) for 6, 24 and 48 hrs and measured *dnmt3a* mRNA in tadpole brain using real-time RT-qPCR. *Dnmt3a* mRNA is normalized to a reference gene *alpha-actinin* mRNA that did not change with T_3 treatment. Points represent the means ± SEM (n=5-6/time point/treatment), and asterisks above the means indicate statistically significant increase in *dnmt3a* mRNA compared to 0h time point (1.6-fold at 24 hr; 2.1-fold at 48 hr; $F_{(6,34)} = 13.420$, $p < 0.001$; ANOVA). Vehicle treatment did not alter the mRNA level at any time point (data not shown). **(B.)** Shown is the dorsal view of *Xenopus* brain (top) and two transverse sections (bottom) at the region of the ventral hypothalamus and thalamic nuclei [1] and the optic tectum and tegmentum [2] (bottom). The bolded lines on the transverse sections highlight the ventricular and subventricular zones. Abbreviations: P, posterior thalamic nucleus; C, central thalamic nucleus; Lpv, lateral thalamic nucleaus, pars posteroventralis; VM, nucleus motorius nervi trigemini; NPv, nucleus of the paraventricular organ; VH, ventral hypothalamic nucleus; LH, Lateral hypothalamus; tect, optic tectum; Tor, torus semicircularis; tegm, mesencephalic tegmentum; Ad, dorsal anterior thalamic nucleus; Av, ventral anterior thalamic nucleus; III, third cranial nerve **(C.) I** treated early prometamorphic (NF stage 54) *X. laevis* tadpole with vehicle or (0.0003% DMSO) or T_3 (5 nM) for 48 hrs and conducted ISHH for *dnmt3a* mRNA (n=3-4/treatment). Shown are representative photomicrographs of two transverse sections. Scale bars = 160 μm. (**D.**) I measured *dnmt3a* mRNA using real-time RT-qPCR at different developmental stages of *X. laevis* metamorphosis in brain regions that contained the hypothalamic area and the pituitary. *Dnmt3a* mRNA is normalized to *alpha-actinin* mRNA that did not change across development. Points represent the means ± SEM (n=5/developmental stage), and the letters above the means indicate statistically significant differences across developmental stages (means with the same letter are not significantly different) ($F_{(4,20)} = 3.963$, $p = 0.017$; ANOVA). **(E.) I** conducted ISHH for *dnmt3a* mRNA on *X. laevis* tadpole brain harvested at different developmental stages of metamorphosis. Shown are representative photomicrographs of two transverse sections. Sense probes did not give signals above background (Supplemental Fig. 1). For region [1] scale bars = 160 μm for NF stages 52 and 59, 200 μm for NF stages 62 and 66; for region [2] scale bars = 160 μm for NF stage 52, 200 μm for NF stages 59, 62 and 66.

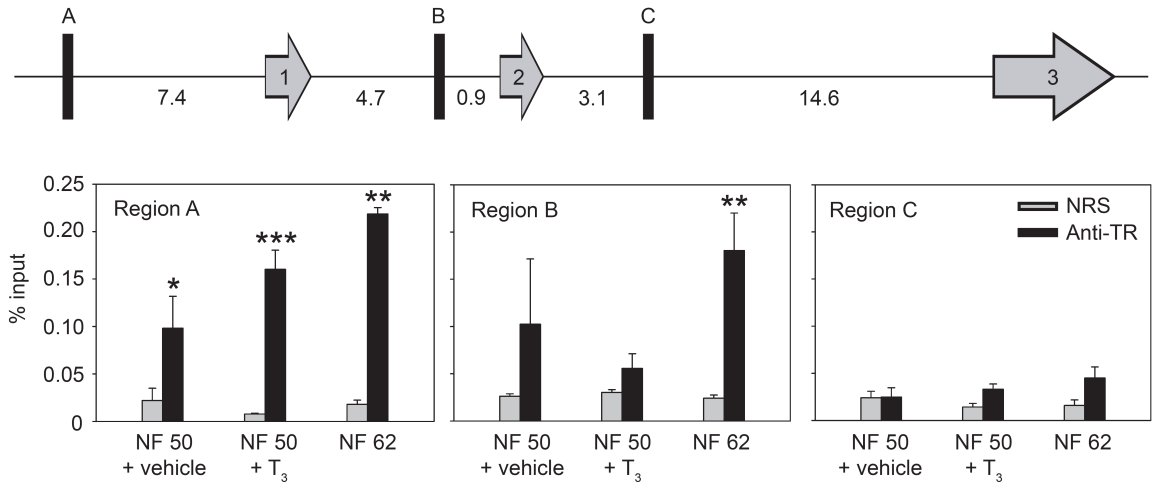

Fig. 2.2. The TRs associate with the *Xenopus dnmt3a* locus in tadpole brain. The schematic diagram (top) shows location of *X. tropicalis dnmt3a* coding exons (arrows; up to third coding exons) and putative TR binding sites identified by a ChIA-PET experiment conducted on *X. tropicalis* tail fin chromatin (L. Sachs and N. Buisine, unpublished data) (black rectangles; regions A, B and C) (distance between features are in kb). **I** conducted targeted ChIP assays for TR at regions A, B and C using brain chromatin isolated from premetamorphic *X. laevis* tadpoles (NF stage 50) treated with vehicle (0.0003% DMSO) or T_3 (5 nM) for 48 hrs, and brain chromatin from tadpoles at metamorphic climax (NF stage 62). Bars represent the mean ± SEM ChIP signal expressed as a percentage of input for TR serum (anti-TR) or normal rabbit serum (NRS; negative control) (n=4/group). Asterisks indicate statistically significant enrichment of TR ChIP signals compared to NRS (* $p < 0.05$, ** $p < 0.01$, *** $p < 0.001$; Student's independent sample *t*-test).

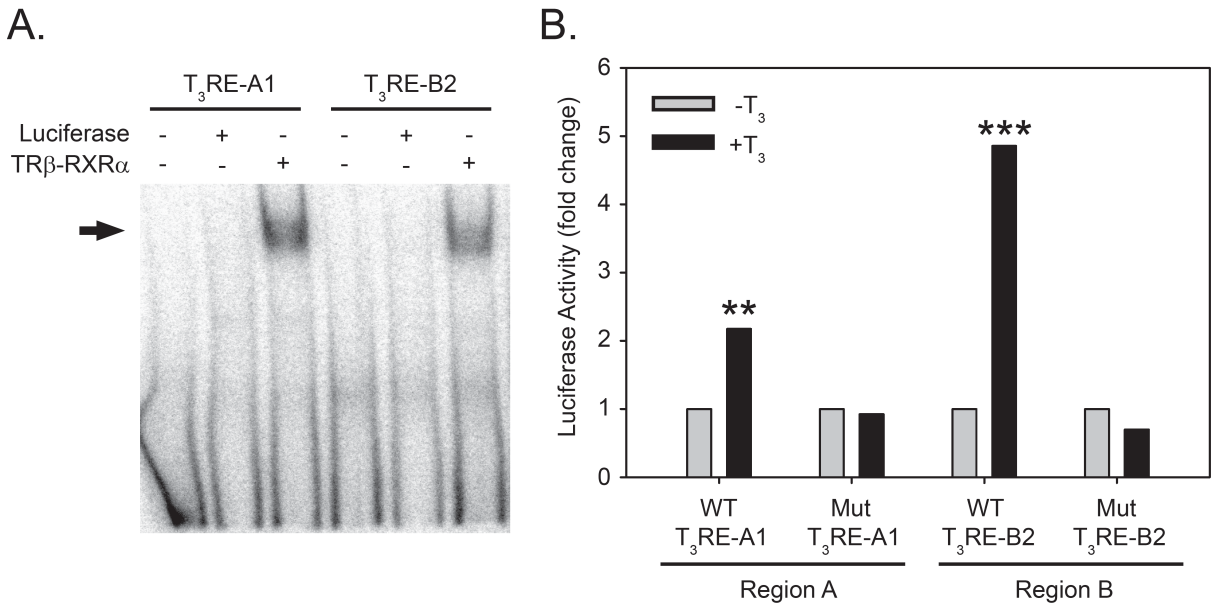

Fig. 2.3. Predicted T_3REs at the *Xenopus dnmt3a* locus bind TR-RXR heterodimers *in vitro* and support T_3-dependent transactivation. **(A.)** I conducted EMSA using [^{32}P]-labeled oligonucleotide probes corresponding to *X. tropicalis dnmt3a* xT_3RE-A1 and xT_3RE-B2 sequences (Supplemental Table 2.2) and *in vitro* synthesized *Xenopus* TRβ plus RXRα. *In vitro* synthesized luciferase was used as a negative control. The arrow indicates the location of supershifted bands due to TRifted binding to the probes. **(B.) I** tested for transactivity of genomic fragments corresponding to *X. tropicalis dnmt3a* regions A (281 bp) and B (322 bp) in transient transfection assays using Neuro2a[TRβ1] cells. After transfection I treated cells with vehicle (0.1% DMSO) or T_3 (30 nM) for 24 hrs before dual luciferase assay. These genomic fragments supported T_3-dependent transactivity, which was abolished by single base mutations introduced into each of the two half sites of xT_3RE-A1 and xT_3RE-B2. Bars represent the mean fold change in corrected luciferase activity (see Materials and Methods) relative to vehicle-treated group (normalized to 1; n=4/treatment). Asterisks indicate statistically significant differences from control ($p < 0.001$; Student's independent sample *t*-test).

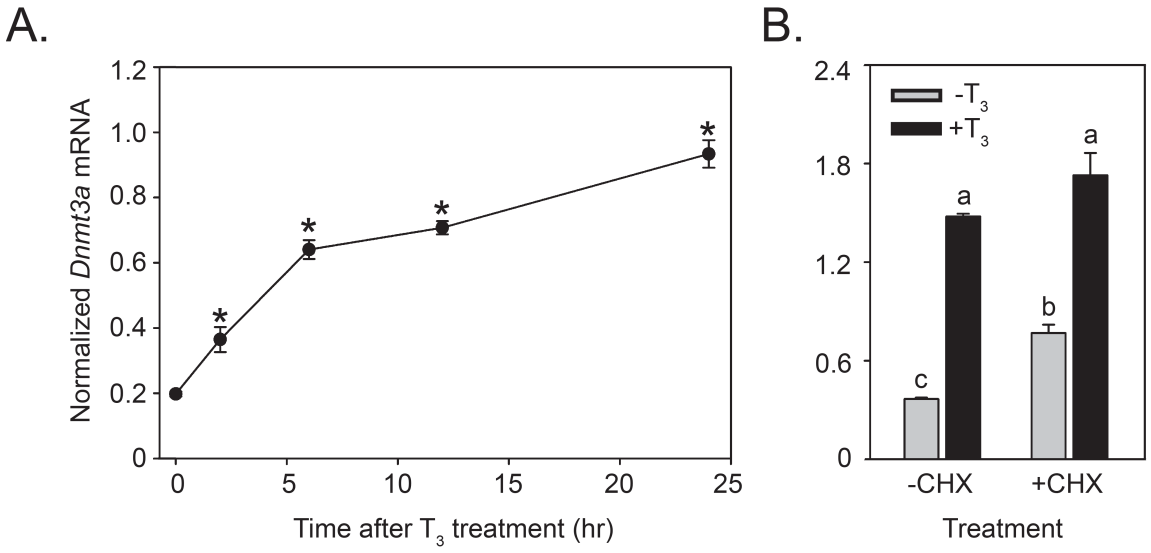

Fig. 2.4. *Dnmt3a* mRNA is induced by T_3 with rapid kinetics in mouse neuroblastoma cells. (**A.**) I treated Neuro2a[TRβ1] cells with vehicle (0.1% DMSO) or T_3 (30 nM) for 2, 6, 12 and 24 hrs and measured *Dnmt3a* mRNA. Points represent means ± SEM, and asterisks above the means indicate statistically significant increase in *Dnmt3a* mRNA compared to 0 hr time point (n=4/treatment/time point) ($F_{(8, 25)} = 103.017$, $p < 0.001$; ANOVA). Vehicle treatment did not alter *Dnmt3a* mRNA level at any time point (data not shown). (**B.**) I pre-treated Neuro2a[TRβ1] cells with the protein synthesis inhibitor cyclohexamide (CHX; 10 μg/ml) for 1 hr and then treated them with vehicle (0.1% DMSO) or T3 (30 nM) for additional 6 hrs in the continuing presence or abosence of CHX. Bars represent means ± SEM, and letters above the means indicate statistically significant differences among treatments (n = 4/treatment) ($F_{(3,12)} = 186.490$, $p < 0.001$; ANOVA). For all experiments, I measured *Dnmt3a* mRNA using real-time RT-qPCR and it was normalized to *GAPDH* mRNA that did not change across development or among treatments (data not shown).

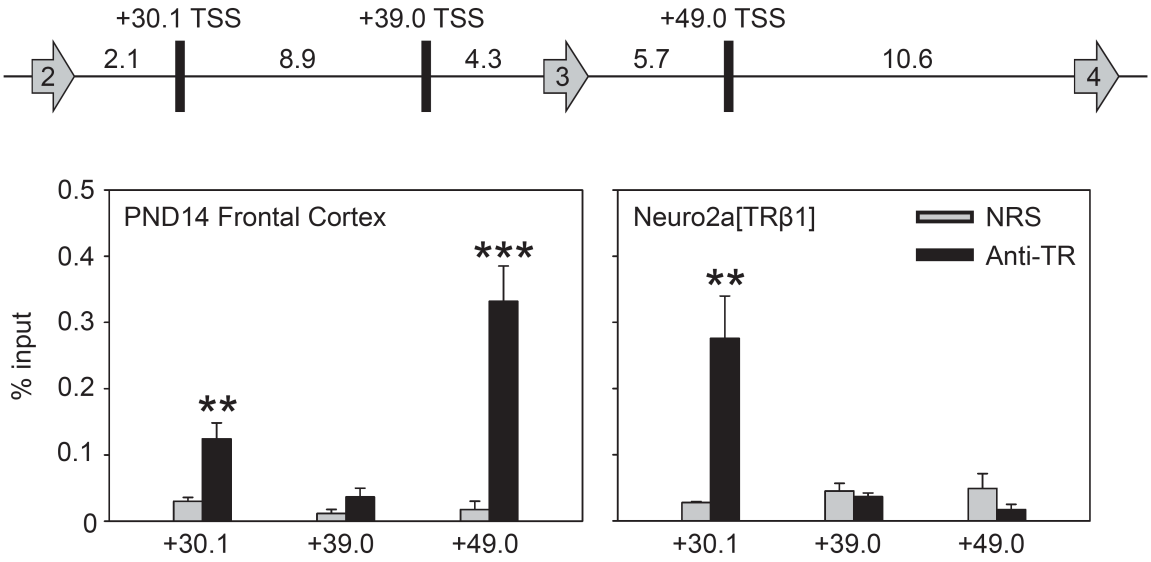

Fig. 2.5. The TRs associate with the mouse *Dnmt3a* locus. The schematic diagram (top) shows putative TR binding sites (rectangles) identified by TR ChIP-seq experiments conducted on mouse liver (REF) and C17.2 mouse cerebellar cell line (REF) that are located between exons 2 and 4 (arrows) of the mouse *Dnmt3a* gene (distance between features are in kb). I conducted targeted ChIP assays for TR at +30.1, +39.0 and +49.0 kb from the TSS of the mouse *Dnmt3a* gene using chromatin isolated from frontal cortex of PND14 mouse that had received intraperatoneal injection of T_3 (25 μg/kg BW) four hrs before sacrifice (n=5/treatment). I also conducted similar ChIP assays for TR using chromatin isolated from Neuro2a[TRβ1] cells treated with T_3 (30 nM) for 24 hrs before harvest (I obtained similar results using chromatin from Neuro2a[TRβ1] cells treated with vehicle (0.1% DMSO); data not shown). Bars represent the mean ± SEM ChIP signal expressed as a percentage of input for TR serum (anti-TR) or normal rabbit serum (NRS; negative control). The asterisks indicate significant enrichment of TR ChIP signals compared to NRS (* $p < 0.01$, ** $p < 0.001$; Student's independent sample *t*-test).

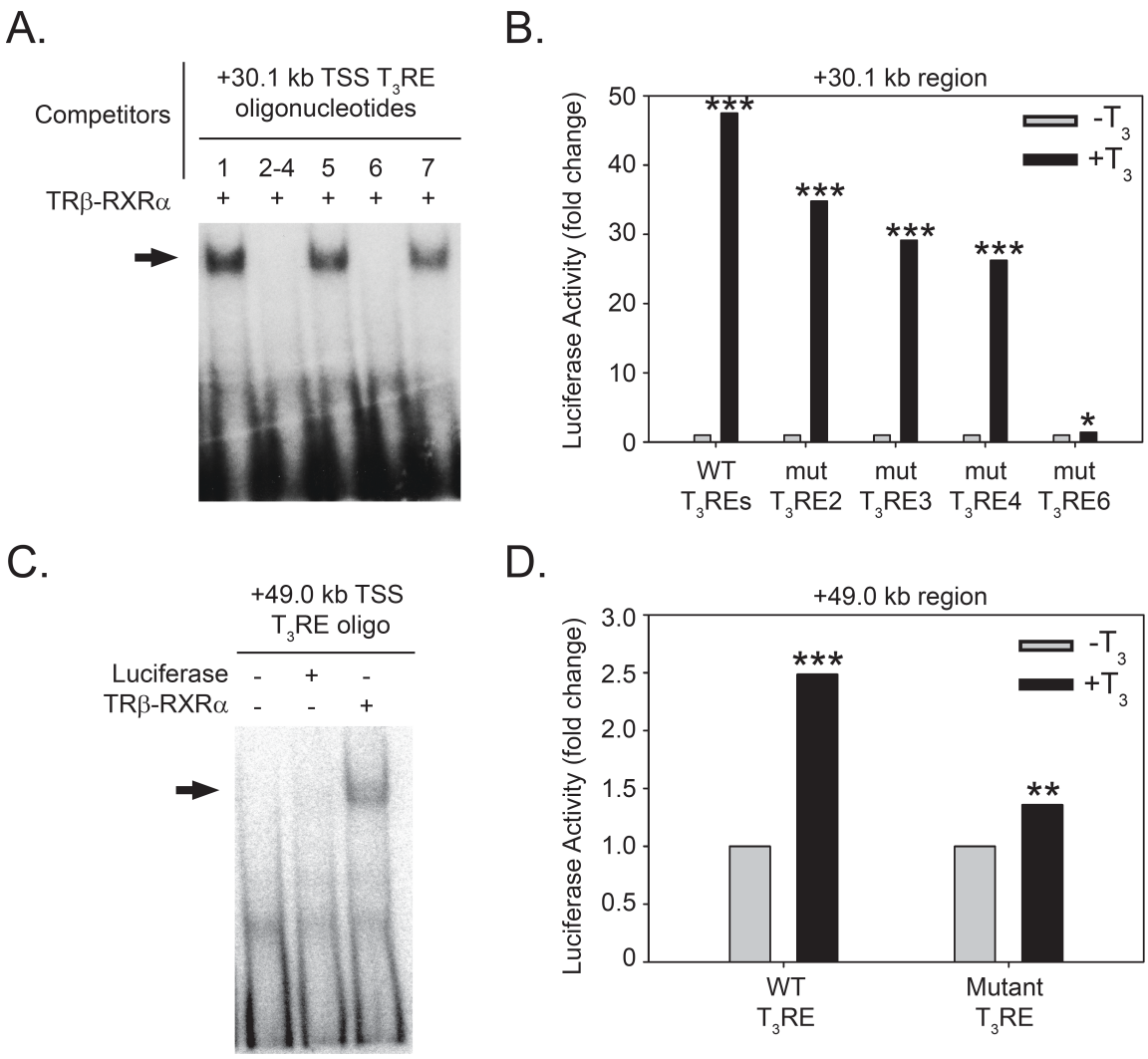
A.
Competitors
+30.1 kb TSS T3RE oligonucleotides
1 2-4 5 6 7
TRβ-RXRα
+ + + + +
B.
+30.1 kb region
Luciferase Activity (fold change)
50
40
30
20
10
0
-T3
+T3
***
***
***
***
*
WT T3REs
mut T3RE2
mut T3RE3
mut T3RE4
mut T3RE6
C.
+49.0 kb TSS T3RE oligo
Luciferase - + -
TRβ-RXRα - - +
D.
+49.0 kb region
Luciferase Activity (fold change)
3.0
2.5
2.0
1.5
1.0
0.5
0
-T3
+T3
***
**
WT T3RE
Mutant T3RE

Fig. 2.6. Predicted T_3REs at the mouse *Dnmt3a* locus bind TR-RXR heterodimers *in vitro* and support T_3-dependent transactivation. (**A.**) I conducted competitive EMSA using a [^{32}P]-labeled oligonucleotide probe corresponding to *X. tropicalis dnmt3a* xT_3RE-B2 and radioinert duplex oligonucleotides with the sequences of seven putative T_3REs found within the region located +30.1 kb from the transcription start site (TSS) of the mouse *Dnmt3a* gene (see Supplemental Fig. 7 for location of the predicted T_3REs; positions #2, 3 and 4 overlap, so I synthesized a single oligonucleotide that encompasses these three predicted T_3REs; oligonucleotide sequences are given in Supplemental Table 2.2). Before gel electrophoresis the probe was incubated with *in vitro* synthesized *Xenopus* TRβ plus RXRα with or without radioinert oligonucleotides (1 mM). The arrow indicates the location of supershifted bands due to TRβ-RXRα binding to the probe. Radioinert oligonucleotides corresponding to T_3REs #2-4 and 6 completely displaced TRβ-RXRα binding to the probe, while those for T_3REs #1, 5 and 7 had no activity. (**B.) I** tested for transactivity of a 500 bp genomic fragment centered at +30.1 kb from the TSS in transient transfection assays using Neuro2a[TRβ1] cells. After transfection I treated cells with vehicle (0.1% DMSO) or T_3 (30 nM) for 5 hr before dual luciferase assay. This fragment supported T_3-dependent transactivity, which was reduced by mutations introduced into T_3REs #2, 3 and 4, and was almost completely abolished by mutation of T_3RE #6 ($p = 0.02$). Bars represent the mean fold change in firefly luciferase activity normalized to *Renilla* luciferase activity relative to vehicle-treated controls (normalized to 1; n=3/treatment) (**C.) I** conducted EMSA using a [^{32}P]-labeled oligonucleotide probe corresponding to the mouse +49.0 kb T_3RE sequence (Supplemental Table 2.2) and *in vitro* synthesized *Xenopus* TRβ plus RXRα. In vitro luciferase protein was used as a negative control. The arrow indicates the location of the supershifted band due to TRβ-RXRα binding to the probe. **(D.) I** tested for transactivity of a 500 bp genomic fragment centered at +49.0 kb from the TSS in transient transfection assays using Neuro2a[TRβ1] cells. After transfection I treated cells with vehicle (0.1% DMSO) or T_3 (30 nM) for 24 hr before dual luciferase assay. This fragment supported T_3-dependent transactivity, which was reduced by mutation of single predicted T_3RE located in this region. Bars represent the mean fold change in corrected firefly luciferase activity normalized to vehicle-treated controls (normalized to 1; n=4/treatment). Asterisks indicate statistically significant differences between treatments ($p < 0.001$; Student's independent sample *t*-test).

Chapter 3

DEVELOPMENTAL AND T_3-DEPENDENT DNA DEMETHYLATION IN *XENOPUS* TADPOLE BRAIN DURING METAMORPHOSIS

Abstract

Methylation of cytosine in DNA (DNA methylation) is an epigenetic modification that plays a critical role during postembryonic neurological development. I used *Xenopus* tadpole metamorphosis, a thyroid hormone (T_3)-dependent postembryonic developmental process, to investigate roles for DNA methylation in gene regulation, and its possible regulation by T_3. Using three independent biochemical assays I saw a progressive decline in whole genome DNA methylation in tadpole brain during metamorphosis, which correlated with increases in mRNAs for genes that code for enzymes that catalyze DNA demethylation (*tet2, tet3, apobec2, gadd45β, gadd45*γ and *tdg*). Treatment of premetamorphic tadpoles with T_3 induced *tet3, gadd45*γ and *tdg* mRNAs in the brain. Using methylation-sensitive restriction digest followed by PCR, I found that genomic regions with T_3 response elements (T_3REs) associated with known T_3-response genes (*klf9* and *dnmt3a*) became demethylated during metamorphosis, which correlated with developmental increases in their mRNAs. Furthermore, T_3 treatment of premetamorphic tadpoles induced DNA demethylation at these loci. *In vitro* methylation of DNA fragments containing the T_3REs subcloned into reporter plasmids abrogated T_3-dependent transactivation. My findings support that T_3 regulates DNA methylation in the tadpole brain during metamorphosis, and that

these changes may be important for the coordination of gene regulation programs that underlie tissue morphogenesis.

Introduction

DNA Methylation at carbon-5 position of cytosine (5-methylcytosines; 5-mC) is a critical epigenetic modification that controls gene expression. In vertebrate genomes 5-mC is predominantly found in the context of cytosine-guanine (CpG) dinucleotides, although recent research has shown that CpH (where H = A, T, and C) methylation is also present in the genome of embryonic stem cells and neural cells (1-4). The dynamics of genome-wide DNA methylation patterns (the methylome) are regulated by DNA methyltransferases (DNMTs: DNMT1, DNMT3a and DNMT3b) that methylate cytosines, and by enzymes that remove 5-mC to demethylate DNA. Active DNA demethylation is initiated by the ten-eleven translocation (TET) enzymes that oxidize 5-mC to 5-hydroxymethylcytosine (5-hmC) (5); the 5-hmC is then removed by two different pathways to complete the process of DNA demethylation. For example, 5-hmC can be de-aminated to unmethylated cytosine by the combined actions of activity-induced cytidine deaminase (AID) and the apolipoprotein B mRNA editing enzyme, catalytic polypeptide (APOBEC) (6). Alternatively, 5-hmC can be further oxidized by TET enzymes to 5-formylcytosine (5-fC), then to 5-carboxylcytosine (5-caC) (7,8) and removed through the base-excision repair pathway catalyzed by thymine DNA glycosylase (TDG), or by nucleotide excision repair pathways catalyzed by growth arrest and DNA damage (GADD45) enzymes (6).

During mammalian embryogenesis global changes in DNA methylation occur in pre-implantation zygotes and in primordial germ cells to establish X-chromosome inactivation, monoallelic expression of imprinted genes and tissue-specific patterns of gene expression (9). Similar global changes in the met(2)hylome have been reported during embryogenesis of other vertebrates such as *Xenopus* (10). Mounting evidence indicates that dynamic changes in the methylome continue beyond embryogenesis, and recent research has highlighted the crucial roles

for modulating DNA methylation in postembryonic maturation of the brain. For example, a recent comprehensive genome-wide analysis of 5-mC in the developing frontal cortex of human and mouse found a dramatic increase in CpA methylation during the early postnatal period that coincided with the period of synaptogenesis and synaptic pruning (2). Other studies also showed that the 5-hmC abundance increased during the same developmental period in the frontal cortex, cerebellum and hippocampus of the mouse brain (2,11,12), indicating that neural cells undergo dynamic rearrangement of their methylomes during early postembryonic brain development.

In all vertebrates studied, postembryonic development is crucially dependent on thyroid hormone (T_3). Thyroid hormone exhibits a dramatic increase during the early postnatal period in mammals and exerts pleiotropic actions on the developing brain (13-15). The molecular actions of T_3 are mediated by T_3 receptors (TRs) that regulate target gene transcription by recruiting histone-modifying enzymes to their binding sites in the genome (T_3 response elements; T_3RE). In addition to this well-known role for posttranslational modification of histones, I recently found that TRs regulate transcription of *Dnmt3a* in the brains of mouse and *Xenopus* during postembryonic development (Chapter 2), suggesting that T_3 may influence key epigenetic changes in the developing brain by modulating a key enzyme that methylates DNA.

In the present study I investigated developmental and T_3-dependent modulation of the methylome of neural cells in the developing brain of *Xenopus* tadpoles during metamorphosis, a T_3-dependent postembryonic process. I found that the neural cell genome in *Xenopus* tadpole brain exhibited a progressive decline in 5-mC during metamorphosis, which correlated with developmental and T_3-dependent increases in mRNAs for genes that encode enzymes that actively remove 5-mC (*tet3, gadd45γ* and *tdg*). I also found that genomic regions that contain T_3RE s for known T_3-response genes (*klf9* and *dnmt3a*) become demethylated in tadpole brain

during metamorphosis and in response to exogenous T_3. Furthermore, *in vitro* methylation of these genomic loci strongly inhibited T_3-dependent transactivity in transient transfection-reporter assays, supporting that developmental DNA demethylation may be important for T_3-dependent transactivation of T_3-response genes in the developing brain. My findings support that T_3 modulates the methylome of neural cells in the developing brain during postembryonic development.

Materials and Methods

Animal care and thyroid hormone (T_3) treatment of *Xenopus* tadpoles

Xenopus laevis and *X. tropicalis* tadpoles were obtained by in-house breeding, reared in dechlorinated tap water (water temperature, 21 – 23 °C for *X. laevis*; 23 – 25 °C for *X. tropicalis*), maintained at 12L:12D photoperiod and fed *ad libitum* with pulverized frog brittle powder (NASCO, Fort Atkinson, WI). The normal table of Nieuwkoop and Faber (NF) (1994) was used to assign developmental stages.

I placed premetamorphic *X. laevis* tadpoles (NF stage 50) in aquaria containing two liters of water 24 hr prior to hormone treatment. Thyroid hormone (3,5,3′-L-triiodothyronine; T_3 sodium salt; Sigma-Aldrich, St. Louis, MO) was first dissolved in dimethylsulfoxide (DMSO) and directly added to the aquarium water. I treated animals with vehicle (0.0003% DMSO) or T_3 (1.5 or 5 nM) for different times before harvest. Twenty-four hours after hormone treatment was initiated, the water was exchanged and T_3 was replenished. Tadpoles were killed by rapid decapitation, whole brains were dissected, and either snap frozen in liquid nitrogen and stored at –80 °C until RNA or genomic DNA extraction.

All procedures involving animals were conducted in accordance with the guidelines of

the University Committee on the Care and Use of Animals of the University of Michigan.

Enzyme-linked immunosorbent assay (ELISA)

I pooled 20 *X. laevis* tadpole brains for NF stage 48 for each biological replicate, 15 for NF 50, 10 for NF 54, 2 for NF stages 58 and 62, and extracted genomic DNA using the DNeasy Blood and Tissue kit (Qiagen, Valencia, CA). I measured the abundance of 5-mC in 150 ng of input genomic DNA using MethylFlash Methylated DNA Quantification Kit (Epigentek, Farmingdale, NY). A relative quantification method was used to compare the abundance of 5-mC across developmental stages by generating a standard curve with known amounts of 5-mC. For each biological sample I averaged the quantity of two technical replicates.

Luminometric Methylation Assay (LUMA)

I conducted LUMA assay as described by Karimi et al. (2006) (16) with modifications. More detail method is described in Head et al. (2014) (17). I extracted genomic DNA using the DNeasy Blood and Tissue kit (Qiagen) from whole brain of premetamorphic (NF stage 50) *X. laevis* tadpole treated with vehicle (0.0003% DMSO) or T_3 (5 nM) for 48 hrs, and from whole brain of untreated *X. laevis* tadpole at metamorphic climax stage (NF stage 62). For each biological replicate I pooled brains from 15 animals for NF stage 50 and 2 animals for NF stage 62. I digested 300 ng of input DNA with either HpaII or MspI (isoschizomers that recognize CCGG; HpaII is sensitve to CpG methylation while MspI is insensitive) for 4 hrs at 37 °C. I quantified the extent of restriction digest using pyrosequencing.

Cytosine Extension Assay

I conducted Cytosine Extension Assay as described by Pogribny et al. (1999) (18) with modifications. I digested 1 μg of genomic DNA with 10 units of either HpaII or MspI isoschizomers (NEB) at 37 °C overnight. I then incubated 200 ng of the digested DNA in 25 μL reaction with [^{32}P]dCTP (10 μCi) and GoTaq DNA polymerase (1U) at 56 °C for 1 hr. I applied 10 μl sample of the reaction to a piece of Whatman DE-81 ion-exchange filter, and then washed it three times with 0.5M sodium phosphate buffer (pH = 7) at room temperature. I air-dried the filter and measured incorporated radioactivity using scintillation counting, which was normalized to the total radioactivity measured from 2.5 μl of the fill-in reaction.

RNA extraction and reverse transcriptase real-time quantitative PCR (RT-qPCR)

I extracted total RNA from whole tadpole brain using TRIZOL reagent (Invitrogen Life Technologies, Carlsbad, CA). Prior to cDNA synthesis, I treated the total RNA with 20 units of deoxyribonuclease I (DNAse I) (Invitrogen) in the presence of RNAse inhibitor (Roche Applied Sicence, Indianapolis, IN). I reverse transcribed cDNA using the High Capacity cDNA Synthesis Kit (Applied Biosystems Inc. (ABI), Foster City, CA). I conducted real-time qPCR using ABsolute Blue qPCR SYBR Low ROX Mix (ABgene Thermo Scientific, Surrey, UK) and Fast 7500 Real-Time PCR System (ABI) or StepOne Real Time PCR Systems (Life Technologies). I designed primers to span exon/exon boundaries for the following *X. laevis* genes: *tet2*, *tet3* (Genbank Accession# HQ220208), *apobec2* (Genbank Accession# NM_001092842.1), *apobec4*, *gadd45α* (Genbank Accession# NM_001086068.1), *gadd45β*, *gadd45γ* (Genbank Accession# NM_001090459.1), *TDG* (Genbank Accession# NM_001090821.1), *AID* (Genbank Accession# NM_001095712.1); and *X. tropicalis klf9* (Genbank Accession# NM_001113674.1) and *dnmt3a* (Genbank Accession# XM_002942354.2) (see Supplemental Table 1 for primer sequences). A

relative quantification method (19,20) was used to compare gene expression levels across developmental stages or among treatments by generating standard curves for each gene with a pool of cDNAs. All mRNAs were normalized to *alpha-actinin* mRNA (NM_001090829.1 for *X. laevis*, NM_001079198.1 for *X. tropicalis*) that did not change across development or with T_3 treatment.

Methylation-sensitive restriction digest followed by qPCR (chop-qPCR)

I extracted genomic DNA from tadpole brain using DNeasy Blood and Tissue Kit (Qiagen). For *X. laevis* tadpoles I extracted genomic DNA from whole brain; for *X. tropicalis I* extracted DNA from the microdissected region of the diencephalon that contained the hypothalamus and the pituitary. I incubated 1 μg of genomic DNA in a 50 μl reaction with 10 units of Hinp1I (NEB) at 37 °C overnight, purified DNA using phenol/chloroform/isoamyl alcohol (Invitrogen, Life Technologies, Carlsbad, CA) and resuspended in 40 μl of buffer AE (Qiagen, 10mM Tris, 0.5mM EDTA, pH 9.0). To measure the extent of restriction digest, I conducted genomic DNA qPCR using primers that flank the restriction sites (see Supplemental Table 1 for primer sequences) and normalized the quantity of amplification to genomic regions that did not contain the restriction sites.

Intracerebroventricular (i.c.v.) injection of 5-aza-2'-deoxycytidine into *Xenopus* tadpole brain

The DNMT inhibitor 5-aza-2'-deoxycytidine (5-aza-2'-dC; Sigma-Aldrich) was first dissolved in 0.6% saline to a final concentration of 10 mM. I first anesthetized premetamorphic (NF stage 50) *X. laevis* tadpoles by immersing them in 0.002% benzocaine and then administered

i.c.v. microinjection of vehicle (0.6% saline) or 5-aza-2'-dC into the third ventricle of tadpole brain (110 nl). Both solutions contained 0.02% Fast Green dye as a tracing marker.

Plasmid constructs

I subcloned DNA fragments corresponding to the sequences of genomic regions that encompassed *X. tropicalis klf9* (179 bp) and *dnmt3a* (322 bp) T_3REs into the CpG-less luciferase reporter vector (pCpGL; gift of Michael Rheli) at the BglII and HindIII sites. I *in vitro* methylated or mock-treated these plasmids in a 100 µl reaction by incubating them with 10 units of M.SssI CpG methyltransferase (NEB) and SAM substrate (640 uM) for eight hrs; I replenished SAM four hrs into reaction. I purified the plasmids using phenol/chloroform/isoamyl alcohol precipitation (Invitrogen) and resuspended them in 25 µl of buffer EB (Qiagen; 10 mM Tris, pH = 8.5). I verified that *in vitro* methylation prevented Hinp1I restriction digest (NEB; 10 units per reaction) (data not shown).

Cell culture and transient transfection assays

I cultured Neuro2a[TRβ1] cells (21) as previously described (22) in DMEM/F12 containing 10% fetal bovine serum that had been stripped of thyroid hormone (23) and was supplemented with hygromycin B (500 µg/ml). I plated cells at a density of 0.15 X 10^6 per well in 24-well plates. When cells had reached 60-70% confluency, I transfected cells with luciferase reporter constructs (described above; 200 ng per well plus 10 ng pRenilla-tk) using FuGene 6 transfection reagent (Promega, Madison, WI). Twenty-four hr after transfection I treated cells with vehicle (0.1% DMSO) or T_3 (30 nM) for 24 additional hrs before harvest for analysis by dual luciferase assay (Promega).

Electrophoretic mobility shift assays (EMSA)

I conducted EMSA as previously described by (24). *Xenopus* TRβ and retinoid X receptor alpha (RXRα) proteins were *in vitro* synthesized using pSp64a-TRβ and pSp64a-RXRα plasmids (gift of Yun-Bo Shi) and the TnT SP6 Quick-Coupled Translation System (Promega).

I conducted competitive EMSA using radioinert double-stranded DNA fragments encompassing the T_3RE regions for *X. tropicalis klf9* (~180 bp) or *dnmt3a* (~320 bp) genes. To synthesize methylated competitors, I first *in vitro* methylated the pCpGL constructs containing these genomic fragments (see above) by incubating them with M.SssI CpG methyltransferases as described above. I then released the inserts with restriction digest (BamHI and HindIII) and gel purified the fragments. I verified successful *in vitro* methylation of these genomic fragments based on resistance to Hinp1I restriction digest, which is sensitive to CpG methylation (Supplemental Fig. 3.1).

Data analysis and statistics

I analyzed data using SPSS statistical software (version 19; SPSS Inc., Chicago, IL). I conducted one-way ANOVA followed by Fisher's least significant difference (Fisher's LSD) *post hoc* test and Student's independent sample *t*-test (α=0.05). Data were Log10-transformed before statistical analysis for the derived values or when the variances were found to be heterogeneous.

Results

The neural cell genome in *Xenopus* tadpole brain becomes demethylated during metamorphosis, which correlated with developmental and T_3-dependent increases in expression of genes involved with DNA demethylation

Using enzyme-linked immunosorbent assay (ELISA) I found that the amount of 5-methylcytosine (5-mC) in the neural cell genome of *X. laevis* tadpole brain remained unchanged from premetamorphosis to early prometamorphosis (NF stages 48 to 54), declined during late prometamorphosis (NF stage 58) and reached its lowest level at metamorphic climax (NF stage 62) (Fig. 3.1A). I confirmed this reduction in whole genome DNA methylation using two other independent assays, cytosine extension assay (18) and luminometric methylation assay (LUMA; (16)). These two assays showed that the neural cell genome in *X. laevis* tadpole brain was less methylated at metamorphic climax (NF stage 62) than during premetamorphosis (NF stage 50) (Table 1).

Given the large decrease in 5-mC occurring in tadpole brain during metamorphosis, I hypothesized that genes that encode enzymes that catalyze DNA demethylation would show correlated changes in expression during metamorphosis. Using real-time RT-qPCR I found that *tet2* and *tet3* mRNAs increased in *X. laevis* tadpole brain between premetamorphosis and early prometamorphosis (NF stage 50 to 54), remained elevated until metamorphic climax (NF stage 62) and then declined to basal level at the end of metamorphosis (NF stage 66) (Fig 1B). The *tdg* and *apobec2* mRNAs showed similar developmental profiles as *tet2* and *tet3* mRNAs (Fig. 3.1B). The *gadd45β* mRNA exhibited basal expression between premetamorphosis and metamorphic climax, and increased at the end of metamorphosis. By contrast, the *gadd45γ* gene exhibited elevated expression during earlier stages of metamorphosis between premetamorphosis and late prometamorphosis and declined towards the end of metamorphosis (Fig. 3.1B). The *gadd45α*

mRNA did not show changes during metamorphosis, and *AID* mRNA was undetectable throughout metamorphosis (data not shown). I also found that treating premetamorphic (NF stage 50) *X. laevis* tadpoles with exogenous T_3 added to the aquarium water (5 nM) caused time-dependent increases in *tet3, gadd45γ* and *tdg* mRNAs in tadpole brain as analyzed by real-time RT-qPCR (Fig. 3.1C); the same treatment did not change *tet2, apobec2* and *gadd45β* mRNA levels (data not shown).

Thyroid hormone response elements (T_3REs) for known T_3-regulated genes become demethylated in tadpole brain during metamorphosis, which correlated with increases in the mRNA levels of the regulated genes

A recent study analyzed genome-wide changes in DNA methylation during *X. tropicalis* gastrulation using methylated DNA capture (MethylCap) followed by high-throughput sequencing (MethylCap-seq) (25). By analyzing their dataset I found that genomic regions that contain T_3REs for the Krüppel-like factor 9 (*klf9*) and *dnmt3a* genes overlapped with regions that are enriched for DNA methylation (Supplemental Fig. 3.2). Because these T_3REs are important for T_3-dependent transactivation of *klf9* and *dnmt3a* genes ((22); Chapter 2), I investigated whether these loci might exhibit changes in DNA methylation in tadpole brain during metamorphosis.

I conducted chop-qPCR analysis targeting *klf9* and *dnmt3a* T_3RE regions in *X. tropicalis* tadpole brain and found that both regions became demethylated during metamorphosis (Fig. 3.2A). Both loci became demethylated between early and mid-prometamorphosis (NF stages 54 and 56) and stayed demethylated throughout the rest of metamorphosis until its completion; the *dnmt3a* T_3RE region reached its lowest methylation level at the end of metamorphosis (NF stage

66) (Fig. 3.2A). Homologous loci in the *X. laevis* genome were also less methylated at metamorphic climax (NF stage 62) than during premetamorphosis (NF stages 52) as analyzed by chop-qPCR (Supplemental Fig. 3.3). Demethylation of the T_3RE regions correlated with increases in *klf9* and *dnmt3a* mRNAs as analyzed by RT-qPCR (Fig. 3.2B). I also conducted MethylCap assay targeting these two genomic loci and confirmed DNA demethylation at the *dnmt3a* T_3RE region; however, this assay did not detect methylation changes around the *klf9* T_3RE region likely due to differences in sensitivity of the two assays (Fig. 3.2C). Chop-qPCR assay analyzes the methylation state of a single CpG site (high resolution), while the MethylCap assay surveys the methylation state of multiple CpG dinucleotides around the target region, the resolution of which is determined by the fragment size of sonicated DNA (low resolution). Also, since I conducted qPCR assay on high-salt fraction of MethylCap assay eluate, this may indicate that the *klf9* T_3RE region is barely methylated (based on the scale of % recovery relative to input samples).

In a first attempt to investigate whether T_3 can induce changes in DNA methylation in tadpole brain, I treated premetamorphic (NF stage 50) *X. laevis* tadpoles with exogenous T_3 (5 nM) for 48 hrs. However, this treatment regimen did not cause DNA demethylation in the whole genome as analyzed by 5-mC ELISA and LUMA (Table 1), or at the *klf9* and *dnmt3a* T_3RE regions using chop-PCR assay (Supplemental Fig. 3.4). However, 48 hr T_3 treatment increased *tet3, gadd45g* and *tdg* mRNAs in tadpole brain (Fig. 3.1C). Therefore, I hypothesized that there may be a temporal delay in DNA demethylation in the genome after mRNAs for DNA demethylase enzymes increased, and so I conducted another experiment by treating tadpoles for a longer period of time (96 hrs) with a lower dose of T_3 (1.5 nM) (I used a lower dose of T_3 because tadpoles do not survive beyond three days with the higher dose – 5 nM). I found that

treating *X. laevis* premetamorphic tadpoles with T_3 for 96 hr caused DNA demethylation of *klf9* and *dnmt3a* T_3RE regions (Fig. 3.3); I did not investigate whether this treatment caused DNA demethylation in the whole genome.

I also investigated whether the DNMT inhibitor 5-aza-2'-deoxycitidine (10 mM) would induce changes in DNA methylation at *klf9* and *dnmt3a* T_3RE regions. Four days of daily intracerebroventricular injection of 5-aza-2'-deoxycitidine caused demethylation of the *dnmt3a* T_3RE region, which was enhanced when combined with T_3 (1.5 nM over 4 days; Fig. 3.3). The 5-aza-2'dC injection alone did not alter DNA methylation at the *klf9* T_3RE region, and the combined treatment did not enhance T_3-induced demethylation at this locus (Fig. 3.3).

CpG Methylation impairs T_3-dependent transactivation

I sublconed DNA fragments corresponding to the *klf9* and *dnmt3a* T_3RE regions into the CpG-less luciferase reporter plasmid (pCpGL; gift of Michael Rheli), *in vitro* methylated (or mock-treated) them with M.SssI CpG methyltransferase and conducted transient transfection-reporter assays using Neuro2a[TRβ1] cells. Both DNA fragments supported robust T_3-dependent transactivity; however, methylating CpG sites within these genomic regions caused a strong reduction in transactivity (Fig. 3.4). I hypothesized that this reduction in T_3-dependent transactivity was due to reduced TR-RXR binding to the *klf9* and *dnmt3a* T_3RE regions. Competitive EMSA showed that radioinert genomic fragments corresponding to the *klf9* and *dnmt3a* T_3RE regions displaced TRβ-RXRα from the radiolabeled oligonucleotide probe in a concentration-dependent manner (Fig. 3.5). It also showed that the radioinert competitor oligonucleotides that had been *in vitro* methylated at CpG sites displaced TRβ-RXRα in a similar manner to oligonucleotides that had not been methyalted (Fig. 3.5)

Discussion

Postembryonic brain development is critically dependent on thyroid hormone. Recent work by Lister and colleagues (2) showed dynamic changes in the neural cell methylome during the early postnatal period in mouse and human. Here, I found that the neural cell genome of *Xenopus* tadpoles became globally and progressively demethylated during metamorphosis, and this correlated with developmental, T_3-dependent upregulation of genes involved with active DNA demethylation (*tet3, gadd45γ* and *tdg*). I also found examples of local DNA demethylation at T_3RE regions associated with known T_3-response genes (*klf9* and *dnmt3a*) during metamorphosis and in response to exogenous T_3. Furthermore, *in vitro* methylation of these DNA sequences strongly inhibited T_3-dependent transactivity. To my knowledge, this is the first report showing that T_3 modulates the neural cell methylome. My findings support that T_3 modulates DNA methylation to regulate developmental gene expression programs.

Developmental DNA demethylation and regulation of genes that catalyze active DNA demethylation in Xenopus tadpole brain during metamorphosis

I found that the tadpole neural cells became demethylated during metamorphosis. The abundance of 5-mC declined by almost 50% between the onset of metamorphosis and metamorphic climax, which is a striking reduction given the size of the *X. laevis* genome to be around 3.1 billion base pairs (26). Three independent assays (ELISA, LUMA and cytosine extension assay) confirmed DNA demethylation in tadpole brain. The percentage change was smaller with LUMA and cytosine extension assays compared with ELISA (Table 1). This is likely due to differences in what these three assays measure. While ELISA measures the

abundance of 5-mC regardless of the context within which it is found, LUMA and cytosine extension assays survey a subpopulation of all 5-mC recognized by MspI/HpaII isoschizomers used in these assays. Therefore, the percentage change detected by LUMA and cytosine extension assay is likely an underestimate, as methylated cytosines are also present in sequence contexts that are not recognized by these restriction enzymes. Furthermore, a recent genome-wide study of 5-mC in the developing mammalian brains showed CpH methylation exhibited more dynamic changes than CpG methylation (2). Future studies should investigate whether CpH methylation is also present in the *Xenopus* genome and whether it exhibits dynamic changes in tadpole brain during metamorphosis.

Because I investigated DNA methylation changes in mixed population of cells in tadpole brain, I do not know whether global DNA demethylation occurred uniformly among all types of neural cells or within a subpopulation. A previous study showed that the intragenic region (gene body) of cell type-specific genes became differentially methylated depending on neural cell type (2); therefore, it is likely that subtypes of neural cells in tadpole brain undergo differential changes in DNA methylation during metamorphosis.

Correlated with global DNA demethylation, I also found that mRNAs for genes that are involved with active DNA demethylation (*tet2*, *tet3*, *apobec2*, *gadd45β*, *gadd45γ* and *tdg*) increased in *X. laevis* tadpole brain during metamorphosis. Of these six genes, *tet3*, *gadd45γ* and *tdg* mRNAs also increased in premetamorphic tadpole brain in response to exogenous T_3. Developmental and T_3-dependent regulation of *tet3, gadd45γ* and *tdg* genes in tadpole brain suggest roles of these enzymes in postembryonic neurological maturation of the brain. Previous study has shown that *Xenopus* TET3 plays a role in neural cell development during embryogenesis through regulation of genes that are involved in neurogenesis (27). Future studies

should further investigate whether activity of DNA demethylases increases in tadpole brain to catalyze global decrease in 5-mC during metamorphosis.

Developmental and T_3-dependent local DNA demethylation at T_3RE associated with known T_3-response genes

The *klf9* and *dnmt3a* T_3REs are important for T_3-dependent transactivation of the associated genes ((22); Chapter 2). I found that these T_3RE regions became demethylated in tadpole brain during metamorphosis, which correlated with developmental increases in *klf9* and *dnmt3a* mRNAs. I also found that T_3 treatment of premetamorphic tadpoles precociously induced DNA demethylation at these T_3REs in tadpole brain. Furthermore, *in vitro* methylation of CpG nucleotides of T_3RE regions strongly reduced T_3-dependent transactivity, although the sequences of *klf9* and *dnmt3a* T_3REs themselves do not contain CpG dinucleotides. These findings together suggest that developmental DNA demethylation of T_3RE regions may be important for regulation of their T_3-dependent transactivity and thus regulation of T_3-response genes in tadpole brain during metamorphosis.

Recent studies have shown that methylated cytosines are also abundantly present in the context of CpA dinucleotides in the neural cell genome (2-4), which could be bound by methyl-CpG binding protein at an equal affinity (MeCP2) (29). Although the sequences of *klf9* and *dnmt3a* T_3REs do not contain CpG dinucleotides, which may explain why CpG methylation of DNA fragments did not alter TRβ-RXRα binding to these sequences (Fig. 3.5), both T_3REs sequences contain CpA dinucleotides at their respective half-sites. As a preliminary experiment to investigate whether CpA methylation inhibits TRβ-RXRα binding, I synthesized DNA fragments encompassing the *klf9* and *dnmt3a* T_3REs in PCR reactions in which all cytosines

became methylated, and then conducted a competitive EMSA using these fragments as radioinert competitors to compete for TRβ-RXRα binding with the radiolabeled probe. I found that methylated DNA fragments competed less efficiently for TRβ-RXRα heterodimers than fragments that were not methylated (Supplemental Fig. 3.5). This result suggests that CpA methylation within T_3REs could be inhibitory to TR-RXR binding, but this needs further investigation whether specifically methylating CpA dinucleotides within the *klf9* and *dnmt3a* T_3REs alter TR-RXR binding.

In conclusion, I showed that *Xenopus* tadpole brain became demethylated during metamorphosis and in response to T_3, which may be catalyzed by T_3 activation of genes that are involved with active DNA demethylation. I previously found that T_3 also activates the *dnmt3a* gene that codes for enzymes that catalyze DNA methylation (Chapter 2). Findings in the current study extended a role for T_3 in modulating the neural cell methylome to regulate gene regulation programs during postembryonic neurological development.

Acknowledgements

I thank Michael Rheli (University Hospital Regensburg, Germany) for kindly providing the pCpGL plasmids, Richard Harland (University of California, Berkley) for generously sharing draft *X. laevis* genome data (Build 5.0) and Ling Huang for conducting bioinformatics analysis to identify some of homologous *X. laevis* genes and for conducting gene expression analyses for *X. laevis* reference genes.

References

1. Lister R, Pelizzola M, Dowen RH, Hawkins RD, Hon G, Tonti-Filippini J, Nery JR, Lee L, Ye Z, Ngo QM, Edsall L, Antosiewicz-Bourget J, Stewart R, Ruotti V, Millar AH, Thomson JA, Ren B, Ecker JR. Human DNA methylomes at base resolution show widespread epigenomic differences. Nature 2009; 462:315-322

2. Lister R, Mukamel EA, Nery JR, Urich M, Puddifoot CA, Johnson ND, Lucero J, Huang Y, Dwork AJ, Schultz MD, Yu M, Tonti-Filippini J, Heyn H, Hu S, Wu JC, Rao A, Esteller M, He C, Haghighi FG, Sejnowski TJ, Behrens MM, Ecker JR. Global epigenomic reconfiguration during mammalian brain development. Science 2013; 341:1237905

3. Varley KE, Gertz J, Bowling KM, Parker SL, Reddy TE, Pauli-Behn F, Cross MK, Williams BA, Stamatoyannopoulos JA, Crawford GE, Absher DM, Wold BJ, Myers RM. Dynamic DNA methylation across diverse human cell lines and tissues. Genome research 2013; 23:555-567

4. Xie W, Barr CL, Kim A, Yue F, Lee AY, Eubanks J, Dempster EL, Ren B. Base-resolution analyses of sequence and parent-of-origin dependent DNA methylation in the mouse genome. Cell 2012; 148:816-831

5. Tahiliani M, Koh KP, Shen Y, Pastor WA, Bandukwala H, Brudno Y, Agarwal S, Iyer LM, Liu DR, Aravind L, Rao A. Conversion of 5-methylcytosine to 5-hydroxymethylcytosine in mammalian DNA by MLL partner TET1. Science 2009; 324:930-935

6. Wu H, Zhang Y. Reversing DNA methylation: mechanisms, genomics, and biological functions. Cell 2014; 156:45-68

7. He YF, Li BZ, Li Z, Liu P, Wang Y, Tang Q, Ding J, Jia Y, Chen Z, Li L, Sun Y, Li X, Dai Q, Song CX, Zhang K, He C, Xu GL. Tet-mediated formation of 5-carboxylcytosine and its excision by TDG in mammalian DNA. Science 2011; 333:1303-1307

8. Ito S, Shen L, Dai Q, Wu SC, Collins LB, Swenberg JA, He C, Zhang Y. Tet proteins can convert 5-methylcytosine to 5-formylcytosine and 5-carboxylcytosine. Science 2011; 333:1300-1303

9. Goll MG, Bestor TH. Eukaryotic cytosine methyltransferases. Annual review of biochemistry 2005; 74:481-514

10. Stancheva I, Meehan RR. Transient depletion of xDnmt1 leads to premature gene activation in Xenopus embryos. Genes & development 2000; 14:313-327

11. Song CX, Szulwach KE, Fu Y, Dai Q, Yi C, Li X, Li Y, Chen CH, Zhang W, Jian X, Wang J, Zhang L, Looney TJ, Zhang B, Godley LA, Hicks LM, Lahn BT, Jin P, He C. Selective chemical labeling reveals the genome-wide distribution of 5-hydroxymethylcytosine. Nature biotechnology 2011; 29:68-72

12. Szulwach KE, Li X, Li Y, Song CX, Wu H, Dai Q, Irier H, Upadhyay AK, Gearing M, Levey AI, Vasanthakumar A, Godley LA, Chang Q, Cheng X, He C, Jin P. 5-hmC-mediated epigenetic dynamics during postnatal neurodevelopment and aging. Nature neuroscience 2011; 14:1607-1616

13. Anderson GW, Schoonover CM, Jones SA. Control of thyroid hormone action in the developing rat brain. Thyroid : official journal of the American Thyroid Association 2003; 13:1039-1056

14. Bernal J. Thyroid hormone receptors in brain development and function. Nature clinical practice Endocrinology & metabolism 2007; 3:249-259
15. Hadj-Sahraoui N, Seugnet I, Ghorbel MT, Demeneix B. Hypothyroidism prolongs mitotic activity in the post-natal mouse brain. Neuroscience letters 2000; 280:79-82
16. Karimi M, Johansson S, Stach D, Corcoran M, Grander D, Schalling M, Bakalkin G, Lyko F, Larsson C, Ekstrom TJ. LUMA (LUminometric Methylation Assay)--a high throughput method to the analysis of genomic DNA methylation. Experimental cell research 2006; 312:1989-1995
17. Head JA, Mittal K, Basu N. Application of the LUminometric Methylation Assay to ecological species: tissue quality requirements and a survey of DNA methylation levels in animals. Molecular ecology resources 2014; 14:943-952
18. Pogribny I, Yi P, James SJ. A sensitive new method for rapid detection of abnormal methylation patterns in global DNA and within CpG islands. Biochemical and biophysical research communications 1999; 262:624-628
19. Crespi EJ, Denver RJ. Leptin (ob gene) of the South African clawed frog Xenopus laevis. Proceedings of the National Academy of Sciences of the United States of America 2006; 103:10092-10097
20. Yao M, Stenzel-Poore M, Denver RJ. Structural and functional conservation of vertebrate corticotropin-releasing factor genes: evidence for a critical role for a conserved cyclic AMP response element. Endocrinology 2007; 148:2518-2531
21. Lebel JM, Dussault JH, Puymirat J. Overexpression of the beta 1 thyroid receptor induces differentiation in neuro-2a cells. Proceedings of the National Academy of Sciences of the United States of America 1994; 91:2644-2648
22. Denver RJ, Williamson KE. Identification of a thyroid hormone response element in the mouse Kruppel-like factor 9 gene to explain its postnatal expression in the brain. Endocrinology 2009; 150:3935-3943
23. Samuels HH, Stanley F, Casanova J. Depletion of L-3,5,3'-triiodothyronine and L-thyroxine in euthyroid calf serum for use in cell culture studies of the action of thyroid hormone. Endocrinology 1979; 105:80-85
24. Hoopfer ED, Huang L, Denver RJ. Basic transcription element binding protein is a thyroid hormone-regulated transcription factor expressed during metamorphosis in Xenopus laevis. Development, growth & differentiation 2002; 44:365-381
25. Bogdanovic O, Long SW, van Heeringen SJ, Brinkman AB, Gomez-Skarmeta JL, Stunnenberg HG, Jones PL, Veenstra GJ. Temporal uncoupling of the DNA methylome and transcriptional repression during embryogenesis. Genome research 2011; 21:1313-1327
26. Hellsten U, Harland RM, Gilchrist MJ, Hendrix D, Jurka J, Kapitonov V, Ovcharenko I, Putnam NH, Shu S, Taher L, Blitz IL, Blumberg B, Dichmann DS, Dubchak I, Amaya E, Detter JC, Fletcher R, Gerhard DS, Goodstein D, Graves T, Grigoriev IV, Grimwood J, Kawashima T, Lindquist E, Lucas SM, Mead PE, Mitros T, Ogino H, Ohta Y, Poliakov AV, Pollet N, Robert J, Salamov A, Sater AK, Schmutz J, Terry A, Vize PD, Warren WC, Wells D, Wills A, Wilson RK, Zimmerman LB, Zorn AM, Grainger R, Grammer T, Khokha MK, Richardson PM, Rokhsar DS. The genome of the Western clawed frog Xenopus tropicalis. Science 2010; 328:633-636
27. Xu Y, Xu C, Kato A, Tempel W, Abreu JG, Bian C, Hu Y, Hu D, Zhao B, Cerovina T, Diao J, Wu F, He HH, Cui Q, Clark E, Ma C, Barbara A, Veenstra GJ, Xu G, Kaiser UB,

Liu XS, Sugrue SP, He X, Min J, Kato Y, Shi YG. Tet3 CXXC domain and dioxygenase activity cooperatively regulate key genes for Xenopus eye and neural development. Cell 2012; 151:1200-1213

28. Hahn MA, Qiu R, Wu X, Li AX, Zhang H, Wang J, Jui J, Jin SG, Jiang Y, Pfeifer GP, Lu Q. Dynamics of 5-hydroxymethylcytosine and chromatin marks in Mammalian neurogenesis. Cell reports 2013; 3:291-300

29. Gabel HW, Kinde B, Stroud H, Gilbert CS, Harmin DA, Kastan NR, Hemberg M, Ebert DH, Greenberg ME. Disruption of DNA-methylation-dependent long gene repression in Rett syndrome. Nature 2015;

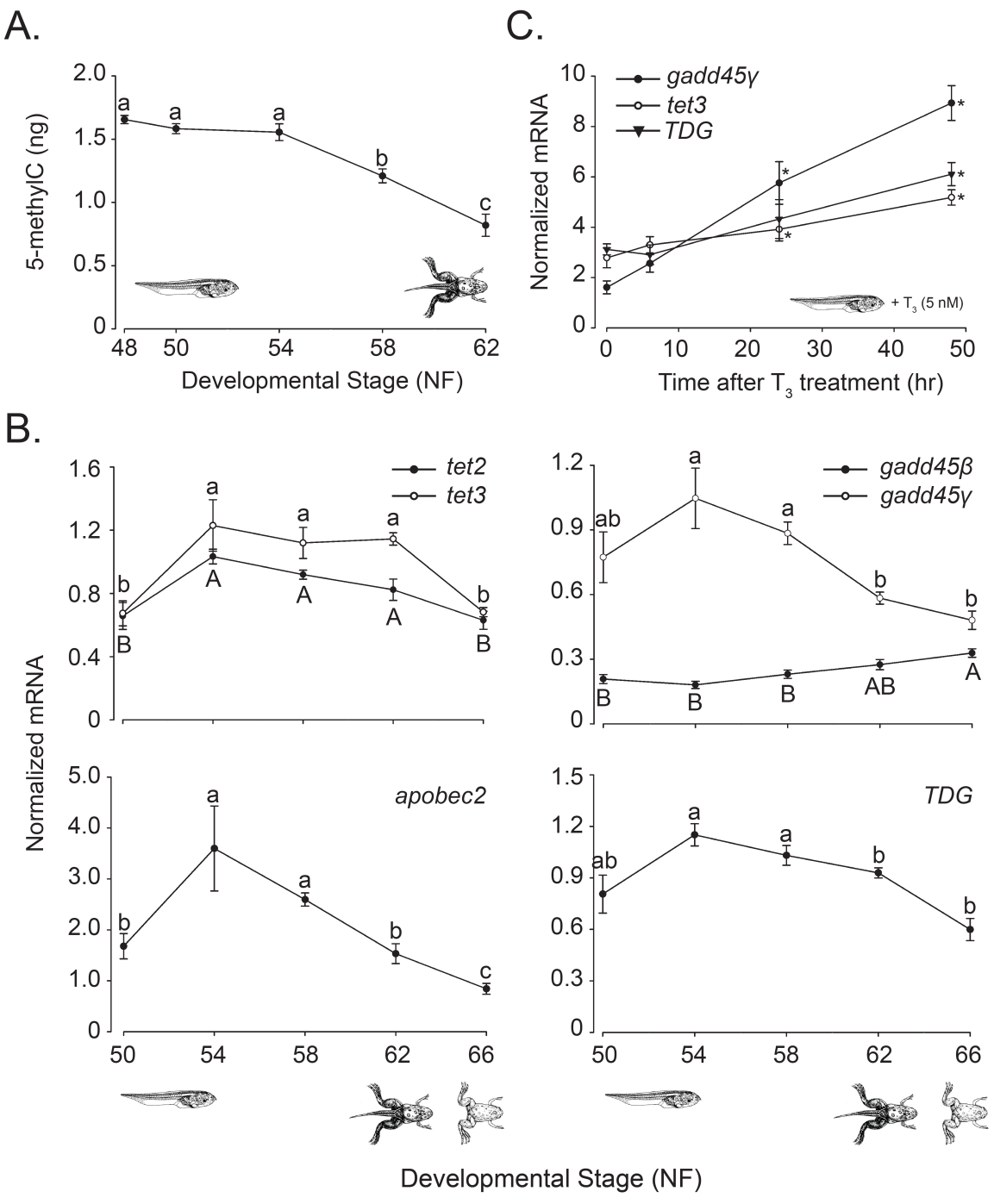
A.
5-methylC (ng)
Developmental Stage (NF)
C.
Normalized mRNA
gadd45γ
tet3
TDG
+ T3 (5 nM)
Time after T3 treatment (hr)
B.
Normalized mRNA
tet2
tet3
gadd45β
gadd45γ
apobec2
TDG
Developmental Stage (NF)

Fig. 3.1. The abundance of 5-methylcytosine in the neural cell genome of *Xenopus* tadpole brain declines during metamorphosis, which correlates with developmental and T_3-dependent increases in expression of genes that are involved in active DNA demethylation. **(A.) I** measured abundance of 5-methylcytosine (5-mC) in the neural cell genome of *X. laevis* tadpole brain at different developmental stages of metamorphosis using enzyme-linked immunosorbent assay (ELISA). Points represent the means ± SEM (n=5/developmental stage), and letters above the means indicate statistically significant differences across development (means with the same letter are not significantly different) ($F_{(4,20)} = 36.096$, $p < 0.001$; ANOVA). **(B.) I** measured *tet2, tet3, gadd45α*, *gadd45β*, *gadd45γ*, *apobec2*, *apobec4, AID* and *TDG* mRNAs in the region of *X. laevis* tadpole brain that contained the hypothalamic area and the pituitary at different developmental stages of metamorphosis using real-time RT-qPCR. All mRNAs were normalized to mRNA for a reference gene (*alpha-actinin*) that did not change across development (Supplemental Fig. 3.1). Points represent the means ± SEM (n=5/developmental stage), and the letters above the means indicate statistically significant differences across development (means with the same letter are not significantly different) (*tet2:* $F_{(4,20)} = 6.742$, $p = 0.001$; *tet3*: $F_{(4,20)} = 10.717$, $p = 0.001$; *gadd45β*: $F_{(4,19)} = 7.867$, $p = 0.001$; *gadd45γ*: $F_{(4,19)} = 6.531$, $p = 0.002$; *apobec2*: $F_{(4,20)} = 11.604$, $p < 0.001$; *TDG*: $F_{(4,19)} = 8.928$, $p < 0.001$; ANOVA). *Gadd45α* and *apobec4* mRNAs did not change during metamorphosis; *AID* mRNA was undetectable in tadpole brain (data not shown). **(C.) I** treated premetamorphic (NF stage 50) *X. laevis* tadpoles with vehicle (0.0003% DMSO) or T_3 (5 nM) for 6, 24 and 48 hrs and measured *tet2, tet3, gadd45β*, *gadd45γ*, *apobec2* and *TDG* mRNAs in tadpole brain using real-time RT-qPCR. All mRNAs were normalized to *alpha-actinin* mRNA that did not change with T_3 treatment. Points represent the means ± SEM (n=5-6/time point/treatment), and asterisks above the means indicate statistically significant increases relative to mRNA levels at 0 hr time point (*tet3*: 1.4-fold at 24 hr; 1.9-fold at 48 hr; $F_{(6,34)} = 3.888$, $p < 0.001$; *gadd45γ*: 1.6-fold at 6 hr, 3.6-fold at 24 hr; 5.5-fold at 48 hr; $F_{(6,34)} = 19.430$, $p < 0.001$; *TDG*: 2.0-fold at 48 hr; $F_{(6,34)} = 3.816$, $p < 0.001$; ANOVA). *Tet2, gadd45β*, *apobec2* and *apobec4* mRNAs did not change with T_3 treatment; vehicle treatment did not change mRNA levels at any time point (data not shown).

A. Luminometric Methylation Assay (LUMA)

Stage + treatment	% Methylation
NF stage 52 + vehicle	91.8 ± 0.2
NF stage 52 + T_3 (5 nM, 48 hrs)	91.9 ± 0.1
NF stage 62 (untreated)	90.2 ± 0.2*

B. Cytosine Extension Assay

	% Methylation
NF stage 50	90.7 ± 0.2
NF stage 62	87.1 ± 0.2*

Table 3.1. The genome of cells in *Xenopus* tadpole brain becomes globally demethylated during metamorphosis. I extracted genomic DNA from whole brain of premetamorphic (NF stage 50-52) *X. laevis* tadpole treated with vehicle (0.0003% DMSO) or T_3 (5 nM) for 48 hr, and untreated tadpole at metamorphic climax stage (NF stage 62). I digested DNA with a pair of HpaII/MspI isoschizomers that recognize 5' – CCGG- 3' then conducted either LUMA (A) or Cytosine extension assay (B) to measure the extent of restriction digest. I did not have T_3-treated brain sample for analysis. The number represents the mean percentage ± SEM of methylated CpG dinucleotides within the HpaII/MspI restriction sites. The asterisk represents statistically significant differences in % methylation (LUMA: $F_{(2,12)} = 13.733$, $p < 0.001$ ANOVA; Cytosine extension assay: $p = 0.032$, Student's independent sample *t*-test)

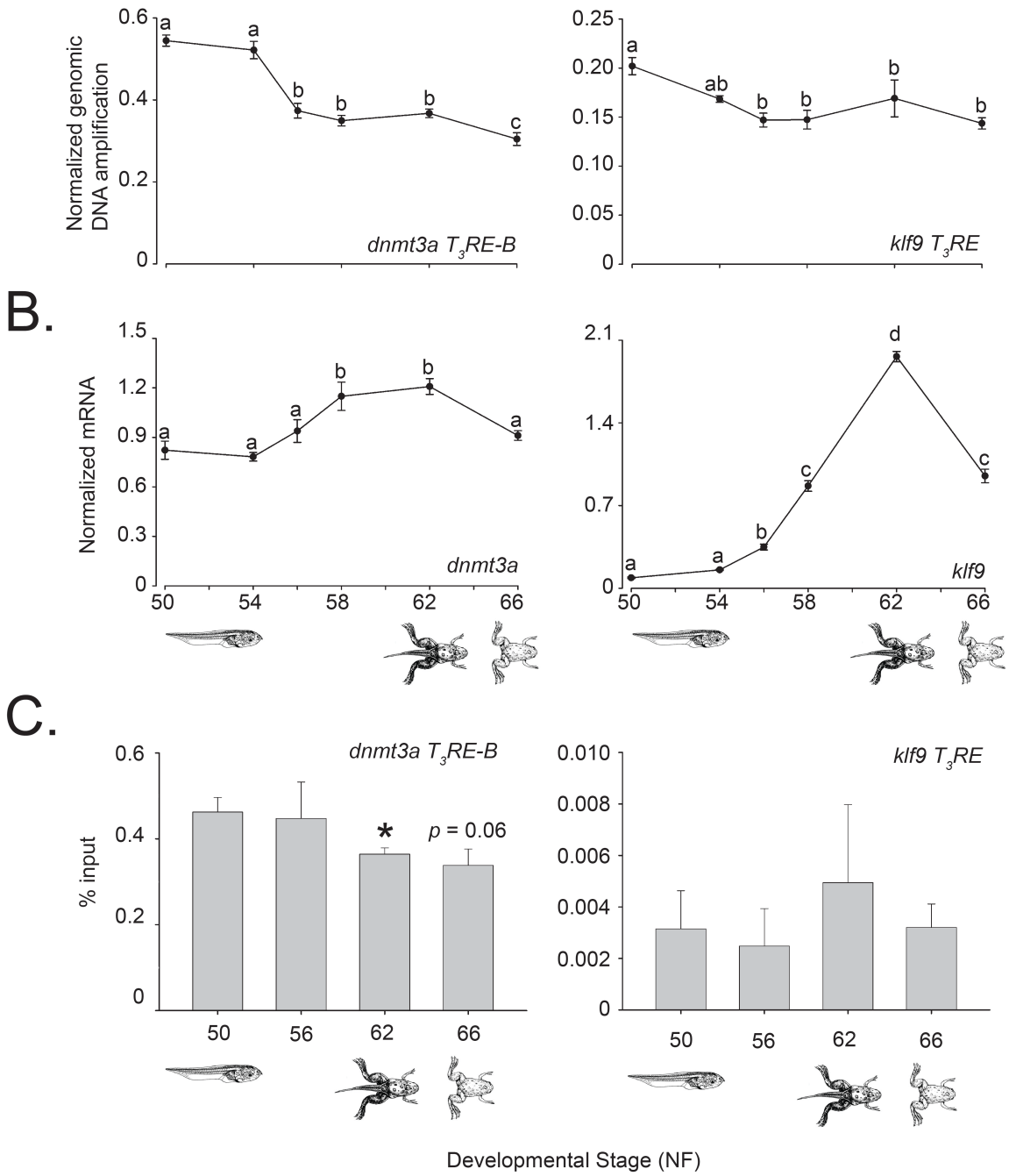
A.
Normalized genomic DNA amplification
dnmt3a T3RE-B
klf9 T3RE
B.
Normalized mRNA
dnmt3a
klf9
C.
% input
dnmt3a T3RE-B
p = 0.06
klf9 T3RE
Developmental Stage (NF)

Fig. 3.2. The *klf9* and *dnmt3a* T_3REs regions become demethylated in *Xenopus* tadpole brain during metamorphosis, which correlated with developmental increases in their mRNAs. (**A.**) I isolated genomic DNA from the region of *X. tropicalis* tadpole brain that contained the hypothalamic area and the pituitary at different developmental stages of metamorphosis, and conducted methylation-sensitive restriction digest/qPCR (chop-qPCR) assays targeting genomic regions that contain T_3REs for the *klf9* and *dnmt3a* loci (primer sequences are given in Supplemental Table 3.1). Amplification of target genomic regions was normalized to that of genomic region that did not contain restriction sites. Points represent the means ± SEM (n=5/developmental stage), and letters above the means indicate statistically significant differences across development (means with the same letter are not significantly different) (*dnmt3a* T_3RE: $F_{(5,18)} = 35.093, p < 0.001$; *klf9* T_3RE : $F_{(5,18)} = 9.847, p < 0.001$; ANOVA) (n=4/developmental stage). (**B.**) I also conducted the MethylCap assay on the same *X. tropicalis* genomic DNA samples as described in Fig. 3.2A targeting the *klf9* and *dnmt3a* T_3REs regions. Bars represent the mean ± SEM signal expressed as a percentage of input. The asterisk above the mean indicates statistically significant differences compared to NF stage 50 ($p = 0.029$, Student's independent sample *t*-test) (n=4/developmental stage) (**C.**) I measured *klf9* and *dnmt3a* mRNAs in the same brain region of *X. tropicalis* tadpole brain as in Fig. 3.2A at different stages of metamorphosis using real-time RT-qPCR. Both mRNAs were normalized to *alpha-actinin* mRNA that did not change across development. Points represent the means ± SEM (n=5/developmental stage), and the letters above the means indicate statistically significant differences across development (means with the same letter are not significantly different) (*klf9:* $F_{(5,23)} = 419.359, p < 0.001$; *dnmt3a*: $F_{(5,23)} = 8.950, p < 0.001$; ANOVA).

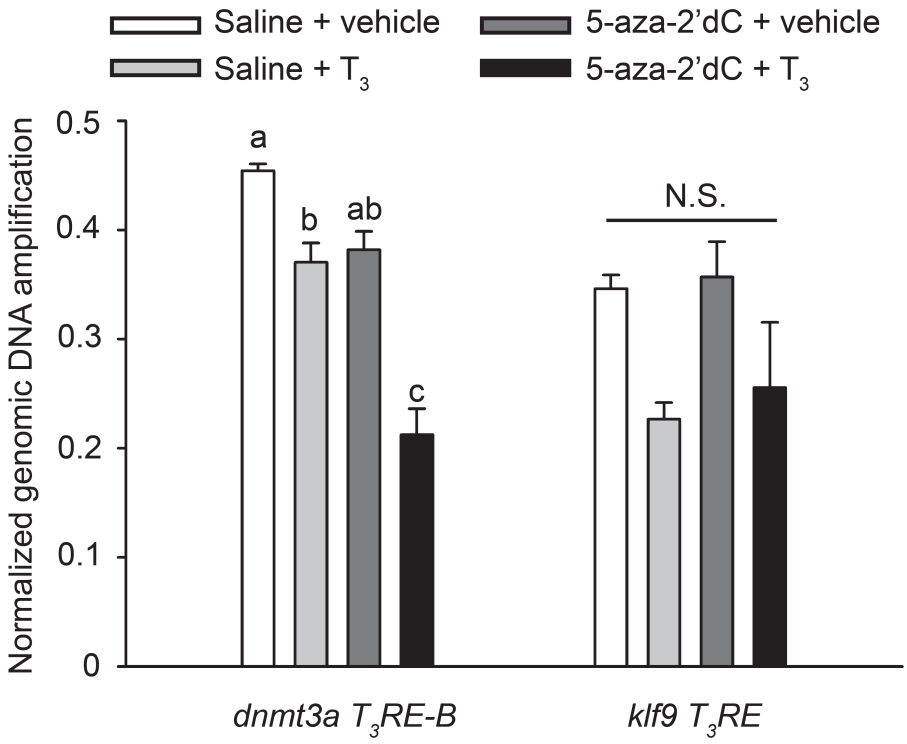

Fig. 3.3. Treating premetamorphic *Xenopus* tadpoles with exogenous T_3 (and/or 5-aza-2'-deoxycytidine) induces DNA demethylation at *klf9* and *dnmt3a* T_3RE regions. I administered daily intracerebroventricular (i.c.v.) injection of vehicle (0.6% saline) or 5-aza-2'deoxycytidine (10 mM) to premetamorphic (NF stage 50) *X. laevis* tadpoles for 4 days. I also treated these tadpoles with vehicle (0.0003% DMSO) or T_3 (1.5 nM) by directly adding them to the aquarium water. I harvested tadpole brain four days after I had initiated T_3 treatment. I isolated genomic DNA from the whole brain and conducted chop-qPCR assays targeting the *klf9* and *dnmt3a* T_3RE regions. Amplification of target genomic regions was normalized to that of genomic region that did not contain restriction sites. Bars represent the means ± SEM (n=4/treatment group), and letters above the means indicate statistically significant differences among treatments (means with the same letter are not significantly different) (*dnmt3a* T_3RE : $F_{(3,12)} = 29.652$, $p < 0.001$; *klf9* T_3RE : N.S.; ANOVA).

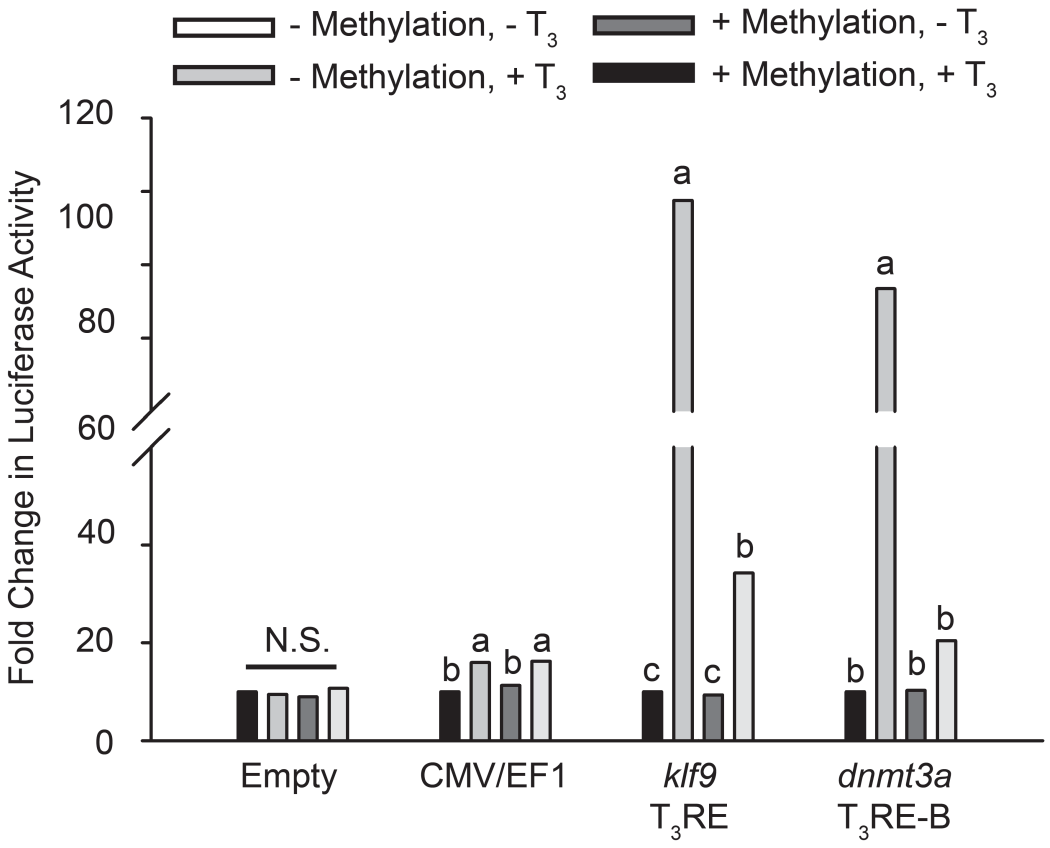

Fig. 3.4. Methylation of CpG sites within *Xenopus klf9* and *dnmt3a* T_3RE regions reduces T_3-dependent transactivity. I *in vitro* methylated or mock-treated CpG-less luciferase reporter plasmids (pCpGL; gift of Michael Rheli) into which I had subcloned genomic fragments that encompass the *X. tropicalis klf9* and *dnmt3a* T_3RE regions, and tested for transactivity in transient transfection assays using Neuro2a[TRβ1] cells. After transfection I treated cells with vehicle (0.1% DMSO) or T_3 (30 nM) for 24 hrs before dual luciferase assay. Both genomic fragments supported T_3-dependent transactivity, which was strongly reduced or abolished by CpG methylation. The genomic fragment of CpG-less CMV/EF1 promoter also supported T_3-dependent transactivity but CpG methylation of this fragment did not affect its transactivity. Bars represent the mean fold changes in firefly luciferase activity normalized to those of respective non-methylated plasmids in cells treated with vehicle (normalized to 1; n=3/treatment). Letters above the means indicate statistically significant differences among treatments (means with the same letter are not significantly different) (*klf9* T_3RE : $F_{(3,8)} = 281.749, p < 0.001$; *dnmt3a* T_3RE : $F_{(3,8)} = 21.630, p < 0.001$; CMV/EF1: $F_{(3,8)} = 57.085, p < 0.001$; ANOVA). I analyzed transfection efficiency by measuring abundance of plasmids in cell lysate using qPCR, which did not differ among treatments (data not shown). Similar results were obtained in two separate experiments.

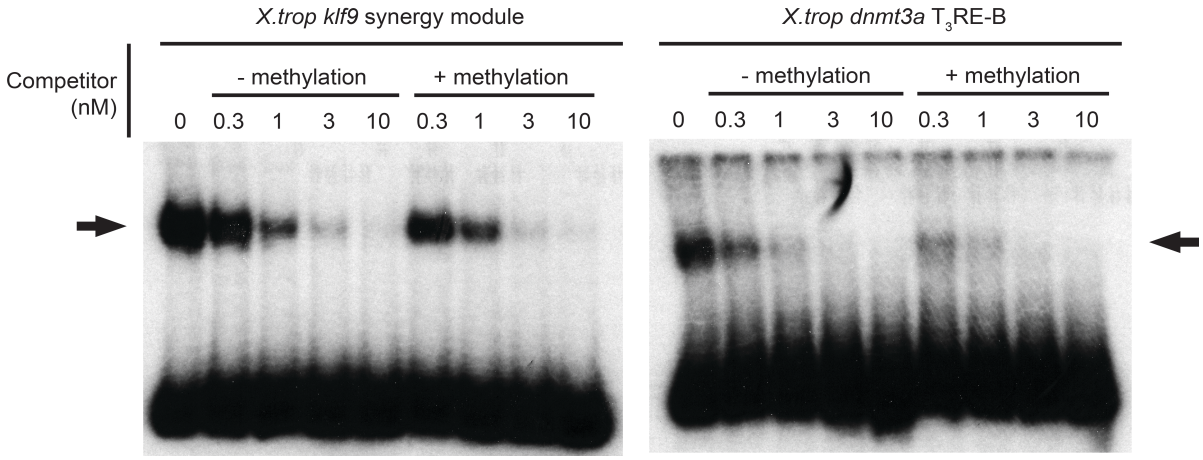

Fig. 3.5. Methylation of CpG sites within the *klf9* and *dnmt3a* T_3RE regions does not affect TRβ-RXRα binding. I conducted a competitive EMSA using [^{32}P]-labeled genomic fragments that encompass *X. tropicalis klf9* (~180 bp) or *dnmt3a* T_3REs (~320 bp) as probes, and corresponding radioinert genomic fragments that had been *in vitro* methylated with or without M.Sssi CpG methyltransferase. Before gel electrophoresis I incubated the probes with *in vitro* synthesized *Xenopus* TRβ plus RXRα, with or without the indicated radioinert genomic fragments (1-10 nM). The arrow indicates the location of supershifted bands due to TRβ-RXRα binding to the probe. Both genomic fragments displaced TRβ-RXRα binding to the probe in a concentration-dependent manner; CpG methylation of both genomic fragments did not change its ability to compete for the probe.

Chapter 4

GENOME-WIDE ANALYSIS OF CHANGES IN DNA METHYLATION AND GENE TRANSCRIPTION IN *XENOPUS* TADPOLE BRAIN DURING METAMORPHOSIS

Abstract

Methylation of cytosines in DNA (DNA methylation) is a key epigenetic modification that influences gene transcription. Recent studies in mammals and my thesis work in *Xenopus* showed a dramatic reorganization of DNA methylation in the developing brain. To investigate a role for DNA methylation in regulation of developmental gene expression programs, I conducted methylated DNA capture sequencing (MethylCap-seq) and RNA-sequencing (RNA-seq) in *X. tropicalis* tadpole brain at four stages of metamorphosis (NF stages 50, 56, 62 and 66). The MethylCap-seq analysis identified 141,700 loci in the neural cell genome that are enriched for methylated cytosines (methylation peaks), among which 855 peaks showed changes during metamorphosis. Consistent with my findings in Chapter 3 that the tadpole brain genome became demethylated during metamorphosis, differentially methylated regions (DMRs) identified between NF stage 66 (end of metamorphosis) and three earlier stages predominantly showed decrease in DNA methylation. Differentially methylated regions between mid-prometamorphosis and metamorphic climax (NF stages 56 and 62) predominantly showed increase in DNA methylation, coincident with upregulation of the *de novo* DNA methyltransferase 3a (*dnmt3a*) gene in tadpole brain. The RNA-seq analysis identified 5,280 unique genes that became

differentially expressed during metamorphosis in tadpole brain. Using clustering and gene ontology analyses, I identified thirteen patterns of gene expression dynamics and found that the cell cycle was the major pathway downregulated during metamorphosis. By combining the MethylCap-seq and RNA-seq data, I investigated the potential correlation between changes in DNA methylation and expression of genes that are found in 50 kb vicinity of DMRs. While the majority of genes did not show correlated changes in expression, my preliminary analysis found a weak, but significant inverse correlation between changes in DNA methylation and changes in gene expression. My findings suggest a role for DNA methylation in regulation of gene transcription in the developing brain.

Introduction

Methylation at carbon-5 position of cytosine in DNA (5-methylcytosine; 5-mC) is a critical epigenetic modification that controls gene transcription. In vertebrate genomes DNA methylation occurs in the context of cytosine-guanine (CpG) dinucleotides in most cells, although recent research has shown that the neural cell genome is enriched for methylated cytosines also in the cytosine-adenine (CpA) context (1-3). Changes in DNA methylation during embryogenesis play an important role in imprinting, X-chromosome inactivation and establishing tissue-specific gene expression programs {Hackett, 2013 #107}.

Recent research has shown that global changes in DNA methylation also occur during postembryonic development. A recent genome-wide analysis of 5-mC conducted in mouse and human cerebral cortex showed a dramatic increase in CpA methylation during early postnatal period (2). In Chapter 3, I also found that the genome of *Xenopus* tadpole brain undergoes global changes in DNA methylation during metamorphosis. The abundance of 5-hydroxymethylcytosine (5-hmC), which is an intermediate substrate of the active DNA demethylation pathway (4), similarly increases in postnatal mouse brain (2,5). Developmental changes in DNA methylation may play a crucial role in neural cell maturation and function. Lister and colleagues (2) found that increase in CpA methylation coincides with a period of synaptogenesis. They also found that decrease in the gene body methylation correlated with downregulation of neuron-specific genes in glial cells, suggesting a specific role for DNA methylation in cell differentiation and establishing neural cell type-specific transcriptome.

To better understand DNA methylation changes in neural cell genome during postembryonic development, I conducted a high-throughput methylated DNA capture sequencing (MethylCap-seq; (6)) analysis on *X. tropicalis* preoptic area/hypothalamus (including

the pituitary) at four stages of metamorphosis: premetamorphosis (NF stage 50), mid-prometamorphosis when cell proliferation peaks in tadpole brain (NF stage 56; (7)), metamorphic climax (NF stage 62) when plasma [T_3] and [T_4] reach their highest titers in tadpole brain (NF stage 62; (8)) and at the completion of metamorphosis (NF stage 66). To correlate changes in DNA methylation with changes in gene transcription, I also conducted RNA-sequencing (RNA-seq) analysis on the same brain regions at the same four stages of metamorphosis.

Materials and Methods

Animal care and thyroid hormone (T_3) treatment of *Xenopus* tadpoles

X. tropicalis tadpoles were obtained by in-house breeding, reared in dechlorinated tap water (23 – 25 °C), maintained at 12L:12D photoperiod and fed *ad libitum* with pulverized frog brittle powder (NASCO, Fort Atkinson, WI). The normal table of Nieuwkoop and Faber (NF) (1994) was used to assign developmental stages. Tadpoles were killed by rapid decapitation, brain tissues were extracted, and snap frozen in liquid nitrogen and stored at –80 °C until RNA or DNA extraction. All procedures involving animals were conducted in accordance with the guidelines of the University Committee on the Care and Use of Animals of the University of Michigan.

Spike-in control for the Methylated DNA Capture (MethylCap) assay

In Chapter 3, I found that the genome of *Xenopus* tadpole brain became demethylated during metamorphosis. Since this might lead to differences in efficiency of methylated DNA capture among samples during the MethylCap assay, I used spike-in control DNA to monitor the

capture efficiency.

I synthesized the spike-in control as described in Taiwo et al. (2012) (9) with modifications. I first PCR amplified four different DNA fragments from the lambda phage genome that differed in CpG density (two with low-CpG and two with high CpG density; see Supplemental Table 4.1 for primer sequences). I methylated two of these DNA fragments (one low-CpG and one high-CpG density) *in vitro* by incubating them with 10 units of M.SssI CpG methyltransferase (New England Biolabs (NEB), Ipsiwich, MA) and S-adenosylmethionine (SAM; 640 μM) for eight hours; four hours into reaction I replenished SAM. I purified the DNA fragments using phenol/chloroform/isoamyl alcohol precipitation (Invitrogen Life Technologies, Carlsbad, CA) and resuspended in buffer EB (Qiagen, Valencia, CA). I verified successful *in vitro* methylation by digesting the DNA fragments with Hinp1I restriction enzyme that is sensitive to CpG methylation (NEB; 10 units per reaction) (data not shown). I combined the four DNA fragments (two methylated and two non-methylated) into one to make a cocktail (0.2 pM). I added this cocktail to Buffer B of the MethylCap kit (Diagenode, Denville, NJ) in 1:30 dilution before the capture reaction.

Real-time qPCR assay showed that the MethylCap assay efficiently captured methylated spike-in DNA in a CpG density-dependent manner and that the capture efficiency did not vary significantly among samples (Supplemental Fig. 4.1). A recent study showed that the methyl CpG-binding domain of human MeCP2 binds to methylated CpAs at a similar affinity as methylated CpGs (10). When this study was published I had already completed the experiment, and therefore, I did not assess whether capture efficiency of methylated CpAs vary among samples

Genomic DNA extraction, the MethylCap assay, and MethylCap-seq

I microdissected the preoptic area/hypothalamus (including the pituitary) from *X. tropicalis* tadpoles at NF stages 50, 54, 56, 58, 62 and 66, and extracted genomic DNA using the DNeasy Blood and Tissue kit (Qiagen) (n=4/stage). For each biological replicate I pooled tissues from fifteen animals for NF stage 50, eight for stage 54, five for stage 56, five for stage 58, six for stage 62 and six for stage 66.

I sonicated 5 μg of genomic DNA to an average size of 400 bp using the Covaris S2 sonicator (Covaris, Woburn, MA), then used 1 μg of sonicated DNA to conduct the MethylCap assay using the MethylCap kit (Diagenode) following the manufacturer's protocol with the following modifications. Before the capture reaction, I added the spike-in control cocktail (described above) to Buffer B in 1:30 dilution to monitor the efficiency of methylated DNA capture. I collected flow-through and fractions that were serially eluted with low-, mid- and high-salt elution buffer. Input and high-salt fractions were further purified with the QIAquick PCR Purification kit (Qiagen), while other fractions were left unpurified and stored at -80 °C. Although the capture efficiency of the spike-in control did not vary significantly among samples as analyzed by real-time qPCR (Supplemental Fig. 4.1), I adjusted the final volume of eluates based on the qPCR result for MethylCap-seq, so that all samples contained the same concentration of the spike-in control. For sequencing I selected three biological replicates of high-salt fractions for each of the following four stages: NF stages 50 (premetamorphosis), 56 (mid-prometamorphosis), 62 (metamorphic climax) and 66 (end of metamorphosis); I also selected one input sample each from NF stage 50, 56 and 62 (one sample each). These 15 samples were submitted to the University of Michigan DNA sequencing core for sequencing library preparation.

The sequencing library was constructed on the Apollo instrument (an automated system) using IntegenX reagents (now Wafergen, Fremont, CA). DNA fragments were end repaired, adenylated, ligated with adapters that contain hexanucleotide barcodes, PCR amplified and pooled. One pool of libraries contained twelve libraries for high-salt fractions, while the other pool of libraries contained three libraries for input samples. Final libraries were assessed for their quality using the TapeStation (Agilent Technologies, Santa Clara, CA), quantified by qPCR using a commercial kit (Kapa Biosystems, Wilmington MA), and sequenced to produce single-end 50 bp reads on Illumina HiSeq 2000 platform with High Output mode using version 3 reagents. The libraries for high-salt fractions were sequenced twice, once using two flow cells and a second time using six additional flow cells to increase the number of reads. The libraries for input samples were sequenced once using two flow cells.

MethylCap-seq data processing and analysis

I filtered raw sequencing reads to remove duplicate reads using a custom script, and then assessed their quality using FastQC software (version 0.10.1) (http://www.bioinformatics.babraham.ac.uk/projects/fastqc/). I mapped the reads to the *X. tropicalis* genome (version 4.1) (11) using Bowtie software (version 1.0.0) (12). Prior to final mapping I conducted preliminary analyses to determine a parameter to produce the maximum number of aligned reads by adjusting the seed-length ("-l"), number of nucleotides to trim from the 5' and/or 3' ends of the reads ("-5" and "-3", respectively) and the number of sequence mismatches allowed ("-n"). Based on this analysis (data not shown), I uniquely mapped the reads using 50 bp as the seed-length with 1 bp mismatch allowed ("–l 50 –m 1 –n 1"). The number of aligned reads is provided in Supplemental Table 4.2. The Bowtie output file was converted to the

BED format for subsequent analyses.

I identified genomic regions that are enriched for methylated DNA ('methylation peaks') using PePr software (13) with the default parameters plus the "--remove artefacts" option included. I identified differentially methylated regions (DMRs) by additionally including the "--diff" option. The "--window_size" parameter was set to "400 (bp)" because this was the average fragment size of sonicated DNA used for the MethylCap assay; my preliminary analysis also showed that this window size yielded an optimal number of peaks among different window sizes tested (data not shown). For each of these analyses I ran the analysis twice by setting the "--peak_type" option to be "sharp" for the first run and "broad" for the second run. I combined these two data sets together using "mergeBed" function of Bedtools software (version 2.20.1) (14) for subsequent analyses.

I used "intersectBed" function of Bedtools software (version 2.20.1) (14) to identify the overlap between methylation peaks (or DMRs) and the following annotated genomic regions: upstream regions (0 to 10 kb 5' from the TSS in 1 kb increments), downstream regions (0 to 10 kb 3' from the TSS in 1 kb increments) and intragenic region (gene body) of the annotated genes. I used the MNHN gene model (described below) to identify these regions.

RNA extraction and RNA-sequencing (RNA-seq) library preparation

I microdissected the preoptic area/hypothalamus (which included the pituitary) from *X. tropicalis* tadpoles at NF stages 50, 54, 56, 58, 62 and 66. I extracted total RNA from tissue using TRIZOL reagent (Invitrogen) and further purified it with the RNeasy Mini kit (Qiagen). For RNA-seq I selected three of five biological replicates for the same four stages of metamorphosis as MethylCap-seq (NF stages 50, 56, 62 and 66), and submitted them to the

University of Michigan DNA sequencing core for sequencing library preparation.

All samples had RIN (RNA Integrity Numbers) of 8 or greater as analyzed by the TapeStation (Agilent). Each library was prepared from 130 ng of RNA using the Illumina TruSeq mRNA Sample Prep v2 kit (Illumina Inc., San Diego, CA), where total RNA was poly-A selected, fragmented and reverse transcribed with random primers. The 3' ends of the cDNA library were adenylated, ligated with adapters that contain hexanucleotide barcodes, and PCR-amplified to construct the final library. The final libraries were assessed for their quality using the TapeStation (Agilent) and quantified by qPCR using a commercial kit (Kapa Biosystems). All libraries were pooled and sequenced to produce single-end 50 bp reads in two flow cells on the Illumina HiSeq 2000 platform with High Output mode using version 3 reagents.

RNA-seq data processing and analysis

I conducted quality control and post-processing of raw sequencing reads, and the same preliminary analysis for Bowtie mapping as described above for MethylCap-seq. Based on the preliminary analysis (data not shown), I used a parameter to first trim 21 bp from the 5'end of the reads and then uniquely map them to the genome using 30 bp as the seed-length with 1 bp mismatch allowed ("-5 21 –l 30 –m 1 –n 1"). The number of aligned reads is provided in Supplemental Table 4.2. The Bowtie output file was converted to the BED format for subsequent analyses.

I used the "intersectBed" function of Bedtools software (version 2.20.1) (14) to count the number of reads that overlapped with each of 22,820 custom annotated *X. tropicalis* genes ('gene counting'). This custom annotation (the MNHN gene model) was built by Laurent Sachs and colleagues based on their unpublished high-throughput RNA pair-end tagging (RNA-PET)

sequencing analysis to identify the 5' and 3' ends of transcripts that were expressed in various *X. tropicalis* tissues including the brain. After gene counting I used DESeq software (version 1.12.0) (15) to identify differentially expressed genes at a false discovery rate of 5% with the following parameters: *method="pooled"; sharing-mode="maximum"; fit-type="parametric"*.

The RNA-seq analysis identified 5,220 unique genes that became differentially expressed in tadpole brain during metamorphosis (see Results). Using a list of genes that became differentially expressed between NF stage 50 (premetamorphosis) and any of the three later stages (1,979 genes), I conducted fuzzy c-mean clustering (which is similar to *k*-means clustering but less sensitive to noise) (16) to identify patterns of gene expression dynamics during metamorphosis. I first sorted the 1,979 genes into 81 clusters, and then grouped similar clusters into 13 general patterns as described in the Results section. I conducted gene ontology and KEGG pathway analyses of differentially expressed genes using g:Profiler software (17) with the default parameters.

Reverse transcriptase real-time quantitative PCR (RTqPCR)

To validate RNA-seq I conducted RTqPCR as described in Chapter 3 for 14 genes chosen based on their type of regulation (up-, down- or non-regulated) and transcript abundance (low, medium and high). For this analysis I included three RNA samples used for sequencing and two additional samples not used for sequencing. The list of 14 genes and primer sequences are provided in Supplementary Table 4.3.

Results

Identification of genomic regions that undergo changes in DNA methylation during

Xenopus metamorphosis using MethylCap-seq

The Methylated DNA capture (MethylCap) assay enriches ('captures') methylated cytosines using the recombinant methyl-CpG-binding domain (MBD) of human MeCP2 protein that has affinity for both CpG and CpA methylation (10). I sequenced fraction that was eluted with high-salt elution buffer and input samples and generated 95.2 million and 72.6 million reads respectively per sample (Supplemental Table 4.2). I aligned the reads to the *X. tropicalis* genome using a parameter to remove sequences that appear more than once in the genome (i.e. unique mapping), and obtained 15.2 million mapped reads for high-salt samples and 30.9 million mapped reads for input samples (Supplemental Table. 4.2). This mapping parameter removed more reads from high-salt samples (31.8%) than input samples (21.0%), suggesting that high-salt samples contained a higher amount of repeat sequences in the genome (Supplemental Table. 4.2).

Using PePr software (13) I identified 141,700 unique genomic regions that are enriched for methylated DNA ('methylation peaks'). The width of methylation peaks ranged from 400 bp to 15.8 kb with the average of ~1 kb. About 57% of peaks overlapped with intra-genic regions, while the rest of the peaks fell within inter-genic regions. Roughly 29% of total peaks overlapped within 10 kb upstream and downstream of transcription start sites. Differential peak analysis using PePr software (13) identified 855 methylation peaks that showed changes during metamorphosis (coordinates of these differentially methylated regions (DMRs) are provided in Supplemental Table 4.4). The extent of overlap in intra-genic regions was similar among DMRs (62%). Roughly 30% of DMRs overlapped within 10 kb upstream and downstream of transcription start sites.

Pair-wise differential peak analysis identified 25 methylation peaks that showed increase and 24 methylation peaks that showed decrease between premetamorphosis (NF stage 50) and

mid-prometamorphosis (NF stages 56) (Fig. 4.1). Larger numbers of methylation peaks exhibited changes between premetamorphosis and metamorphic climax (NF stage 62; 144 increase and 149 decrease), and between premetamorphosis and the end of metamorphosis (NF stage 66; 41 increase and 195 decrease) (Fig. 4.1), indicating that more changes in DNA methylation occurred during later stages of metamorphosis. Similar pair-wise analyses between the end of metamorphosis (NF stage 66) and three earlier stages showed that the majority of DMRs (76-91%) showed decrease in DNA methylation (Fig. 4.1), consistent with my findings in Chapter 3 that the tadpole brain genome became demethylated during metamorphosis. In Chapter 2, I found that mRNA for the *de novo* DNA methyltransferase 3a (*dnmt3a*) gene increased in tadpole brain between mid-prometamorphosis and metamorphic climax (NF stages 56 and 62). Consistent with this there were more peaks that showed increase in DNA methylation (82) than those that showed decrease (29) between these two stages (Fig. 4.1).

Identification of differentially expressed genes in *Xenopus* tadpole brain during metamorphosis using RNA-sequencing (RNA-seq)

To identify genes that might show correlated changes in expression, I conducted RNA-sequencing (RNA-seq) analysis on the preoptic area/hypothalamus (including the pituitary) of *X. tropicalis* tadpoles at the same four stages of metamorphosis as for MethylCap-seq analysis. I generated 27.4 million reads and uniquely mapped 10.8 million reads to the *X. tropicalis* genome per sample (Supplemental Table 4.1). To validate RNA-seq results I conducted RTqPCR for 14 genes (6 up-, 6 down- and 2 non-regulated) chosen based on their transcript abundance (low, medium and high). All genes tested by RTqPCR showed similar developmental expression dynamics as they did by RNA-seq (Supplemental Fig. 4.2; gene annotation and primer sequences

are provided in Supplemental Table 4.3).

Using DESeq software (15) I found that 5,220 of 22,820 annotated genes showed changes in expression in tadpole brain during metamorphosis. Using the list of differentially expressed genes between premetamorphosis (NF stage 50) and any one of the three later stages (NF stages 56, 62, and 66) (1,979 genes), I conducted fuzzy *c*-means clustering analysis and identified thirteen patterns of gene expression dynamics (Fig. 4.2 and Supplemental Fig. 4.3). While there was one pattern that was unique to a group of upregulated genes (pattern 1) in which they showed highest expression at mid-prometamorphosis (NF stage 56) and declined towards the end of metamorphosis, the remaining twelve patterns could be divided into six pairs of upregulated and downregulated genes based on their roughly inverse expression patterns (Fig. 4.2). The first pair exhibited a simple pattern as they increased (pattern 2) or decreased (pattern 3) continuously throughout metamorphosis, while another pair exhibited a more complex dynamics that involved a transient increase or decrease (patterns 4 and 5). The third and fourth pairs exhibited peak expression at metamorphic climax (NF stage 62) and either reached a plateau (pattern 6 and pattern 7), or decreased (pattern 8) or increased (pattern 9) between metamorphic climax and the end of metamorphosis (NF stage 62 and 66). The fifth pair exhibited a sharp increase (pattern 10) or decrease (pattern 11) between premetamorphosis and mid-prometamorphosis (NF stages 50 and 56) but did not show further changes for the remainder of metamorphosis. The last pair had unique characteristics in that they did not change until after mid-prometamorphosis (NF stage 56; patterns 12 and 13) (see Supplemental Table 4.5 for the list of genes in each pattern).

I also identified differentially expressed genes among the four stages of metamorphosis by pair-wise comparisons (Fig. 4.3) (the complete list of differentially expressed genes is

provided in Supplemental Table 4.6), and then investigated enrichment of pathways using gene ontology (GO) and KEGG/Reactome pathway analyses. Between premetamorphosis and mid-prometamorphosis (NF stages 50 and 56), I found 311 upregulated and 627 downregulated genes (Fig. 4.3). While there was no enrichment of pathways among upregulated genes, I found enrichment of pathways involved in cell cycle and p53 signaling (apoptosis) among downregulated genes (Supplemental Table 4.7).

The RNA-seq analysis identified 655 upregulated and 732 downregulated between mid-prometamorphosis and metamorphic climax (NF stages 56 and 62), coinciding with a dramatic increase in plasma [T_3] (Fig. 1.1). The cell cycle pathway was again enriched among downregulated genes, consistent with previous findings from my laboratory that the rate of cell proliferation in tadpole brain peaks at mid-prometamorphosis and declines towards metamorphic climax (7). The metabolic and biosynthetic pathways were other major pathways enriched among downregulated genes (Supplemental Table 4.7). Although there were similar numbers of upregulated and downregulated genes, only a few pathways were enriched among upregulated genes (Supplemental Table 4.7), one of which was hormone-mediated signaling pathway that included genes that code for thyroid hormone (TR) β and its heterodimerization partner Retinoid X receptor (RXR) α.

A small set of genes (137) showed changes in expression between metamorphic climax and the completion of metamorphosis (NF stage 62 and 66) (Fig. 4.3). Again, I found no enrichment of pathways among 69 upregultad genes, while I found enrichment of pathways involved in metabolism of lipids and lipoproteins among 68 downregultaed genes (Supplemental Table 4.7).

Correlation between changes in DNA methylation and gene expression changes in during metamorphosis

I investigated possible correlations between developmental changes in DNA methylation and expression of genes that are in the 50 kb vicinity of DMRs. While I did not find such correlations for changes that occur during short developmental time intervals (i.e. between NF stages 50 and 56, NF stages 56 and 62, and NF stages 62 and 66), I found some correlations for changes that occur during longer developmental time intervals (NF stages 50 and 62, NF stages 56 and 66 and NF stages 50 and 66) (the complete list of genes that showed correlated changes is provided in Supplemental Table 4.8).

The RNA-seq analysis identified 311 upregulated and 627 downregulated genes (among 22,820 annotated genes) between premetamorphosis and metamorphic climax (NF stages 50 and 62) (Fig. 4.3). This predicted that I would find 21 upregulated and 24 downregulated genes by random correlation among 268 genes that are in 50 kb vicinity of methylation peaks that showed decrease (i.e. demethylated) between these two stages. My analysis identified 38 upregulated and 28 downregulated genes, which statistically exceeded the number of genes predicted by random correlation (Fig. 4.4). I found 229 genes in the 50 kb vicinity of peaks that showed increase in DNA methylation (i.e. methylated) between the two stages; however, I did not find statistically significant correlation for these genes (data not shown).

Between mid-prometamorphosis and the end of metamorphosis (NF stages 56 and 66) I identified 833 upregulated and 854 downregulated genes (Fig. 4.3). Among 193 genes in 50 kb vicinity of methylation peaks that showed decrease, a random correlation predicted to find 7 upregulated and downregulated genes each; my analysis found 17 upregulated genes (2.4-fold enrichment) and 3 downregulated genes (2.3-fold underrepresentation) (Fig. 4.4). There were 44

genes in 50 kb vicinity of methylation peaks that showed increase; I found 4 upregulated and downregulated genes each while random correlation predicted to find 2 of each (Fig. 4.4).

Between the beginning and end of metamorphosis (NF stages 50 and 66) RNA-seq analysis identified 1,926 upregulated and 2,172 downregulated genes. A random correlation predicated to find 37 upregulated genes and 42 downregulated genes among 440 genes that are found in 50 kb vicinity of methylation peaks that showed decrease between these two stages. While I found roughly twice as many number of upregulated genes predicted by random correlation (75 genes), I found the same number of downregulated genes predicted by chance (i.e. no enrichment; 42 genes) (Fig. 4.4). There were 56 genes in 50 kb vicinity of methylation peaks that showed increase. I found 7 upregulated and 13 downregulated genes, while random correlation predicted to find 5 of each (Fig. 4.4).

Discussion

The neural cell genome undergoes dramatic changes in DNA methylation during postembryonic development. To identify genomic regions that go through deveopmntal changes in DNA methylation, and also to investigate the role of such changes in gene transcription in the brain, I conducted MethylCap-seq and RNA-seq on *X. tropicalis* tadpole brain at different stages of metamorphosis. The MethylCap-seq analysis identified distinct loci in the genome that showed increase and decrease in DNA methylation, while RNA-seq analysis identified genes that became differentially expressed in tadpole brain during metamorphosis. I also found a weak, but significant inverse correlation between changes in DNA methylation and changes in expression of genes that are found in 50 kb vicinity of differentially methylated regions (DMRs). Although more rigorous analysis of both MethylCap-seq and RNA-seq is required, my findings

suggest that DNA methylation may play a role in transcriptional regulation of genes in the developing brain.

DNA methylation changes in Xenopus tadpole brain during metamorphosis

Using MethylCap-seq I identified 141,700 distinct regions that are enriched for methylated DNA ('methylation peaks') in the genome of *X. tropicalis* tadpole brain. However, the majority of these methylation peaks did not show changes during metamorphosis, and I only found 855 methylation peaks that became differentially methylated. In Chapter 3, I found ~50% reduction in methylated cytosines in the developing tadpole brain using 5-mC ELISA; in comparison, changes detected by MethylCap-seq analysis were much smaller (0.6% of all methylation peaks).

There are several factors that might have contributed to the difference in the magnitude of changes detected by ELISA and MethylCap-seq. First, while 5-mC ELISA detects methylated cytosines in any sequence context, the MethylCap assay can detect only those in CpG and CpA contexts (10). Second, although I used low-, mid- and high-salt elution buffers to serially elute captured DNA during the MethylCap assay, I only analyzed the high-salt fraction for sequencing analysis, which restricted my analysis to a small subpopulation of all methylated cytosines present in the genome. Third, I also conducted the assays using two different frog species: while I used *X. laevis* tadpoles for 5-mC ELISA in Chapter 3, I used *X. tropicalis* tadpoles for MethylCap-seq analysis. A previous study by Head and colleagues (18) has shown that the genome of *X. tropicalis* frog brain is relatively less methylated than that of *X. leavis* (76% and 91% of MspI/HpaII restriction sites were methylated as analyzed by Luminometric Methylation Assay (LUMA) (19)). Because of this species difference, changes in DNA methylation may be

less dynamic in *X. tropicalis* than in *X. laevis*. In support of this, I found larger DNA demethylation at regions that contain *klf9* and *dnmt3a* T_3REs in *X. laevis* than in *X. tropicalis* (Chapter 3). Lastly, mapping of MethylCap-seq reads showed that the high-salt fraction had a higher content of sequences that are repeated in the genome, as more reads were removed from high-salt samples than input samples during alignment (31.8% versus 21.0% of reads) (Supplemental Table 4.1), which may be consistent with a role for DNA methylation in silencing of repetitive elements (20). Taken together, changes in DNA methylation identified by MethylCap-seq analysis may not be representative of changes that occur at the whole genome scale, particularly in regions that have a lower density of methylated cytosines. Sequencing of the low- and mid-salt fractions is required for more comprehensive analysis of changes in DNA methylation that occur in the tadpole brain.

Gene expression changes in Xenopus tadpole brain during metamorphosis

To better understand the molecular basis of tissue morphogenesis during postembryonic development, and to investigate a potential correlation between gene expression and DNA methylation changes, I conducted RNA-seq on *X. tropicalis* tadpole brain at the same stages of metamorphosis as in MethylCap-seq. My study represents the first transcriptome analysis of *Xenopus* tadpole brain (or any tadpole tissue) following their development; prior transcriptome analyses using microarrays have been conducted only on premetamorphic tadpole after T_3 treatment or inhibition of T_3 synthesis (reviewed in Kulkarni and Buchholz, 2013 (21)). My RNA-seq analysis identified 5,220 unique genes that became differentially expressed, thirteen distinct patterns of gene expression dynamics, and enriched pathways among differentially expressed genes during metamorphosis.

Genes that are involved in cell cycle control were strongly downregulated during metamorphosis. Gene ontology analysis identified the pathway twice during the transition from premetamorphosis to mid-prometamorphosis (NF stages 50 and 56), and then again during the transition from mid-prometamorphosis to metamorphic climax (NF stages 56 and 62). The repressed genes included the cyclins (*ccna2, ccnb2, ccnb3, ccne1, ccne2*), cyclin-dependent kinases (*cdk1, cdk4*), and subunits of protein complexes that are involved in DNA synthesis and replication, such as MCM replication licensing factor complex and ORC origin recognition complex. All of these genes are known targets of E2F transcription factors, the master regulators of the transition between G1 and S phase of the cell cycle (22); the genes that code for E2F protein (*e2f1, e2f3*, *e2f5*) also exhibited decreases by the time tadpole reaches metamorphic climax. Robust downregulation of cell cycle genes may explain the decline of cell proliferation in tadpole brain that occurs during metamorphosis (7), although this needs further investigation.

On the contrary I found only a small number of enriched pathways among upregulated genes; this was not due to a low number of genes included in the analysis (311 genes for comparison between NF stages 50 and 56; 655 genes for comparison between NF stages 56 and 62; and 69 genes between stages 62 and 66). This may imply that there is a greater diversity of pathways regulated by genes that are induced during metamorphosis than those that are repressed. The annotation of the *X. tropicalis* genome is still far from complete (23); therefore, it is also possible that functions are not assigned for a large number of activated genes.

Identification of genes that exhibit correlated changes in expression with changes in DNA methylation

I investigated whether genes that are found in the 50 kb vicinity of DMRs would exhibit correlated changes in expression, and my analysis supported a weak, but statistically significant inverse correlation between changes in DNA methylation and gene expression changes (Fig. 4.4). For example, I found twice as many upregulated genes (75 genes found; 37 genes predicted by chance) that are close to regions that became demethylated between NF stage 50 and 66; whereas, I did not find such enrichment for downregulated genes within the same regions (42 genes found; 42 genes predicted by chance) (Fig. 4.4). It is noteworthy that I found a correlation between DNA demethylation and activation of genes that are important for neural cell maturation and function. This includes genes that code for subunits of neurotransmitter receptors (*grin1, gabra2*), the enzyme that synthesize GABA, the major inhibitory neurotransmitters in the brain (*gad2*), subunits of potassium and calcium voltage-gated channels that regulate neural cell excitability (*kcng2*, *cacna1g*) and receptors for brain-derived and glial-derived tropic factors (BDNF and GDNF) (*ntrk2, gfra1*).

Further analysis is required to identify the precise location of DMRs with respect to the genes that showed correlated changes in expression, and to investigate if these DMRs overlap with gene regulatory regions such as promoters and enhancers. In mouse brain DMRs that exhibit changes in CpG methylation were more likely to overlap with enhancers that are marked by mono methylation of lysine 4 of histone 3 (H3K4me1) and acetylation of lysine 27 of histone 3 (H3K27ac) (2). No genome-wide analyses of these histone marks have been conducted in *Xenopus* tadpole brain. Conducting such experiments to identify enhancers in tadpole brain may be informative for understanding the functional relevance of DNA methylation changes identified by MethylCap-seq.

While my analysis supported a general correlation between DNA demethylation and activation of genes nearby, the majority (76-91%) of genes did not show such correlated changes in expression, which may be due to limitations of my approach. First, I included all DMRs for analysis regardless of whether they overlap with gene regulatory regions, which may have diluted the overall effect in the analysis. Previous studies supported correlated changes in gene expression and methylation changes at gene bodies and enhancer regions (24). Therefore, investigating the correlation for a subset of DMRs that overlap with defined genomic regions may support a stronger correlation. Another limitation of my approach was that I investigated the correlation based only on physical distance (i.e. within 50 kb) between genes and DMRs. Gene regulatory regions such as enhancers could be located more than 50 kb away from regulated genes. For example, my lab recently identified an enhancer located 72 kb upstream of human Krupple-like factor 9 (*KLF9*) gene that interacts with its promoter through long-range chromosomal interaction (25). Investigating such interaction between DMRs and genes using a technique such as 5C (26) will establish a more direct functional linkage between changes in DNA methylation and correlated changes in gene expression.

In conclusion, I identified genomic regions that showed changes in DNA methylation and genes that became differentially expressed in *Xenopus* tadpole brain during metamorphosis. My preliminary analysis found an inverse correlation between changes in DNA methylation and expression of genes that are close to DMRs. To my knowledge, this is the first study to investigate DNA methylation changes in any *Xenopus* tadpole tissues during metamorphosis, and is also the first to conduct RNA-seq in tadpole brain. The present study laid an important groundwork for investigating roles of DNA methylation and gene expression changes in *Xenopus* tadpole brain during metamorphosis.

References

1. Guo JU, Su Y, Shin JH, Shin J, Li H, Xie B, Zhong C, Hu S, Le T, Fan G, Zhu H, Chang Q, Gao Y, Ming GL, Song H. Distribution, recognition and regulation of non-CpG methylation in the adult mammalian brain. Nature neuroscience 2014; 17:215-222

2. Lister R, Mukamel EA, Nery JR, Urich M, Puddifoot CA, Johnson ND, Lucero J, Huang Y, Dwork AJ, Schultz MD, Yu M, Tonti-Filippini J, Heyn H, Hu S, Wu JC, Rao A, Esteller M, He C, Haghighi FG, Sejnowski TJ, Behrens MM, Ecker JR. Global epigenomic reconfiguration during mammalian brain development. Science 2013; 341:1237905

3. Varley KE, Gertz J, Bowling KM, Parker SL, Reddy TE, Pauli-Behn F, Cross MK, Williams BA, Stamatoyannopoulos JA, Crawford GE, Absher DM, Wold BJ, Myers RM. Dynamic DNA methylation across diverse human cell lines and tissues. Genome research 2013; 23:555-567

4. Wu SC, Zhang Y. Active DNA demethylation: many roads lead to Rome. Nature reviews Molecular cell biology 2010; 11:607-620

5. Szulwach KE, Li X, Li Y, Song CX, Wu H, Dai Q, Irier H, Upadhyay AK, Gearing M, Levey AI, Vasanthakumar A, Godley LA, Chang Q, Cheng X, He C, Jin P. 5-hmC-mediated epigenetic dynamics during postnatal neurodevelopment and aging. Nature neuroscience 2011; 14:1607-1616

6. Brinkman AB, Simmer F, Ma K, Kaan A, Zhu J, Stunnenberg HG. Whole-genome DNA methylation profiling using MethylCap-seq. Methods 2010; 52:232-236

7. Denver RJ, Hu F, Scanlan TS, Furlow JD. Thyroid hormone receptor subtype specificity for hormone-dependent neurogenesis in Xenopus laevis. Developmental biology 2009; 326:155-168

8. Krain LP, Denver RJ. Developmental expression and hormonal regulation of glucocorticoid and thyroid hormone receptors during metamorphosis in Xenopus laevis. The Journal of endocrinology 2004; 181:91-104

9. Taiwo O, Wilson GA, Morris T, Seisenberger S, Reik W, Pearce D, Beck S, Butcher LM. Methylome analysis using MeDIP-seq with low DNA concentrations. Nature protocols 2012; 7:617-636

10. Gabel HW, Kinde B, Stroud H, Gilbert CS, Harmin DA, Kastan NR, Hemberg M, Ebert DH, Greenberg ME. Disruption of DNA-methylation-dependent long gene repression in Rett syndrome. Nature 2015;

11. Hellsten U, Harland RM, Gilchrist MJ, Hendrix D, Jurka J, Kapitonov V, Ovcharenko I, Putnam NH, Shu S, Taher L, Blitz IL, Blumberg B, Dichmann DS, Dubchak I, Amaya E, Detter JC, Fletcher R, Gerhard DS, Goodstein D, Graves T, Grigoriev IV, Grimwood J, Kawashima T, Lindquist E, Lucas SM, Mead PE, Mitros T, Ogino H, Ohta Y, Poliakov AV, Pollet N, Robert J, Salamov A, Sater AK, Schmutz J, Terry A, Vize PD, Warren WC, Wells D, Wills A, Wilson RK, Zimmerman LB, Zorn AM, Grainger R, Grammer T, Khokha MK, Richardson PM, Rokhsar DS. The genome of the Western clawed frog Xenopus tropicalis. Science 2010; 328:633-636

12. Langmead B, Trapnell C, Pop M, Salzberg SL. Ultrafast and memory-efficient alignment of short DNA sequences to the human genome. Genome biology 2009; 10:R25

13. Zhang Y, Lin YH, Johnson TD, Rozek LS, Sartor MA. PePr: a peak-calling prioritization pipeline to identify consistent or differential peaks from replicated ChIP-Seq data. Bioinformatics 2014; 30:2568-2575
14. Quinlan AR, Hall IM. BEDTools: a flexible suite of utilities for comparing genomic features. Bioinformatics 2010; 26:841-842
15. Anders S, Huber W. Differential expression analysis for sequence count data. Genome biology 2010; 11:R106
16. Kumar L, M EF. Mfuzz: a software package for soft clustering of microarray data. Bioinformation 2007; 2:5-7
17. Reimand J, Arak T, Vilo J. g:Profiler--a web server for functional interpretation of gene lists (2011 update). Nucleic acids research 2011; 39:W307-315
18. Head JA, Mittal K, Basu N. Application of the LUminometric Methylation Assay to ecological species: tissue quality requirements and a survey of DNA methylation levels in animals. Molecular ecology resources 2014; 14:943-952
19. Karimi M, Johansson S, Stach D, Corcoran M, Grander D, Schalling M, Bakalkin G, Lyko F, Larsson C, Ekstrom TJ. LUMA (LUminometric Methylation Assay)--a high throughput method to the analysis of genomic DNA methylation. Experimental cell research 2006; 312:1989-1995
20. Goll MG, Bestor TH. Eukaryotic cytosine methyltransferases. Annual review of biochemistry 2005; 74:481-514
21. Kulkarni SS, Buchholz DR. Developmental programs and endocrine disruption in frog metamorphosis: the perspective from microarray analysis. Current topics in developmental biology 2013; 103:329-364
22. Bracken AP, Ciro M, Cocito A, Helin K. E2F target genes: unraveling the biology. Trends in biochemical sciences 2004; 29:409-417
23. Grimaldi AG, Buisine N, Bilesimo P, Sachs LM. High-throughput sequencing will metamorphose the analysis of thyroid hormone receptor function during amphibian development. Current topics in developmental biology 2013; 103:277-303
24. Baubec T, Schubeler D. Genomic patterns and context specific interpretation of DNA methylation. Current opinion in genetics & development 2014; 25:85-92
25. Bagamasbad PD, Bonett RM, Sachs L, Buisine N, Raj S, Knoedler JR, Kyono Y, Ruan Y, Ruan X, Denver RJ. Deciphering the regulatory logic of an ancient, ultraconserved nuclear receptor enhancer module. Molecular endocrinology 2015:me20141349
26. Shin J, Ming GL, Song H. Decoding neural transcriptomes and epigenomes via high-throughput sequencing. Nature neuroscience 2014; 17:1463-1475

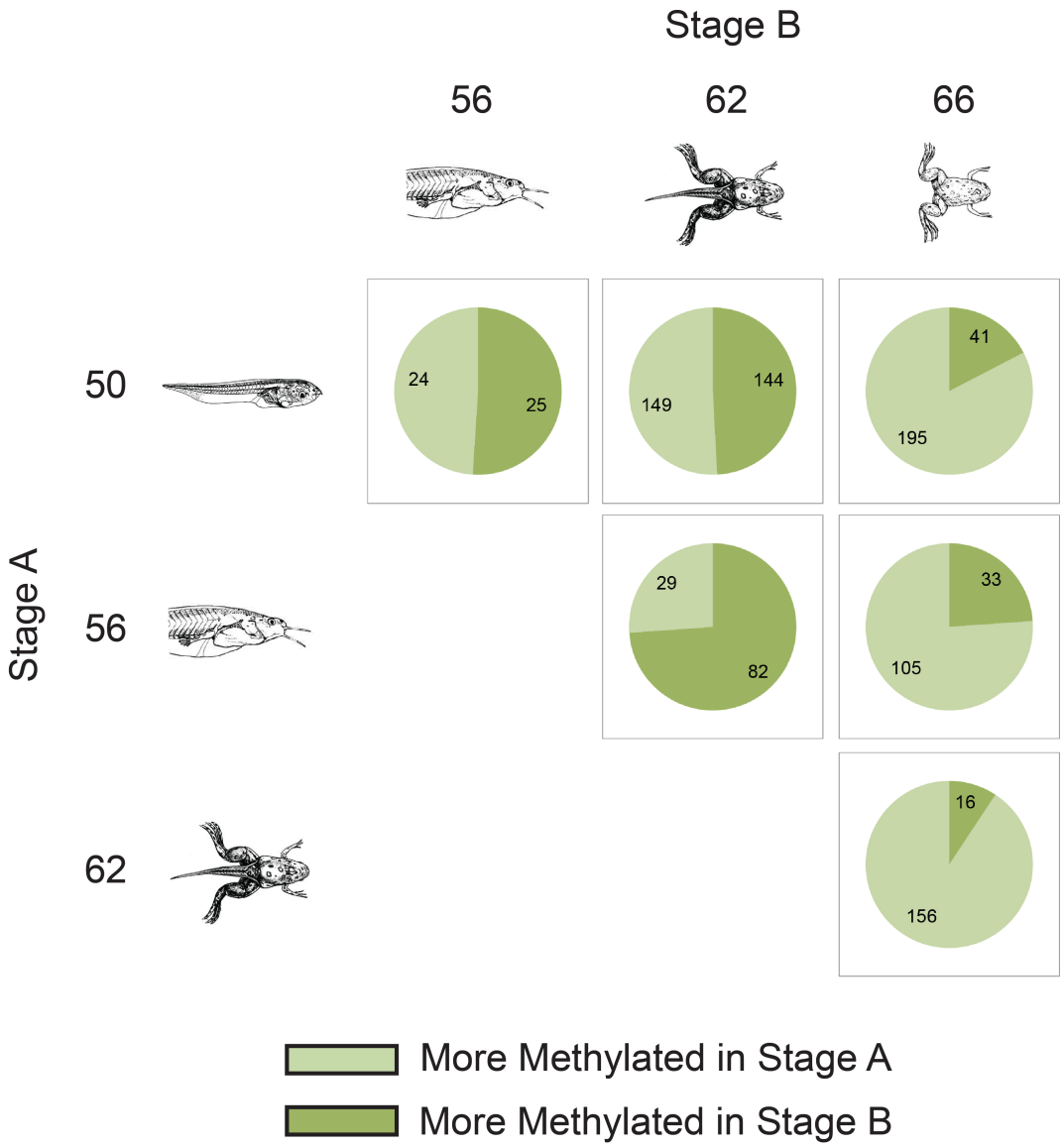

Fig. 4.1. Identification of genomic regions that exhibit changes in DNA methylation in *X. tropicalis* tadpole brain during metamorphosis using MethylCap-seq. I conducted MethylCap-seq analysis on genomic DNA isolated from *X. tropicalis* tadpole brain at four different developmental stages of metamorphosis. Using peak-calling software PePr I identified genomic regions that are enriched for methylated DNA across the genome ('methylation peaks'). I then conducted differential peak analysis to identify methylation peaks that exhibit developmental changes during metamorphosis ('differentially methylated regions – DMRs'). The results of this analysis are summarized as pie charts. The numbers in the lighter area of pie charts indicate the number of DMRs that are more methylated in Stage A (i.e. demethylated in Stage B), and the numbers in the darker area of pie charts indicate the number of DMRs that are more methylated in Stage B.

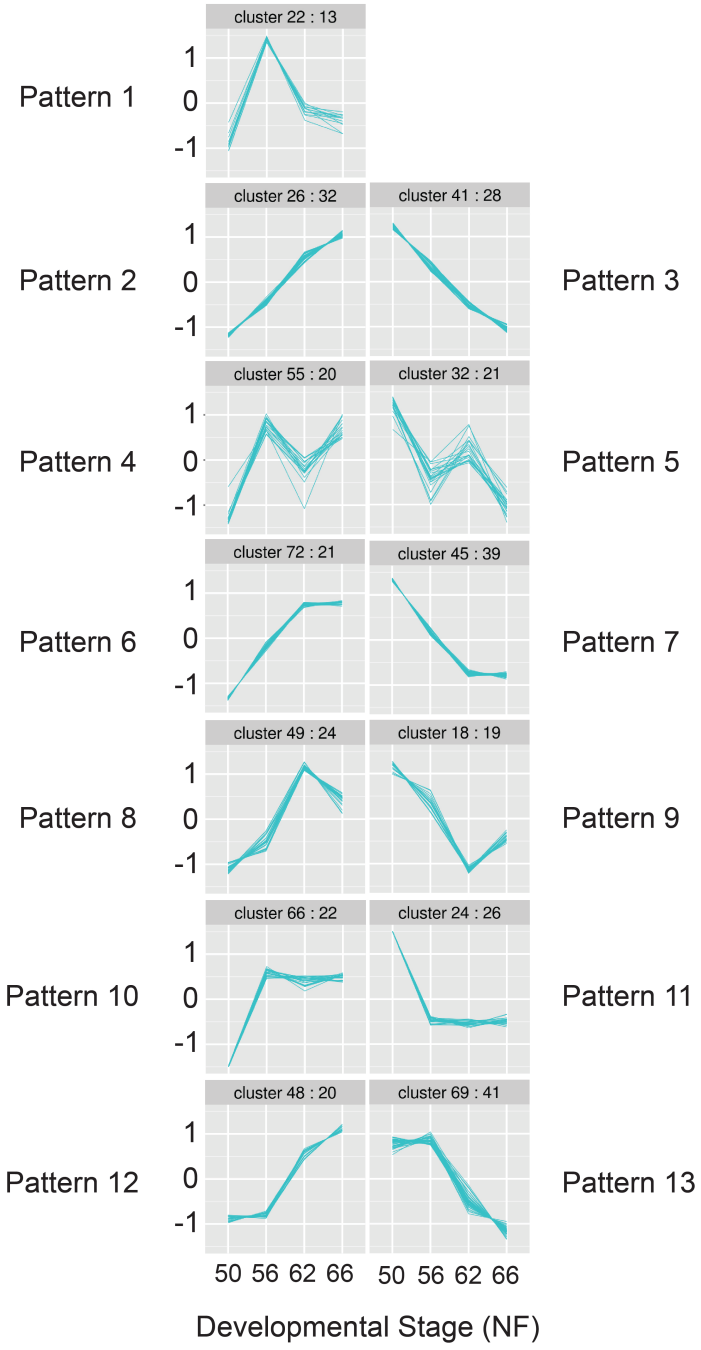

Fig. 4.2. Differentially expressed genes in *X. tropicalis* tadpole brain exhibit distinct patterns of expression dynamics during metamorphosis. Using RNA-seq analysis I identified 5,220 unique genes that exhibited changes in expression in *X. tropicalis* tadpole brain during metamorphosis. Using this list of differentially expressed genes, I conducted *c*-means clustering analysis to identify groups of genes that exhibited similar developmental dynamics of expression during metamorphosis. I first grouped these genes into 81 different clusters (see Supplemental Fig. 3 for all patterns), and then further grouped those clusters into 13 general patterns. Presented in this figure are representatives of those 13 patterns.

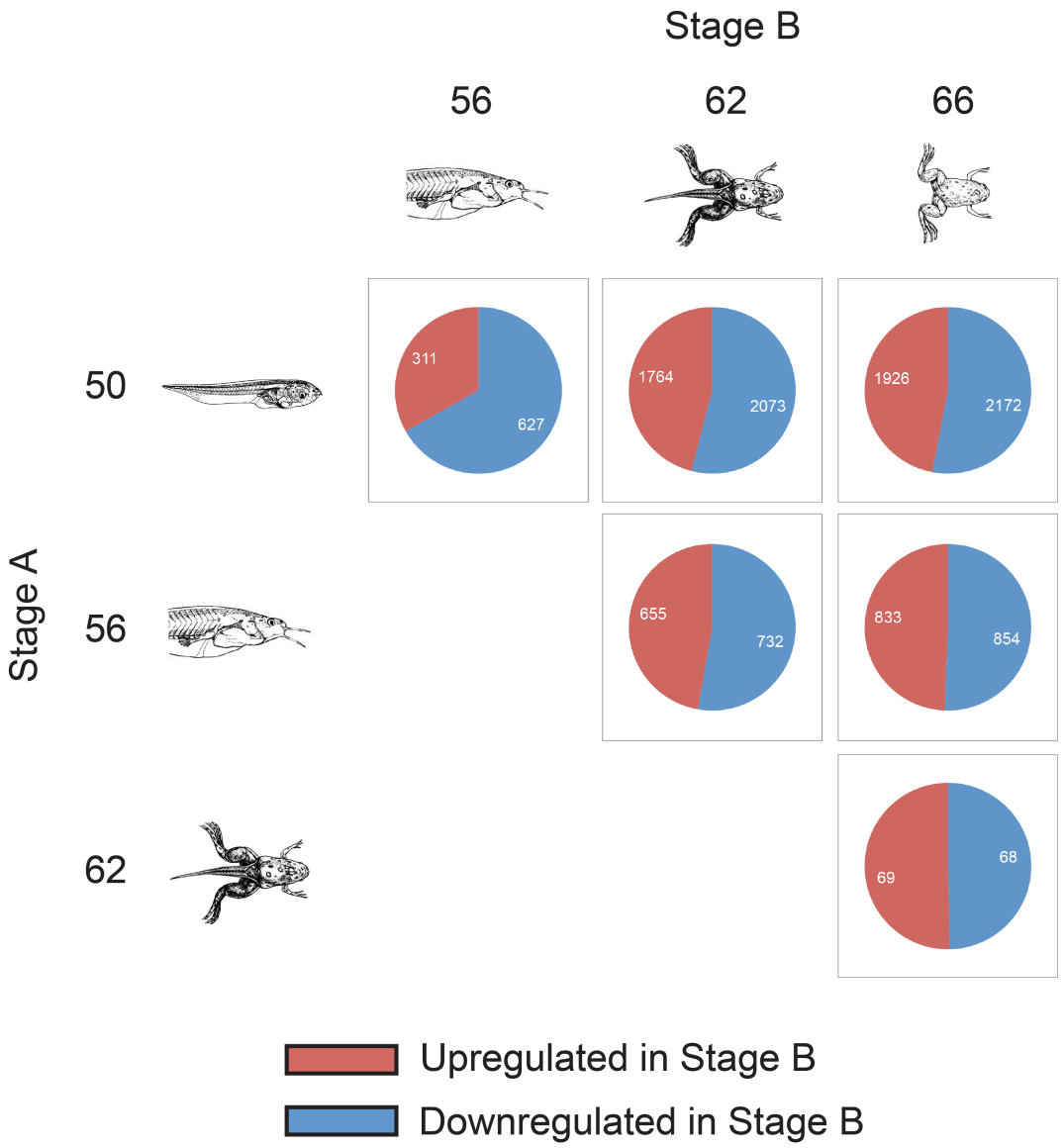

Fig. 4.3. The transcriptome of *X. tropicalis* tadpole brain exhibits dynamic changes during metamorphosis.. I conducted RNA-seq analysis on RNA isolated from *X. tropicalis* tadpole brain at the same four different developmental stages of metamorphosis as in MethylCap-seq. Using DESeq software I identified genes that exhibited changes in expression during metamorphosis ('differentially expressed genes'). Shown are pie charts that summarize the number of differentially expressed genes. The numbers in red area of pie charts indicate the number of upregulated genes in Stage B, while the numbers in blue area of pie charts indicate the number of downregulated genes in Stage B.

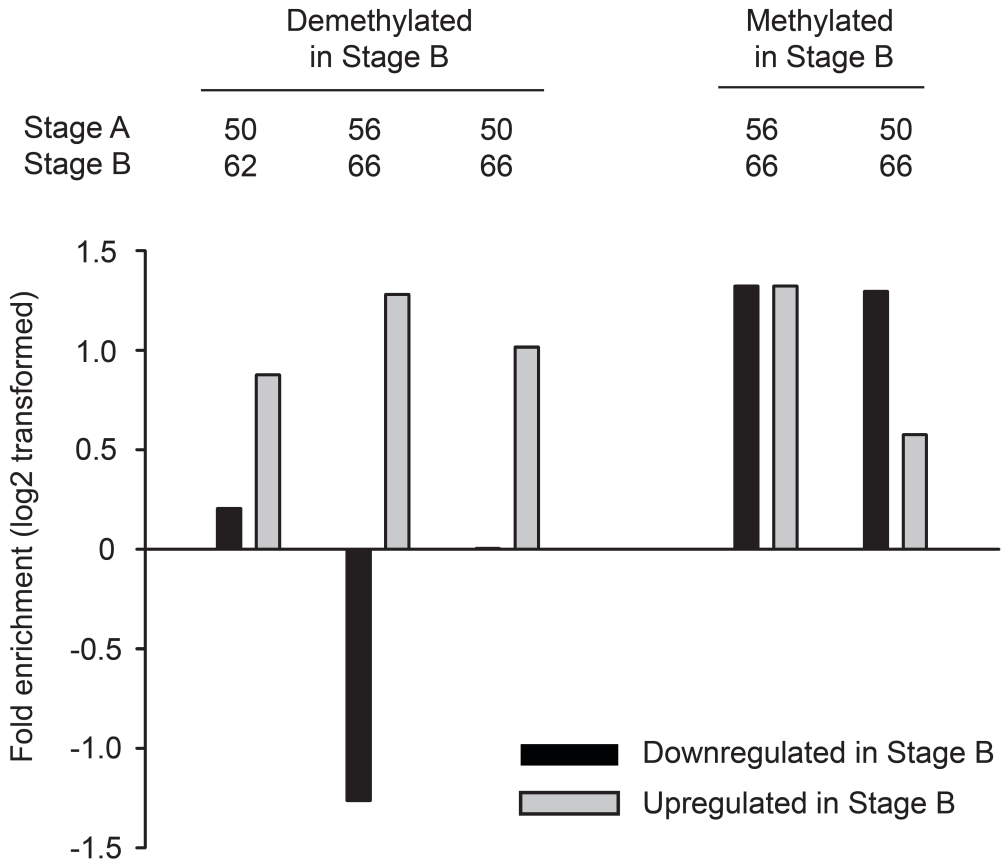

Fig. 4.4. Changes in DNA methylation correlate with expression of genes that are found within 50 kb. I investigated correlation between developmental changes in DNA methylation at differentially methylated regions (DMRs) and expression of genes that are in the neighbor of DMRs. To investigate this I first listed all genes that I found within the 50 kb flanking regions of DMRs, and then categorized those genes as upregulated, downregulated, or no changes in expression. I found statistically significant enrichment in the number of differentially expressed genes within the 50 kb flanking regions over the number of genes predicted by random association (χ^2, $p < 0.05$). Bars represent log2-transformed fold enrichment in the number of genes that exhibited changes in expression.

Chapter 5

CONCLUSIONS AND FUTURE DIRECTIONS

Postembryonic neurological development is critically dependent on thyroid hormone (T_3). The actions of T_3 are mediated by ligand-modulated T_3 receptors (TRs) that control target gene transcription through recruitment of histone-modifying enzymes. Compared to this known role of T_3 in modulating posttranslational modification of histones, virtually nothing is known about the linkage between T_3 signaling and DNA methylation, another critical epigenetic modification that controls gene transcription. It was previously thought that the genome-wide pattern of DNA methylation (methylome) is fixed throughout the life of an organism once it is established during embryogenesis. However, mounting evidence suggest that dynamic changes in the methylome continue beyond embryogenesis and particularly play crucial roles for neural cell development and function.

In this thesis I described studies in which I investigated T_3-dependent modulation of DNA methylation in the developing brain. My discoveries support that in addition to posttranslational modification of histones, T_3 modulates the neural cell methylome through activation of genes that code for enzymes that methylate and demethylate the genome.

Developmental and T_3-dependent regulation of genes that code for enzymes that modulate DNA methylation and demethylation

I investigated developmental and T_3-dependent regulation of the gene that code for the *de novo* DNA methyltransferase 3a (*dnmt3a*), the key enzyme that catalyzes DNA methylation (1) in *Xenopus* tadpole brain (Chapter 2). Using real-time RT-qPCR I found that *dnmt3a* mRNA increased in tadpole brain during metamorphosis, coincident with increases in plasma [T_3] and [T_4] (2) (Fig. 5.1); treating premetamorphic tadpoles with exogenous T_3 also induced *dnmt3a* mRNA. I further conducted molecular characterization of T_3 response elements (T_3RE) associated with the *dnmt3a* gene. By analyzing data from a ChIA-PET experiment conducted on tadpole tail fin chromatin with TR as the target protein (L. Sachs and N. Buisine, unpublished data), I identified three putative TR binding sites associated with the gene. Using this information I conducted targeted ChIP assays for TRs on brain chromatin and found that the receptors associated with 7.4 kb upstream and 4.7 kb downstream of the predicted translation start site of the frog *dnmt3a* gene. Within each locus I identified direct repeat plus a four nucleotide spacer (DR+4) T_3REs using bioinformatics and comparative genomics approaches. I conducted EMSA, transient transfection-reporter assays and site-directed mutagenesis to show that they are functional T_3REs that support T_3-dependent transactivity, which may explain developmental and T_3-dependent regulation of the frog *dnmt3a* gene.

Given the findings in frog, evolutionarily conserved roles for T_3 in vertebrate neurological development (3), and previous work showing a positive correlation between plasma thyroid hormone level and expression of *Dnmt3a* in the early postnatal mouse brain (4-7), I investigated whether the orthologous mouse *Dnmt3a* gene was similarly regulated by T_3. I found that T_3 rapidly induced *Dnmt3a* mRNA both in the neonatal brain and in Neuro2a[TRβ1] cells (Neuro2a neuroblastoma cell line that is engineered to express TRβ1 (8)); this induction was resistant to ongoing protein synthesis inhibition in Neuro2a[TRβ1] cells, further supporting that

Dnmt3a is directly regulated by T_3. Using the same approaches as I used for characterizing the frog *dnmt3a* T_3REs, I identified two functional T_3REs at 30.1 and 49.0 kb downstream from the transcription start site of the mouse *Dnmt3a* gene. These findings strongly suggest that T_3 modulates DNA methylation in the developing brain through direct activation of the *Dnmt3a* gene.

Future studies should investigate roles for DNMT3a in mediating T_3 actions on the developing brain. Cell proliferation in the ventricular and subventricular zones (VZ/SVZ; neurogenic regions) of the tadpole brain exhibits a T_3-dependent increase at the onset of metamorphosis (NF stage 50), peaks at mid-prometamorphosis (NF stage 56), then declines through late prometamorphosis and climax (9) (Fig. 5.1); this decline of cell proliferation inversely correlates with an increase in *dnmt3a* mRNA (Fig. 5.1). *In situ* hybridization histochemistry showed that in tadpole brain *dnmt3a* mRNA is widely expressed in cells that have migrated out of the VZ/SVZ, but not in neural stem cells that reside within the neurogenic regions (Chapter 2). Thyroid hormone is known to induce cell cycle exit and differentiation of neuronal progenitors (Neuro2a[TRβ1] cells) (8,10). Conversely, hypothyroidism prolongs cell proliferation in the postnatal mouse brain (4). These findings together suggest that DNMT3a may play a role in mediating T_3 actions on cell differentiation, and I hypothesize that DNMT3a maintains cell cycle exit in differentiating neural cells through repression of cell cycle genes, such as *Cyclin D1*. Deletion of *Dnmt3a* gene in mouse causes dysregulation of cell cycle genes in neural stem cells derived from the SVZ (11). Thyroid hormone treatment of Neuro2a[TRβ1] cells reduces *Cyclin D1* mRNA (10). DNA methylation of the *Cyclin D1* promoter inversely correlates with *Cyclin D1* gene expression (12), which may be catalyzed by DNMT3a (13,14).

Future studies should investigate whether T_3 influences DNA methylation of cell cycle genes in the developing brain.

I also investigated developmental and T_3-dependent regulation of genes that code for enzymes that catalyze active DNA demethylation in the tadpole brain (Chapter 3). Using real-time RT-qPCR I found that mRNAs for the *tet2, tet3, apobec2, gadd45β, gadd45γ* and *tdg* genes increased during metamorphosis. Of these six genes, *tet3, gadd45γ* and *tdg* mRNAs also showed T_3-dependent increases in premetamorphic tadpole brain, suggesting that these three enzymes may be responsible for T_3-dependent DNA demethylation of neural cells during metamorphosis (discussed below).

It is still not well understood what roles TET3, GADD45γ and TDG proteins play in postembryonic neurological development, but studies in embryos suggest their roles for neural cell differentiation. The ten-eleven translocation dioxygenase 3 (*tet3*) catalyze the conversion of 5-mC to 5-hydroxymethylcytosine (5-hmC) in vertebrate genomes to initiate active DNA demethylation (15). *In situ* hybridization analysis of embryonic mouse brain shows that *Tet3* mRNA increases between embryonic days 13.5 and 15.5 at the cortical plate where neuronal cells undergo differentiation, which correlated with increase in the abundance of 5-hmC (16). In the *Xenopus* genome two homologous *Tet* genes (*tet2* and *tet3*) have been identified. A previous study showed that TET3 plays a role in neural cell (eye) development during embryogenesis by controlling expression of genes that are involved in neurogenesis (17). The growth arrest and DNA damage 45 gamma (GADD45γ*)* is a scaffold protein that interacts with various types of enzymes that are involved in nucleotide excision repair (NER) and base-excision repair (BER) pathways (reviewed in Shafer, 2013 (18)). Histochemical analyses showed that *gadd45γ* mRNA is expressed in cells undergoing differentiation, such as primary neuron precursors in *Xenopus*

neurula (19) and in the developing central nervous system of mouse embryos (20). Thymine DNA glycosylase (TDG) recognizes T:G mismatch in the genome and activates the BER pathway to correct the mismatch (reviewed in Kohli and Zhang, 2013 (21)). In addition to this known role, recent studies showed that TDG catalyzes the removal of 5-formylcytosine (5-fC) and 5-carboxycytosine (5-caC) (22), modified cytosines generated by TET-mediated oxidation of 5-hmC (23,24). Nothing is known about expression pattern of the *TDG* gene in the developing nervous system.

Conducting histochemical analysis using *in situ* hybridization or immunohistochemistry for *tet3, gadd45γ* and *tdg* genes will be informative for developing more specific hypotheses about their potential roles in the developing brain. Whole body deletion of either *Tet3* or *Tdg* gene is embryonic lethal in mouse (25,26), while deletion of the *Gadd45γ* gene does not interfere with normal mouse development (27). Generating mice carrying neural cell-specific deletion of *Tet3* and/or *Tdg* genes will also be useful for studying their roles in postnatal neurological development. Future studies should also investigate roles for TET3, GADD45γ and TDG proteins in mediating T_3 actions on DNA demethylation. One approach is to knock down expression of these genes, for example, in tadpole brain by delivering morpholino antisense oligonucleotides using electroporation-mediated gene transfer (28), and then to analyze the effect of such manipulation on T_3-dependent DNA demethylation at specific loci such as T_3REs for *klf9* and *dnmt3a* genes (Chapter 3; discussed below). If *tet3, gadd45γ* and/or *tdg* mediate T_3-dependent DNA demethylation, I predict that the knock down will impair T_3-dependent changes in DNA methylation, such that the locus will remain methylated in response to T_3.

Developmental and T_3-dependent modulation of the neural cell methylome

I found that the genome of tadpole neural cells became demethylated during metamorphosis using ELISA, LUMA, cytosine extension assays (Chapter 3) and MethylCap-seq (Chapter 4). As discussed before, the degree of changes in DNA methylation detected by these independent assays varied. While 5-mC ELISA detected roughly 50% reduction in methylated cytosines between the onset of metamorphosis and metamorphic climax (NF stages 50 and 62), the other three assays detected reduction ranging between 0.6 and 2%. This discrepancy is likely due to differences in the sensitivity of these assays; ELISA can detectmethylated cytosines in any sequence context, while other assays detect methylated cytosines mainly in CpG context. This discrepancy, however, may also suggest that non-CpG (CpH) methylation may undergo more dynamic changes in tadpole brain during metamorphosis. A recent genome-wide analysis of 5-mC in the developing mouse and human brains showed that CpH methylation exhibited more dynamic changes than CpG methylation did (5). Future studies should investigate whether changes in CpH methylation account for a larger decline of 5-mC detected by ELISA in the tadpole brain. As a preliminary approach, it will be informative to conduct sequence motif analysis of MethylCap-seq data to investigate if CpH sequence is enriched in captured DNA.

Cell proliferation in tadpole brain exhibits a robust increase around mid-prometamorphosis (NF stage 56) (9) (Fig. 5.1). Therefore, while activation of *tet3, gadd45γ* and *tdg* genes suggests active DNA demethylation of tadpole neural cells during metamorphosis, passive DNA demethylation through cell divisions may also contribute to the overall decline of 5-mC, which plays a prominent role during mammalian embryogenesis (reviewed in Hackett and Surani, 2013 (29)). More research is required to support that the active mechanism is responsible for DNA demethylation that occurred during metamorphosis in the tadpole brain. The TET enzymes catalyze the conversion of 5-mC to 5-hmC to initiate active DNA demethylation (15).

Therefore, if the active mechanism is involved, I predict that there is a corresponding increase in the abundance of 5-hmC in tadpole brain during metamorphosis. This can be measured at the whole genome level using ELISA or in a locus-specific manner using a targeted approach, such as 5-hmC DNA immunoprecipitation. Another approach is to measure the enzymatic activity of DNA demethylases in tadpole brain, which can be assayed by mixing cell extract isolated from the brain with DNA fragments of known methylation status (e.g. *in vitro* methylated plasmids). If active DNA demethylation is supported, I predict that brain cell extract from later stage of metamorphosis exhibits a higher DNA demethylase activity than th cell extract isolated from an earlier stage tadpole.

More research is required to determine the extent to which T_3 accounts for developmental changes in DNA methylation. While I found a few examples of T_3-dependent locus-specific DNA demethylation, I did not find evidence to support T_3-dependent DNA demethylation at a global scale (Chapter 3). There are several possibilities to explain the lack of such evidence. First, the duration of T_3 treatment may be too short to recapitulate developmental changes in DNA methylation. While four-day treatment of premetamorphic tadpoles with exogenous T_3 was enough to induce locus-specific DNA demethylation, during spontaneous metamorphosis *Xenopus* tadpoles are exposed to endogenous T_3 for a much longer period of time, as it takes roughly 40 days to complete tadpole metamorphosis (2). Second, as I discovered that T_3 activates both groups of genes that are involved in DNA methylation (*dnmt3a*) and DNA demethylation (*tet3, gadd45γ* and *tdg*) in tapole brain (Chapter 2 and 3), it is likely that T_3 treatment of premetamorphic tadpoles causes simultaneous, opposing changes in DNA methylation, and hence, T_3-dependent changes in DNA methylation may not be detectable by approaches to measure the bulk level of 5-mC such as ELISA and LUMA. A better approach to investigate T_3-

dependent change in DNA methylation is to conduct analysis that allows us to detect locus-specific changes, and therefore, conducting MethylCap-seq analysis on DNA isolated from premetamorphic tadpoles treated with T_3 will be informative to determine the extent to which T_3 is responsible for developmental changes in DNA methylation.

Role of thyroid hormone receptors in modulation of the local DNA methylome

I discovered that genomic regions that contain T_3REs for known T_3-response genes (krüpple-like factor 9 - *klf9* and *dnmt3a*) became demethylated during metamorphosis in tadpole brain; treatment of premetamorphic tadpoles with exogenous T_3 also induced DNA demethylation around these loci. Although *klf9* and *dnmt3a* T_3REs themselves do not contain CpG sequences, *in vitro* methylating DNA sequences that encompass these T_3REs (where flanking regions contain CpG dinucleotides) strongly inhibited T_3-dependent transactivity.

These findings together suggest two things. First, DNA demethylation of T_3REs may be important for activation of T_3-regulated genes in tadpole brain during metamorphosis. Future study should extend this finding by conducting TR ChIP-seq analysis in tadpole brain to determine the extent of overlap between TR binding sites and regions that become demethylated during metamorphosis. Second, the findings suggest that liganded TRs may play a role in recruitment of enzymes that catalyze DNA demethylation to modulate the local methylation state of their binding sites, and future studies should investigate the mechanisms by which *klf9* and *dnmt3a* T_3REs become demethylated. This may occur through several non-mutually exclusive mechanisms. First, through their ability to recruit histone-modifying enzymes, liganded TRs may modulate chromatin architecture to expose binding sites in the genome for enzymes that demethylate DNA, such as for the TET enzymes with the CXXC DNA-binding motif (30).

Second, liganded TRs may recruit enzymes that demethylate DNA through direct protein-protein interaction, as previous study has shown that the TDG protein interacts *in vitro* with nuclear hormone receptors including TRα and RXRα (31). Future studies should address these possibilities by investigating: whether T_3-dependent DNA demethylation requires recruitment of histone-modifying enzymes at TR binding sites; whether DNA demethylases are recruited to TR binding sites upon hormone binding; and whether liganded TRs can directly interact with enzymes that catalyze DNA demethylation, such as TDG.

Published studies generally support the correlation between changes in gene expression and DNA methylation changes that occur within regulatory loci such as promoters and enhancers (5,32,33). In Chapter 4, I also found a weak, but statistically significant correlation between DNA demethylation and activation of genes that are found within 50 kb vicinity of differentially methylated regions. However, more research is required to establish a clear functional connection between these correlated changes. It is still unclear whether changes in DNA methylation lead to gene expression changes (cause), or whether gene expression changes precede changes in DNA methylation at regulatory loci (consequence). My findings of DNA demethylation at T_3REs may provide a useful model to investigate the functional linkage between changes in DNA methylation and changes in gene expression, as a regulatory role of T_3RE is clearly established for some of T_3-regulated genes, such as *klf9* (34). Future study should investigate the effect of modulating the methylation state at T_3REs on expression of the regulated genes using TALEN- or CRISPR/Cas9-mediated targeting of the TET1 catalytic domain (35). Since DNA demethylation at T_3REs correlated with activation of T_3-regulated genes in tadpole brain during metamorphosis (Chapter 3), I predict that TET1-mediated DNA demethylation at

T_3REs either causes precocious activation of the regulated genes, or causes those genes to be more responsive to T_3 by potentially lowering the dose of T_3 that requires for activation.

Concluding remarks

Thyroid hormone and DNA methylation both play crucial roles in postembryonic brain development; however, roles for T_3 in modulating DNA methylation have not been investigated prior to my dissertation research. My discoveries support the hypothesis that T_3 modulates DNA methylation through activation of genes involved in DNA methylation and active DNA demethylation. Although more work is required to identify gene expression programs that are commonly regulated by T_3 signaling and DNA methylation, my thesis work laid an important groundwork to establish the linkage between T_3 signaling and DNA methylation, and broadened our understanding of the mechanisms by which T_3 regulates gene expression programs in the developing brain.

References

1. Goll MG, Bestor TH. Eukaryotic cytosine methyltransferases. Annual review of biochemistry 2005; 74:481-514

2. Shi Y-B. Amphibian Metamorphosis: From Morphology to Molecular Biology. New York: John Wiley and Sons, Inc.

3. Bernal J. Thyroid hormone receptors in brain development and function. Nature clinical practice Endocrinology & metabolism 2007; 3:249-259

4. Hadj-Sahraoui N, Seugnet I, Ghorbel MT, Demeneix B. Hypothyroidism prolongs mitotic activity in the post-natal mouse brain. Neuroscience letters 2000; 280:79-82

5. Lister R, Mukamel EA, Nery JR, Urich M, Puddifoot CA, Johnson ND, Lucero J, Huang Y, Dwork AJ, Schultz MD, Yu M, Tonti-Filippini J, Heyn H, Hu S, Wu JC, Rao A, Esteller M, He C, Haghighi FG, Sejnowski TJ, Behrens MM, Ecker JR. Global epigenomic reconfiguration during mammalian brain development. Science 2013; 341:1237905

6. Chestnut BA, Chang Q, Price A, Lesuisse C, Wong M, Martin LJ. Epigenetic regulation of motor neuron cell death through DNA methylation. The Journal of neuroscience : the official journal of the Society for Neuroscience 2011; 31:16619-16636

7. Westberry JM, Trout AL, Wilson ME. Epigenetic regulation of estrogen receptor alpha gene expression in the mouse cortex during early postnatal development. Endocrinology 2010; 151:731-740

8. Lebel JM, Dussault JH, Puymirat J. Overexpression of the beta 1 thyroid receptor induces differentiation in neuro-2a cells. Proceedings of the National Academy of Sciences of the United States of America 1994; 91:2644-2648

9. Denver RJ, Hu F, Scanlan TS, Furlow JD. Thyroid hormone receptor subtype specificity for hormone-dependent neurogenesis in Xenopus laevis. Developmental biology 2009; 326:155-168

10. Perez-Juste G, Aranda A. The cyclin-dependent kinase inhibitor p27(Kip1) is involved in thyroid hormone-mediated neuronal differentiation. The Journal of biological chemistry 1999; 274:5026-5031

11. Wu H, Coskun V, Tao J, Xie W, Ge W, Yoshikawa K, Li E, Zhang Y, Sun YE. Dnmt3a-dependent nonpromoter DNA methylation facilitates transcription of neurogenic genes. Science 2010; 329:444-448

12. Kitazawa S, Kitazawa R, Maeda S. Transcriptional regulation of rat cyclin D1 gene by CpG methylation status in promoter region. The Journal of biological chemistry 1999; 274:28787-28793

13. Brenner C, Deplus R, Didelot C, Loriot A, Vire E, De Smet C, Gutierrez A, Danovi D, Bernard D, Boon T, Pelicci PG, Amati B, Kouzarides T, de Launoit Y, Di Croce L, Fuks F. Myc represses transcription through recruitment of DNA methyltransferase corepressor. The EMBO journal 2005; 24:336-346

14. Hervouet E, Vallette FM, Cartron PF. Dnmt3/transcription factor interactions as crucial players in targeted DNA methylation. Epigenetics : official journal of the DNA Methylation Society 2009; 4:487-499

15. Wu SC, Zhang Y. Active DNA demethylation: many roads lead to Rome. Nature reviews Molecular cell biology 2010; 11:607-620

16. Hahn MA, Qiu R, Wu X, Li AX, Zhang H, Wang J, Jui J, Jin SG, Jiang Y, Pfeifer GP, Lu Q. Dynamics of 5-hydroxymethylcytosine and chromatin marks in Mammalian neurogenesis. Cell reports 2013; 3:291-300
17. Xu Y, Xu C, Kato A, Tempel W, Abreu JG, Bian C, Hu Y, Hu D, Zhao B, Cerovina T, Diao J, Wu F, He HH, Cui Q, Clark E, Ma C, Barbara A, Veenstra GJ, Xu G, Kaiser UB, Liu XS, Sugrue SP, He X, Min J, Kato Y, Shi YG. Tet3 CXXC domain and dioxygenase activity cooperatively regulate key genes for Xenopus eye and neural development. Cell 2012; 151:1200-1213
18. Schafer A. Gadd45 proteins: key players of repair-mediated DNA demethylation. Advances in experimental medicine and biology 2013; 793:35-50
19. Kaufmann LT, Niehrs C. Gadd45a and Gadd45g regulate neural development and exit from pluripotency in Xenopus. Mechanisms of development 2011; 128:401-411
20. Kaufmann LT, Gierl MS, Niehrs C. Gadd45a, Gadd45b and Gadd45g expression during mouse embryonic development. Gene expression patterns : GEP 2011; 11:465-470
21. Kohli RM, Zhang Y. TET enzymes, TDG and the dynamics of DNA demethylation. Nature 2013; 502:472-479
22. Maiti A, Drohat AC. Thymine DNA glycosylase can rapidly excise 5-formylcytosine and 5-carboxylcytosine: potential implications for active demethylation of CpG sites. The Journal of biological chemistry 2011; 286:35334-35338
23. He YF, Li BZ, Li Z, Liu P, Wang Y, Tang Q, Ding J, Jia Y, Chen Z, Li L, Sun Y, Li X, Dai Q, Song CX, Zhang K, He C, Xu GL. Tet-mediated formation of 5-carboxylcytosine and its excision by TDG in mammalian DNA. Science 2011; 333:1303-1307
24. Ito S, Shen L, Dai Q, Wu SC, Collins LB, Swenberg JA, He C, Zhang Y. Tet proteins can convert 5-methylcytosine to 5-formylcytosine and 5-carboxylcytosine. Science 2011; 333:1300-1303
25. Cortellino S, Xu J, Sannai M, Moore R, Caretti E, Cigliano A, Le Coz M, Devarajan K, Wessels A, Soprano D, Abramowitz LK, Bartolomei MS, Rambow F, Bassi MR, Bruno T, Fanciulli M, Renner C, Klein-Szanto AJ, Matsumoto Y, Kobi D, Davidson I, Alberti C, Larue L, Bellacosa A. Thymine DNA glycosylase is essential for active DNA demethylation by linked deamination-base excision repair. Cell 2011; 146:67-79
26. Gu TP, Guo F, Yang H, Wu HP, Xu GF, Liu W, Xie ZG, Shi L, He X, Jin SG, Iqbal K, Shi YG, Deng Z, Szabo PE, Pfeifer GP, Li J, Xu GL. The role of Tet3 DNA dioxygenase in epigenetic reprogramming by oocytes. Nature 2011; 477:606-610
27. Hoffmeyer A, Piekorz R, Moriggl R, Ihle JN. Gadd45gamma is dispensable for normal mouse development and T-cell proliferation. Molecular and cellular biology 2001; 21:3137-3143
28. Haas K, Jensen K, Sin WC, Foa L, Cline HT. Targeted electroporation in Xenopus tadpoles in vivo--from single cells to the entire brain. Differentiation; research in biological diversity 2002; 70:148-154
29. Hackett JA, Surani MA. DNA methylation dynamics during the mammalian life cycle. Philosophical transactions of the Royal Society of London Series B, Biological sciences 2013; 368:20110328
30. Wu H, Zhang Y. Reversing DNA methylation: mechanisms, genomics, and biological functions. Cell 2014; 156:45-68
31. Chen D, Lucey MJ, Phoenix F, Lopez-Garcia J, Hart SM, Losson R, Buluwela L, Coombes RC, Chambon P, Schar P, Ali S. T:G mismatch-specific thymine-DNA

glycosylase potentiates transcription of estrogen-regulated genes through direct interaction with estrogen receptor alpha. The Journal of biological chemistry 2003; 278:38586-38592

32. Guo JU, Ma DK, Mo H, Ball MP, Jang MH, Bonaguidi MA, Balazer JA, Eaves HL, Xie B, Ford E, Zhang K, Ming GL, Gao Y, Song H. Neuronal activity modifies the DNA methylation landscape in the adult brain. Nature neuroscience 2011; 14:1345-1351

33. Hon GC, Rajagopal N, Shen Y, McCleary DF, Yue F, Dang MD, Ren B. Epigenetic memory at embryonic enhancers identified in DNA methylation maps from adult mouse tissues. Nature genetics 2013; 45:1198-1206

34. Bagamasbad PD, Bonett RM, Sachs L, Buisine N, Raj S, Knoedler JR, Kyono Y, Ruan Y, Ruan X, Denver RJ. Deciphering the regulatory logic of an ancient, ultraconserved nuclear receptor enhancer module. Molecular endocrinology 2015:me20141349

35. Maeder ML, Angstman JF, Richardson ME, Linder SJ, Cascio VM, Tsai SQ, Ho QH, Sander JD, Reyon D, Bernstein BE, Costello JF, Wilkinson MF, Joung JK. Targeted DNA demethylation and activation of endogenous genes using programmable TALE-TET1 fusion proteins. Nature biotechnology 2013; 31:1137-1142

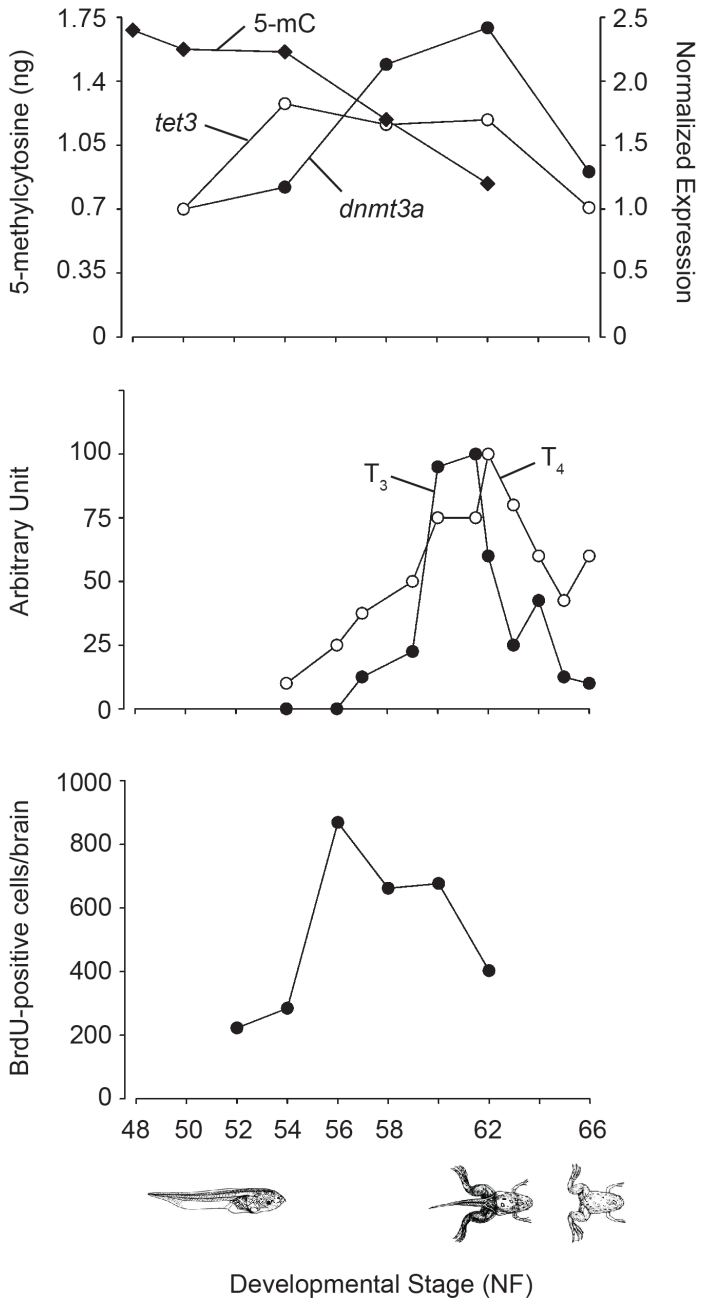

Fig. 5.1. Summary of changes in *Xenopus* tadpole brain during metamorphosis. *Top*: 5-methylcytosine (analyzed by ELISA; Fig 3.1A) and expression of genes that are involved in DNA methylation (*dnmt3a*; Fig. 2.1D) and active DNA demethylation (*tet3* only; *gadd45γ* and *tdg* showed similar profiles; Fig 3.1B). *Middle*: Plasma thyroid hormone concentration (T_3 and T_4; Fig 1.1). *Bottom*: Cell proliferation as quantified by BrdU immunohistochmistry. The middle and bottom figures were adapted and modified with permission (Middle – Shi (2000); Bottom - Denver et al. (2009))